INVESTIGATION OF THE ATMOSPHERIC IMPACTS AND OZONE FORMATION POTENTIALS OF STYRENE

Final Report to the
Styrene Information and Research Center

by
William P. L. Carter, Dongmin Luo, and Irina L. Malkina

March 10, 1999

College of Engineering
Center for Environmental Research and Technology
University of California
Riverside, California 92521

98-AP-RT2H-001-FR

ABSTRACT

Environmental chamber experiments and computer model calculations were conducted to assess the impacts of the gas-phase reactions of styrene on the atmospheric formation of ozone and styrene's known oxidation products. The experiments consisted of determining the effects of adding styrene on ozone formation, NO oxidation, integrated OH radical levels, and formation of benzaldehyde, formaldehyde, and peroxybenzoyl nitrate (PBzN) in various simulated photochemical smog systems in a dual ~2500-liter, xenon-arc-irradiated Teflon environmental chamber. The gas-phase mechanism for the atmospheric reactions of styrene was updated based on available literature data, and model predictions using the mechanism were compared with the results of the chamber experiments. The model predictions were consistent with the observed effects of styrene on benzaldehyde and formaldehyde and not inconsistent with the qualitative PBzN data, but the effect of styrene on radical levels and ozone could only be simulated if it was assumed that the reaction of styrene with ozone does not result in radical formation. The mechanisms which fit the chamber data was used to used to predict the impacts of styrene on ozone formation under various atmospheric conditions. The changes to the ozone + styrene mechanism caused the Maximum Incremental Reactivity (MIR) for styrene, relative to the average of all VOC emissions, to decrease from ~0.7 to ~0.6, on a mass basis. Uncertainties in the mechanism for the styrene + NO_3 reactions were found not to significantly impact ambient ozone impact predictions. The impact of styrene on ozone formation depended significantly on NO_x conditions, being greater than that of ethane (but less than the average of all emissions on a mass basis and therefore not "highly reactive") under the high NO_x conditions of the MIR scale, but becoming significantly negative in scenarios with lower NO_x levels. The reactivities in the MIR scenarios were the same regardless of whether the ozone impact was defined in terms of peak ozone or the maximum 8-hour average, but the 8-hour average ozone reactivities declined much more slowly as NO_x was reduced than reactivities in terms of effects on peak ozone yields. It is concluded that models with an appropriate styrene mechanism (and an explicit representation of benzaldehyde) can probably reliably represent the effects of styrene on the formation of ozone, benzaldehyde, formaldehyde, PBzN, and overall radical levels in the atmosphere. However, the known products from styrene's reactions account for only ~60% of the carbon reacted, and atmospheric impacts of the unknown products may not be well represented in current models.

ACKNOWLEDGEMENTS

The authors acknowledge Mr. Dennis Fitz for assistance in administering this program, Dr. Antonio Miguel for assistance with developing the PBzN analysis, and Mr. Kurt Bumiller with assistance in carrying out the environmental chamber experiments. Helpful discussions with Dr. Roger Atkinson of the Statewide Air Pollution Research Center, Dr. Greg Yarwood of Environ, Inc. and the members of Air Fate Subgroup of the Styrene Information and Research Center (SIRC) are also acknowledged.

Although this work was funded by the SIRC, the opinions and conclusions expressed in this report are entirely those of the primary author, Dr. William P. L. Carter. Mention of trade names or commercial products do not constitute endorsement or recommendation for use.

TABLE OF CONTENTS

Section	Page
INTRODUCTION	1
METHODS	3
Environmental Chamber Experiments	3
Overall Experimental Approach	3
Environmental Chamber	4
Experimental Procedures	5
Analytical Methods	6
Characterization Methods	7
Data Analysis Methods	8
Reactivity Data Analysis Methods	8
Chemical Mechanisms Used in the Model Simulations	10
General Atmospheric Photooxidation Mechanism	10
Environmental Chamber Modeling Methods	15
Atmospheric Reactivity Modeling Methods	15
Scenarios Used for Reactivity Assessment	15
Quantification of Atmospheric Reactivity	18
Chemical Models and Mechanisms Used	19
REACTIONS OF STYRENE AND REPRESENTATION IN THE MODEL	20
OH Radical Reaction	20
Ozone Reaction	21
NO_3 Radical Reactions	23
Reaction with $O(^3P)$	25
Reactions of Benzaldehyde and PBzN	26
RESULTS AND DISCUSSION	28
Summary of Chamber Experiments and Characterization Results	28
Results of the Base Case Experiments and Adjustments to the Assumed Light Intensities	28
Results of The Reactivity Experiments	34
Atmospheric Reactivity Calculations	48
Discussion of Factors Affecting Styrene's Ozone Reactivities	52
CONCLUSIONS	55
REFERENCES	58
APPENDIX A LISTING OF THE CHEMICAL MECHANISM	A-1

LIST OF TABLES

Number page

1. Summary of the conditions of the scenarios used for atmospheric reactivity assessment. 17

2. Chronological listing of all the chamber experiments carried out for this program. 29

3. Summary of conditions and results of the incremental reactivity experiments. 35

4. Summary of calculated incremental reactivities (gram basis) for ethane, toluene, and the two styrene models, relative to the average of all VOC emissions. 49

A-1. List of species in the chemical mechanism used in the model simulations for this study. A-1

A-2. List of reactions in the chemical mechanism used in the model simulations for this study. . . . A-5

A-3. Absorption cross sections and quantum yields for photolysis reactions. A-13

A-4. Values of chamber-dependent parameters used in the model simulations of the environmental chamber experiments for this study. A-21

LIST OF FIGURES

Number page

1. Plots of experimental and calculated 5-hour d(O_3-NO) data for all the base case surrogate - NO_x experiments carried out in the CTC since November, 1996. 31

2. Plot of trends in NO_2 photolysis rates in the CTC, as derived by various methods. 33

3. Plots of experimental and calculated d(O3-NO) and IntOH incremental reactivities and concentration-time plots for selected species for the mini-surrogate + styrene experiment CTC250. 36

4. Plots of experimental and calculated d(O3-NO) and IntOH incremental reactivities and concentration-time plots for selected species for the mini-surrogate + styrene experiment CTC246. 37

5. Plots of experimental and calculated d(O3-NO) and IntOH incremental reactivities and concentration-time plots for selected species for the full surrogate + styrene experiment CTC248. 39

6. Plots of experimental and calculated d(O3-NO) and IntOH incremental reactivities and concentration-time plots for selected species for the full surrogate + styrene experiment CTC251. 40

7. Plots of experimental and calculated d(O3-NO) and IntOH incremental reactivities and concentration-time plots for selected species for the low NOx full surrogate + styrene experiment CTC253. . 41

8. Plots of experimental and calculated d(O3-NO) and IntOH incremental reactivities and concentration-time plots for selected species for the low NOx full surrogate + styrene experiment CTC249. . 42

9. Plots of experimental and calculated d(O3-NO) and IntOH incremental reactivities and concentration-time plots for selected species for the modified mini- surrogate + benzaldehyde experiment CTC266. 44

10. Plots of experimental and calculated d(O3-NO) and IntOH incremental reactivities and concentration-time plots for selected species for the low NOx full surrogate + benzaldehyde experiment CTC267. 45

11. Plots of calculated relative reactivities for styrene against the NO_x / NO_x^{MO} ratio for the base case and the adjusted NO_x averaged conditions scenarios. 51

INTRODUCTION

Many different types of volatile organic compounds (VOCs) are emitted into the atmosphere, each reacting at different rates and with different photooxidation mechanisms. Because of this, VOCs can differ significantly in their effects on ground-level ozone formation and other measures of air quality. The effect of a VOC on ground-level ozone is often referred to as its "reactivity." Some compounds, such as CFCs, do not react in the lower atmosphere at all, and thus make no contribution to ground-level ozone formation. Others, such as methane, react and contribute to ozone formation, but react so slowly that their practical effect on local ozone formation is negligible, and still others, such as volatile silicone compounds (Carter et al., 1992) inhibit the formation of ozone. In recognition of this, the EPA has exempted these and other compounds from regulation as VOC ozone precursors, and has informally used the ozone impact as the standard to define the borderline of "negligible" reactivity (Dimitriades, 1996). Although at present the EPA only takes reactivity into account when considering exempting individual compounds on the basis of negligible ozone impact, it has been proposed that it consider grouping non-exempt compounds into "reactive" and "highly reactive" classes, to serve as a basis for regulations for encouraging or requiring use of less reactive compounds (Dimitriades, 1996). The ozone impact of toluene has been proposed as the dividing line in this regard (Dimitriades, 1996). Furthermore, the California Air Resources Board (CARB) has already adopted reactivity-based regulations in its Clean-Fuel/Low Emissions Vehicle regulations (CARB, 1993), and is now studying the possibility of using reactivity adjustment in consumer product VOC emissions. Therefore, it is clear that producers and users of VOCs will eventually need to know the ozone impacts of their VOCs, and how they would be classified in any reactivity ranking system used in any regulatory approach.

Styrene is a compound which is used in a number of industrial applications, whose normal use may result in its emissions into the atmosphere. Styrene is known to react relatively rapidly in the atmosphere (Marchello and Sterling, 1991), and its reactions may contribute to the formation of ground-level ozone and other secondary pollutants. Based on available kinetic and mechanistic data (Atkinson, 1994, and references therein) we derived an estimated atmospheric reaction mechanism for styrene and used it to estimate its atmospheric ozone impact for various conditions (Carter, 1994a). The results indicated that the ozone impact of styrene is highly dependent on the ambient levels of oxides of nitrogen (NO_x), being calculated to have ~70% the ozone impact (on an ozone formed per gram emitted basis) as the weighed average of all VOC emissions under the relatively high NO_x conditions where ozone formation is most sensitive to VOC emissions, but to be an ozone inhibitor under lower NO_x conditions. However the mechanism used to make these estimates has not been adequately documented, has potentially significant uncertainties, and its ability to accurately predict styrene's ozone impacts has not been experimentally verified. Therefore, it is uncertain how to appropriately classify styrene in any reactivity-based ozone control program.

To address research needs concerning the atmospheric impacts of styrene, the Styrene Information and Research Center (SIRC) contracted with the College of Engineering Center for Environmental Research and Technology (CE-CERT) to carry out an experimental and modeling study to assess the atmospheric impacts of styrene due to its gas-phase atmospheric reactions. This has involved the following tasks: (1) updating the atmospheric reaction mechanism for styrene to be consistent with recent laboratory results and implementing it in the most current atmospheric photochemical reaction mechanism; (2) carrying out environmental chamber studies to determine the effects of styrene on O_3 formation, NO oxidation, organic product formation and rates of reaction of other species under various conditions useful for mechanism evaluation; (3) using the results of the chamber experiments to evaluate the predictions of the mechanism, and revising or adjusting uncertain portions of the styrene oxidation mechanism as appropriate for model predictions to be consistent with the experimental data; (4) carrying out EKMA or box model calculations to estimate styrene's impacts under various representative airshed conditions; and (5) developing recommendations for how best to represent the gas-phase atmospheric reactions of styrene in comprehensive model assessments of the impacts of styrene and its major oxidation products in real-world scenarios of interest to SIRC and the regulatory community. The results of this effort are presented in this report.

METHODS

Environmental Chamber Experiments

Overall Experimental Approach

Most of the environmental chamber experiments for this program consisted of measurements of "incremental reactivities" of styrene under various conditions. These involve two types of irradiations of model photochemical smog mixtures. The first is a "base case" experiment where a mixture of reactive organic gases (ROGs) representing those present in polluted atmospheres (the "base ROG surrogate") is irradiated in the presence of oxides of nitrogen (NO_x) in air. The second is the "test" experiment which consists of repeating the base case irradiation except that the VOC whose reactivity is being assessed is added. The differences between the results of these experiments provide a measure of the atmospheric impact of the test compound, and the difference relative to the amount added is a measure of its reactivity. These data can then be used to test the ability of various chemical mechanisms or models for styrene's atmospheric reactions to predict the impacts of its gas-phase reactions under various conditions in the atmosphere.

To provide data to test predictions of impacts of styrene under varying atmospheric conditions, three types of incremental reactivity experiments were carried out:

1. Mini-Surrogate Experiments. The base case for this type of experiment employed a simplified ROG surrogate and relatively high NO_x levels and low ROG/NO_x ratios. Low ROG/NO_x ratios represent "maximum incremental reactivity" (MIR) conditions (Carter, 1994a), which are most sensitive to VOC effects. Low ROG/NO_x experiments are useful because they provide a sensitive test for the model, and also because it is most important that the model correctly predict a VOC's reactivity under conditions where the atmosphere is most sensitive to the VOCs. The ROG mini-surrogate mixture employed consisted of ethene, n-hexane, and m-xylene. As discussed by Carter et al (1993a), this mixture was designed to be a vert approximate representation of the general types of VOCs measured in the atmosphere. This same surrogate was employed in our previous studies (Carter et al, 1993a,b; 1995a,b.), and was found to provide a more sensitive test of aspects of the mechanism concerning radical initiation and termination effects than the more complex surrogates which more closely represent atmospheric conditions (Carter et al, 1995b). This high sensitivity to these important mechanistic effects makes the mini-surrogate experiments highly useful for mechanism evaluation.

2. Full Surrogate Experiments. The base case for this type of experiment employed a more complex ROG surrogate under somewhat higher, though still relatively low, ROG/NO_x conditions. While less sensitive to radical initiation and termination effects in the mechanisms of the VOCs studied, they provide a means to test other aspects of the mechanisms, such as numbers of NO to NO_2 conversions, etc. Furthermore,

experiments with a more representative ROG surrogate are needed to evaluate the mechanism under conditions that more closely resembling the atmosphere. The ROG surrogate employed was the same as the 8-component "lumped molecule" surrogate as employed in previous studies (e.g., Carter et al. 1995b), and consists of n-butane, n-octane, ethene, propene, trans-2-butene, toluene, m-xylene, and formaldehyde. As discussed by Carter et al (1995b), this surrogate was designed to mixture of VOCs measured in urban atmospheres using a similar level of detail as employed in current airshed models, with a single compound representing each type of model species. Calculations have indicated that use of this 8-component mixture will give essentially the same results in incremental reactivity experiments as actual ambient mixtures (Carter et al. 1995b).

3. Full Surrogate, low NO_x Experiments. The base case for this type of experiment employed the same 8-component lumped molecule surrogate as used in the full surrogate experiments described above, except that lower NO_x levels (higher ROG/NO_x ratios) were employed to represent NO_x-limited conditions. Such experiments are necessary to assess the ability of the model to properly simulate reactivities under conditions where NO_x is low. The initial ROG and NO_x reactant concentrations were comparable to those employed in our previous studies (Carter et al. 1995b).

A limited number of experiments were also carried out using benzaldehyde as the test compound, because this is a major photooxidation product for styrene and data to test its photooxidation mechanism are also needed. In this case, a modified mini-surrogate experiment (where the m-xylene was replaced by toluene and 1,3,5-trimethylbenzene)[1] and a full surrogate experiment were carried out with added benzaldehyde.

An appropriate set of control and characterization experiments necessary for assuring data quality and characterizing the conditions of the runs for mechanism evaluation were also carried out. These are discussed where relevant in the Modeling Methods or Results sections.

Environmental Chamber

The environmental chamber system employed in this study was the CE-CERT dual-reactor Xenon Arc Teflon Chamber (CTC). This consists of two 4' x 4' x 8' FEP Teflon reaction bags located adjacent to each other at one end of an 8' x 12' room with reflective aluminum paneling on all surfaces. The two reactors are referred to as the two "sides" of the chamber (Side A and Side B) in the subsequent discussion. Four 6.5 KW xenon arc lights were mounted on the wall opposite the reaction bags, all in a room with walls and ceiling covered with reflective aluminum paneling to maximize light intensity and homogeneity. The reaction bags were interconnected with two ports, each containing a fan to exchange the contents of the bags to assure that

[1]The modification was made as part of a separate program to investigate the use of alternative radical tracers in the surrogate experiments. 1,3,5-trimethylbenzene reacts with OH radicals more rapidly than does m-xylene, thus its use provides a more sensitive and precise measurement of OH levels. This substitution is not expected to affect the interpretation of the data for this study.

the common reactants were adequately mixed. This was important in order to evaluate the effect of adding a test compound to a standard mixture. Two separate fans are also employed to mix the contents within each chamber. As discussed elsewhere (Carter et al. 1995b,c), this light source gives the closest approximation available of the ground-level solar spectrum for an indoor chamber. Except for the fact that it uses two reactors, the chamber was very similar to the Statewide Air Pollution Research Center's Xenon arc Teflon Chamber (SAPRC XTC) which is described in detail elsewhere (Carter et al. 1995b,c).

Experimental Procedures

The reaction bags were flushed with dry air produced by an AADCO air purification system for 14 hours (6 PM - 8 AM) on the nights before experiments. The continuous monitors were connected prior to reactant injection and the data system began logging data from the continuous monitoring systems. The reactants were injected as described below (see also Carter et al, 1993a,, 1995c). The common reactants were injected in both sides simultaneously using a three-way (one inlet and two outlets connected to side A and B respectively) bulb of 2 liters in the injection line and were well mixed before the chamber was divided. The contents of each side were blown into the other using two box fans located between them. Mixing fans were used to mix the reactants in the chamber during the injection period, but these were turned off prior to the irradiation. The sides were then separated by closing the ports which connected them, after turning all the fans off to allow their pressures to equalize. After that, reactants for specific sides (the test compound in the case of reactivity experiments) were injected and mixed. The irradiation began by turning on the lights and proceeded for 6 hours. After the run, the contents of the chamber were emptied by allowing the bag to collapse, and then was flushed with purified air. The contents of the reactors were vented into a fume hood.

The procedures for injecting the various types of reactants were as follows. The NO and NO_2 were prepared for injection using a high vacuum rack. Known pressure of NO, measured with MKS Baratron capacitance manometers, were expanded into Pyrex bulbs with known volumes, which were then filled with nitrogen (for NO) or oxygen (for NO2). The contents of the bulbs were then flushed into the chamber with AADCO air. The other gas reactants were prepared for injection either using a high vacuum rack or a gas-tight syringes whose amounts were calculated. The gas reactant in a gas-tight syringe was usually diluted to 100-ml with nitrogen in a syringe. The volatile liquid reactants, including styrene, were injected, using a micro syringe, into a 1-liter Pyrex bulb equipped with stopcocks on each end and a port for the injection of the liquid. The port was then closed and one end of the bulb was attached to the injection port of the chamber and the other to a dry air source. The stopcocks were then opened, and the contents of the bulb were flushed into the chamber with a combination of dry air and heat gun for approximately 5 minutes. Formaldehyde was prepared in a vacuum rack system by heating paraformaldehyde in an evacuated bulb until the pressure corresponded to the desired amount of formaldehyde. The bulb was then closed and detached from the vacuum system and its contents were flushed into the chamber with dry air through the injection port.

The concentrations of the reactants calculated from the amounts injected were compared with the experimentally measured concentrations, and generally agreed to within the uncertainties of the calculations or measurements.

Analytical Methods

Ozone and nitrogen oxides (NO_x) were continuously monitored using commercially available continuous analyzers with Teflon sample lines inserted directly into the chambers. The sampling lines from each side of the chamber were connected to solenoids which switched from side to side every 10 minutes, so the instruments alternately collected data from each side. Ozone was monitored using a Dasibi 1003AH UV photometric ozone analyzer and NO and total oxides of nitrogen (including HNO_3 and organic nitrates) were monitored using a Teco Model 14B chemiluminescent NO/NO_x monitor. The output of these instruments, along with that from the temperature sensors and the formaldehyde instrument, were attached to a computer data acquisition system, which recorded the data at 10 minutes intervals for ozone, NO and temperature (and at 20 minutes for formaldehyde), using 60 second averaging times. This yielded a sampling interval of 20 minutes for taking data from each side.

The Teco instrument and Dasibi CO analyzer were calibrated with a certified NO and CO source and CSI gas-phase dilution system. It was done prior to chamber experiment for each run. The NO_2 converter efficiency was checked at regular intervals. The Dasibi ozone analyzer was calibrated against transfer standard ozone analyzer using transfer standard method in a interval of three months and was check with CSI ozone generator (set to 400 ppb) for each experiment to assure that the instrument worked properly. The details were discussed elsewhere (Carter et al, 1995c)

Organic reactants other than formaldehyde were measured by gas chromatography with FID detection as described elsewhere (Carter et al. 1993a; 1995c). GC samples were taken for analysis at intervals from 20 minutes to 30 minutes either using 100 ml gas-tight glass syringes or by collecting the 100 ml sample from the chamber onto Tenax-GC solid adsorbent cartridge. These samples were taken from ports directly connected to the chamber after injection and before irradiation and at regular intervals after irradiation. The sampling method employed for injecting the sample onto the GC column depended on the volatility or "stickiness" of the compound. For analysis of the more volatile species, the contents of the syringe were flushed through a 2 ml or 3 ml stainless steel or 1/8' Teflon tube loop and subsequently injected onto the column by turning a gas sample valve.

The calibrations for the GC analyses for most compounds were carried out by sampling from chambers or vessels of known volume into which known amounts of the reactants were injected, as described previously (Carter et al, 1995c).

Styrene and benzaldehyde were monitored by GC-FID with loop injection. The analysis of nitrophenols were attempted by using GC-FID with Tenax injection system but no significant peaks were found and identified in the course of the experiments.

Peroxylbenzoyl Nitrate (PBzN) was monitored by GC Electron Capture Detector (ECD). It was collected using an all Teflon loop and injected onto a 0.5 meter packed glass column coated with SE30. Purified nitrogen was used as carrier gas at a flow of 10 cc/min, and isothermal oven temperature program was applied in the course of the GC analysis. The retention time of PBzN was approximately 25 minutes. The PBzN was calibrated by preparing it in the Statewide Air Pollution Research Center (SAPRC) Evacuable Chamber by the photolysis of chlorine in the presence of benzaldehyde and NO_2. The PBzN was quantified by assuming 100% conversion of benzaldehyde to PBzN, and measuring the amount of benzaldehyde consumed.

Characterization Methods

Three temperature thermocouples were used to monitor the chamber temperature, two of which were located in the sampling line of continuous analyzers to monitor the temperature in each side (though the temperature monitor in the line for Side B was not functioning during this period). The third one was located in the outlet of the air conditioning system used to control the chamber temperature. The temperature range in these experiments was typically 25-30° C.

The spectrum of the xenon arc light source was measured several (usually five) times during each experiment using a LiCor LI-1800 spectroradiometer. The absolute light intensity in this chamber was previously measured by "photostationary state" NO_2 actinometry experiments and by Cl_2 actinometry (Carter et al, 1995c,d, 1997a). The photostationary state experiments consisted of simultaneous measurements of photostationary state concentrations of NO, NO_2, and O_3 in otherwise pure air, with the NO_2 photolysis rate being calculated from the $[NO][O_3]/[NO_2]$ ratio (Carter et al. 1997a). The Cl_2 actinometry experiments consisted of photolyzing ~0.1 ppm of Cl_2 in ~1 ppm of n-butane, calculating the Cl_2 photolysis rate from the rate of consumption of n-butane, and then calculating the corresponding NO_2 photolysis rate from the absorption cross sections and quantum yields for NO_2 and Cl_2 (assuming unit quantum yields for Cl_2) and the spectral distribution of the light source (Carter et al, 1997a). The results of these two methods are generally in good agreement when carried out around the same time, and were used to place the somewhat more precise data of the relative light intensity methods, discussed below, on an absolute basis (Carter et al, 1997a).

Relative trends in light intensity with time can be obtained using the quartz tube method of Zafonte et al. (1977), modified as discussed by Carter et al. (1995c; 1997a), and from absolute intensities of spectra taken several times during each run using a Li-Cor LI-1800 spectroradiometer. Absolute light intensities are measured periodically using $NO/NO_2/O_3$ steady state method and by Cl_2 + n-butane actinometry as discussed above. Because the quartz tube during the actinometry experiments was located closer to the lights than the

reaction bags, the NO_2 photolysis rates obtained using this method were corrected by multiplying them by a factor of 0.79 to make them consistent with the absolute values obtained using the steady state or Cl_2 actinometry methods (Carter et al, 1997a). The LiCor data gave the most precise indication of the relative trend in light intensity, and NO_2 photolysis rates calculated using it (and NO_2 absorption cross sections and quantum yields) have been used as the primary method for determining how the light intensity varied with time. These data indicated that the NO_2 photolysis rates declined slowly with time, with the data being fit by a curve giving an NO_2 photolysis rates of around 0.165 min^{-1} during the period of this study.

However, as discussed in more detail in the Results section of this report, the long term trend in the amounts of ozone formed in the replicated base case surrogate - NO_x experiments suggested that the NO_2 photolysis rate inside the chamber declined at a somewhat faster rate than this, and that the actual NO_2 photolysis rate inside the chamber during the period of this study was closer to 0.13 min^{-1}. The results of the periodic (though relatively infrequent) Cl_2 + n-butane actinometry are also consistent with the trend indicated by modeling the base case surrogate experiments. This is discussed further later in this report.

The dilution of the CTC chamber due to sampling is expected to be small because the flexible reaction bags can collapse as samples are withdrawn for analysis. Also, the chamber was designed to operate under slightly positive pressure, so any small leaks would result in reducing the bag volume rather than diluting the contents of the chamber. Information concerning dilution in an experiment can be obtained from relative rates of decay of added VOCs which react with OH radicals with differing rate constants (Carter et al. 1993a; 1995c). Most experiments had more reactive compounds such as m-xylene and n-octane present either as a reactant or added in trace amounts to monitor OH radical levels. Trace amounts (~0.1 ppm) of n-butane were also added to experiments if needed to provide a less reactive compound for monitoring dilution. In addition, specific dilution check experiments such as CO irradiations were carried out. Based on these results, the dilution rate was found to be negligible in this chamber during this period, being less than 0.3% per hour in all runs, and usually less than 0.1% per hour.

Data Analysis Methods

Reactivity Data Analysis Methods

The results of the environmental chamber experiments are analyzed to yield two measures of reactivity for styrene. The first is the effect of styrene on the change in the quantity $[O_3]$-[NO], ory $([O_3]_t$-$[NO]_t)$-$([O_3]_0$-$[NO]_0)$, which is abbreviated as d(O -NO) in the subsequent discussion. As discussed elsewhere (e.g., Johnson, 1983; Carter and Atkinson, 1987; Carter and Lurmann, 1990, 1991, Carter et al, 1993a, 1995a), this gives a direct measure of the amount of conversion of NO to NO_2 by peroxy radicals formed in the photooxidation reactions, which is the process that is directly responsible for ozone formation in the atmosphere. (Johnson calls it "smog produced" or "SP".) The incremental reactivity of the compound relative to this quantity, which is calculated for each hour of the experiment, is given by

$$IR[d(O_3\text{-}NO)]_t^{VOC} = \frac{d(O_3\text{-}NO)_t^{test} - d(O_3\text{-}NO)_t^{base}}{[VOC]_0} \qquad (I)$$

where $d(O_3\text{-}NO)_t^{test}$ is the $d(O_3\text{-}NO)$ measured at time t from the experiment where the test compound was added, $d(O_3\text{-}NO)_t^{base}$ is the corresponding value from the corresponding base case run, and $[VOC]_0$ is the amount of test compound added. The units used are ppm for O_3, NO, and $[VOC]_0$, so the incremental reactivity units are moles of O_3 formed and NO oxidized per mole VOC sample added. An estimated uncertainty for $IR[d(O_3\text{-}NO)]$ is derived based on assuming an ~3% uncertainty or imprecision in the measured $d(O_3\text{-}NO)$ values. This is consistent with the results of side equivalency tests carried out previously, where equivalent base case mixtures are irradiated on each side of the chamber.

Note that reactivity relative to $d(O_3\text{-}NO)$ is essentially the same as reactivity relative to O_3 in experiments where O_3 levels are high, because under such conditions $[NO]_t^{base} \approx [NO]_t^{test} \approx 0$, so a change $d(O_3\text{-}NO)$ caused by the test compound is due to the change in O_3 alone. However, $d(O_3\text{-}NO)$ reactivity has the advantage that it provides a useful measure of the effect of the compound on processes responsible for O_3 formation even in experiments (or portions of experiments) where O_3 formation is suppressed by relatively high NO levels.

The second measure of reactivity is the effect of the test compound on integrated hydroxyl (OH) radical concentrations in the experiment, which is abbreviated as "IntOH" in the subsequent discussion. This is an important factor affecting reactivity because radical levels affect how rapidly all VOCs present, including the ROG surrogate components, react to form ozone. If a compound is present in the experiment which reacts primarily with OH radicals, then the IntOH at time t can be estimated from

$$IntOH_t = \int_0^t [OH]_\tau \, d\tau = \frac{\ln\left(\frac{[tracer]_0}{[tracer]_t}\right) - D\,t}{kOH^{tracer}}, \qquad (II)$$

where $[tracer]_0$ and $[tracer]_t$ are the initial and time=t concentrations of the tracer compound, kOH^{tracer} is its OH rate constant, and D is the dilution rate in the experiments. The latter was found to be small and was neglected in our analysis. The concentration of tracer at each hourly interval was determined by linear interpolation of the experimentally measured values. M-xylene was used as the OH tracer in most of these experiments because it is a base case component present in all incremental reactivity experiments, its OH rate constant is known (the value used was 2.36×10^{-11} cm^3 $molec^{-1}$ s^{-1} [Atkinson, 1989]), and it reacts sufficiently rapidly that its consumption rate can be measured with reasonable precision. In one added benzaldehyde experiment, 1,3,5-trimethylbenzene was used as the OH tracer rather than m-xylene. The OH radical rate constant used for it was 5.75×10^{-11} cm^3 $molec^{-1}$ s^{-1} (Atkinson, 1989).

The effect of styrene on OH radicals can thus be measured by its IntOH incremental reactivity, which is defined as

$$IR[IntOH]_t = \frac{IntOH_t^{test} - IntOH_t^{base}}{[VOC]_0} \qquad \text{(III)}$$

where $IntOH_t^{test}$ and $IntOH_t^{base}$ are the IntOH values measured at time t in the added compound and the base case experiment, respectively. The results are reported in units of 10^6 min per ppm. The uncertainties in IntOH and IR[IntOH] are estimated based on assuming an ~2% imprecision in the measurements of the m-xylene concentrations. This is consistent with the observed precision of results of replicate analyses of this compound.

The effects of styrene on the formation of formaldehyde, benzaldehyde, and PBzN was also determined. This is examined by comparing the concentration-time profiles of these products in the experiment with the added styrene with those in the simultaneous base case experiment.

Chemical Mechanisms Used in the Model Simulations

General Atmospheric Photooxidation Mechanism

Ozone formation in photochemical smog is due to the gas-phase reactions of oxides of nitrogen (NO_x) and various reactive organic gases (ROGs) in sunlight. Various reaction schemes have been developed to represent these processes (e.g., Gery et al., 1988; Carter, 1990; Stockwell et al., 1990), but the one used in this work is the latest in the series of the detailed SAPRC mechanisms, previous versions of which have been described previously (Carter, 1990, 1995; Carter et al., 1993b, 1997a). These mechanisms are detailed in the sense that they explicitly represents a large number of different types of organic compounds, but use a condensed representation for most of their reactive products. The major characteristics of this mechanism are similar to the "SAPRC-90" mechanism described by Carter (1990). The reactions of inorganics, CO, formaldehyde, acetaldehyde, peroxyacetyl nitrate, propionaldehyde, peroxypropionyl nitrate, glyoxal and its PAN analog, methyl glyoxal, and several other product compounds are represented explicitly. The reactions of unknown photoreactive products formed in the reactions of aromatic hydrocarbons are represented by model species whose yields and photolysis rate are adjusted based on fits of model simulations to environmental chamber experiments. A "chemical operator" approach is used to represent peroxy radical reactions. Generalized reactions with variable rate constants and product yields are used to represent the primary emitted alkane, alkene, aromatic, and other VOCs (with rate constants and product yields appropriate for the individual compounds being represented in each simulation). Most of the higher molecular weight oxygenated product species are represented using the "surrogate species" approach, where simpler molecules such as propionaldehyde, 2-butanone, or 5-hydroxy-2-pentanone are used to represent the reactions of higher molecular weight analogues that are assumed to react similarly.

The mechanism of Carter (1990) was updated several times prior to this work. The most recent and comprehensive update of this mechanism, was carried out immediately prior to the completion of this project. A report documenting evaluation of this mechanism, and its evaluation with the existing environmental chamber data base, is in preparation (Carter, 1999), and the major features of this mechanism are summarized below.

This version of the mechanism, which can be referred to as the "SAPRC-98" mechanism, incorporates the first complete update of the SAPRC mechanisms since the SAPRC-90 was developed (Carter, 1990). The IUPAC (Atkinson et al, 1997) and NASA (1997) evaluations, the various reviews by Atkinson (1989, 1990, 1991, 1994, 1997), and other available information were used to update all the applicable rate constants, absorption cross sections, quantum yields, and reaction mechanisms where appropriate. Although many small changes were made, none of the changes are considered to have obviously important impacts on reactivity predictions, with a possible exception being the ~30% reduction in important OH + NO_2 rate constant based on the new evaluation by NASA (1997). [The high rate constant in the current IUPAC (Atkinson et al, 1997) evaluation is probably inappropriate (Golden, personal communication, 1998).] However, a complete analysis of the effects of all the changes has not been carried out, and other changes may also be important.

The automated procedure for generated alkane reaction mechanisms incorporated in the SAPRC-90 mechanism (Carter, 1990; Carter and Atkinson, ??) was updated based on the results of the evaluation of Atkinson (1997) and an independent evaluation of alkoxy radial reactions (Carter, 1999). More significantly in terms of general VOC reactivity assessment, it was extended to include not only alkanes, but also alkenes (though presently only for those with no more than one double bond), and many classes of oxygenates including alcohols, ethers, glycols, esters, aldehydes, ketones, glycol ethers, etc. Although many of the estimated rate constants and rate constant ratios are highly uncertain, this procedure provides a consistent basis for deriving "best estimate" mechanisms for chemical systems for which mechanistic data limited or not available, and which are too complex to be examined in detail in a reasonable amount of time. The mechanism generation program allows for assigning or adjusting rate constants or branching ratios in cases where data are available, or where adjustments are necessary for model simulations to fit chamber data. The program outputs programs which can (for larger molecules) involve hundreds or even thousands of reactions or products. Various "lumping rules" are then used to convert the detailed generated mechanisms and product distributions into the lumped reactions and model species distributions actually used in the model. The program also outputs documentation for the generated mechanism, indicating the source of the estimates or assumptions or explicit assignments which were used. The use of this program has permitted estimation of detailed mechanisms for a much larger number of compounds than otherwise would be possible.

The new mechanism was completely re-evaluated using the indoor SAPRC and CE-CERT environmental data base. This included relevant runs from the data base given by Carter et al (1995c) as well as runs more recently carried out at CE-CERT for various programs (e.g., Carter et al, 1995b,d, 1997a,b; and

others[2]). All data from the recently completed program on reactivities of selected consumer product VOCs (Carter et al, in preparation, 1999) were also used in this evaluation. Over 1100 chamber runs were simulated, including ~60 characterization runs, ~380 single compound runs, ~360 reactivity runs, and ~340 complex mixture or base case runs. Insufficient time was available to evaluate the mechanism using data from outdoor chamber runs, though our experience with the SAPRC-90 (Carter and Lurmann, 1991) and RADM-2 (Carter and Lurmann 1990) evaluations indicate that models which perform satisfactorily simulating indoor runs will generally satisfactorily simulate outdoor runs if the latter are sufficiently well characterized.

Given below is a brief summary of the status and updates to the mechanism for the various major classes of compounds, and the results of the evaluation of those mechanisms, where applicable. This discussion will be restricted to the major compounds important when simulating the base case mixture in the environmental chamber experiments and in the atmospheric reactivity calculations discussed in this report. The mechanisms specific to styrene and its major products are discussed separately below, and the mechanisms for other VOCs for which this mechanism has been used to estimate ozone reactivities are summarized elsewhere[3].

Alkanes. Under CARB funding, Atkinson (unpublished results) has obtained new product yields for alkyl nitrates from C_5 - C_{10} n-alkanes indicating that the previously published yields in these systems may be high by ~30%. When the nitrate yields for the higher alkanes are reduced accordingly, it is now possible to fit the chamber data for the C_{8+} n-alkanes without making the unreasonable assumption that nitrate formation does not occur from the peroxy radicals formed after 1,4-H shift isomerizations. In terms of net effects on ozone formation, the updated n-alkane mechanisms are essentially the same as previous, because the increased nitrate formation from the radicals formed after isomerization balances out the reduced yields in the individual reactions. However, the estimated mechanisms for the branched and cyclic alkanes are in some cases significantly different. The estimated mechanism gave generally satisfactory fits to reactivity data for most alkanes except for iso-octane (2,2,4-trimethylpentane), where some adjustments were necessary. There may be a tendency for the mechanism to overpredict the inhibition by the higher alkanes in the mini-surrogate runs, but it is unclear whether this is a consistent bias.

Alkenes. The automated mechanism generation procedure now allows for more realistic and complex mechanisms to be generated for the higher alkenes, though it is still assumed that all the reaction with OH radicals is by addition to the double bond. However, the evaluations of the mechanisms for the simpler

---

[2] See http://cert.ucr.edu/~carter/bycarter.htm for a complete listing of the project reports by Carter et al. which can be downloaded from the internet. Most of these reports describe environmental chamber studies for various VOCs whose data were used to evaluate this mechanism.

[3] See http://cert.ucr.edu/~carter/r98tab.htm for a summary of the updated mechanism with respect to all classes of compounds it currently represents.

alkenes (whose mechanisms are not significantly affected by the use of this automated procedure) indicate problems and inconsistencies which have not been satisfactorily been resolved. In particular, in order to fit chamber data for 1-butene and 1-hexene, it is necessary to assume lower OH radical yields in the reactions of O_3 with these compounds than is consistent with recommendations of Atkinson (1997) based on results of various other laboratory studies. In fact, the most recent previous version of the mechanism (Carter et al, 1997a) also performed poorly in simulating experiments with these compounds, though this had not been recognized until this re-evaluation. It is also necessary to assume essentially no radicals are formed in the reactions of $O(^3P)$ with C_{3+} monoalkenes, contrary to the assumptions of previous models. On the other hand, the isoprene data are still best fit if the relative high radical yields in the O_3 and $O(^3P)$ reactions of this compound are assumed, and the terpene data are also reasonably well fit using the recommended (generally relatively high) OH yields in their O_3 reactions. Although the mechanisms for the various alkenes were adjusted if needed to fit the available chamber data, their mechanisms must be considered to be somewhat uncertain until these inconsistencies are resolved.

Aromatics. Despite considerable research in recent years and some progress, the details of the aromatic ring opening process is remains sufficiently poorly understood that use of parameterized and adjusted mechanisms is still necessary. Some changes were made to the details of the parameterization to permit use in the model of the actual observed dicarbonyl products, but the general parameterization approach was the same. The parameters were optimized to fit the chamber data for the various compounds for which data are available, and the fits to the chamber data were comparable (though usually slightly better) to those for the SAPRC-97 mechanism (Carter et al, 1997a). The naphthalene, 2,3-dimethyl naphthalene and tetralin mechanisms were also optimized; the SAPRC-97 mechanism was not optimized for those compounds. It is interesting to note that to satisfactorily fit the data for those bycyclic aromatics it is necessary to assume significant formation of intermediates which are represented in the model as precursors to PAN analogues. This is not the case for the alkylbenzenes.

The approach for representing the higher aromatics in the model was also modified somewhat. Ethylbenzene, which was found to have a lower mechanistic reactivity than toluene, was used rather than toluene to represent the higher monoalkylbenzenes. The generic di- and tri- or polyalkylbenzenes were represented by mixtures of xylene or trialkylbenzene isomers, rather than just m-xylene or 1,3,5-trimethylbenzene, as was the case previously. This was done to eliminate a source of bias in the mechanism by representing each of these classes by what is essentially the most reactive member of the class. In particular, p-xylene and 1,2,4-trimethylbenzene are much less reactive than the other isomers, and may also be present in these unspeciated generic mixtures. The representation of styrene and its major products is discussed in more detail in a separate section of this report.

Ketones. The previous mechanism used MEK to represent essentially all ketones other than acetone, and chamber data with MIBK has shown this to be unsatisfactory. The current mechanism represents

individual ketones based on their estimated individual reactions, generated as discussed above for alkanes and other oxygenates. Satisfactory simulations of the MIBK data were obtained with the estimated mechanism without adjustments. However, this change does not significantly affect simulations of base case scenarios.

Representation of Reactive Products. As with the previous versions of the mechanisms (e.g., Carter, 1990), most of the higher molecular weight organic products formed in the oxidations of the emitted VOCs are represented by a relatively small set of simpler species on a molecule-for-molecule basis (e.g., using the "lumped molecule" approach). The set of compounds used to represent aromatic ring fragmentation was increased to include biacetyl and to (hopefully) more realistically represent unsaturated dicarbonyls and similar compounds. In addition, a new saturated organic product species (designated "PROD2") was used to represent the reactions of the more rapidly reacting non-aldehyde oxygenated products formed from higher molecular weight alkanes and other compounds, such as glycol ethers, etc. In the SAPRC-90 and the previous versions of this mechanism, all the C_{4+} non-aromatic, non-aldehyde products were represented by methyl ethyl ketone (2-pentanone or MEK), including products with much higher OH radical rate constants. In this mechanism, such products with OH radical rate constants less than 5×10^{-12} cm^3 $molec^{-1}$ s^{-1} were still represented by MEK, but those with higher OH radical rate constants were represented by this new PROD2 model species, whose reactions are derived based on those estimated for 5-hydroxy-2-pentanone, a representative alkane oxidation product. Although this does not significantly affect model simulations of chamber experiments, it results in somewhat higher predicted incremental reactivities for higher molecular weight alkanes and other species forming such products.

This mechanism was used to calculate a preliminary updated version of the Maximum Incremental Reactivity (MIR) scale for use in consumer product regulations being considered by the California Air Resources Board[4]. This mechanism and its associated updated MIR scale are considered preliminary because the documentation is not yet complete, and because it is undergoing a comprehensive peer review under funding by the California Air Resources Board. However, it is used for this work because it is believed to be significant improvement over previous versions, and because incremental reactivities estimates have been derived for a wide range of VOCs, which can be directly compared with those developed for styrene in this work[5].

A complete listing of the reactions, rate constants, and other parameters relevant to the mechanism as used in the calculations presented in this report are given in Appendix A. The mechanisms used for styrene and its major oxidation products are discussed separately later in this report.

---

[4] This scale and related information is available at http://cert.ucr.edu/~carter/r98tab.htm.

[5] The MIR and other reactivity measures developed for styrene in this work supersede those given at http://cert.ucr.edu/~carter/r98tab.htm, but can be directly compared with the reactivities given there for the other VOCs.

Environmental Chamber Modeling Methods

The ability of the chemical mechanisms to appropriately simulate the atmospheric impacts of styrene was evaluated by conducting model simulations of the environmental chamber experiments from this study. This requires including in the model appropriate representations of chamber-dependent effects such as wall reactions and characteristics of the light source. The methods used are based on those discussed in detail by Carter and Lurmann (1990, 1991), updated as discussed by Carter et al. (1995c,d 1997a). Tables A-1 in Appendix A includes the reactions used to represent the chamber effects in the simulations of the experiments for this program, and Table A-4 show the values of the chamber-dependent parameters which were used, and indicate how they were derived.

The photolysis rates were derived from results of NO_2 actinometry experiments and measurements of the relative spectra of the light source. In the case of the xenon arc light source used in these experiments, where the light source spectrum was measured several times during each experiment, the relative spectrum used was based on averaging all such spectra measured during this time period. Data concerning the trend in light intensity during the course of the experiments, and how it was represented in the chamber model simulations, are discussed separately in the Results section (see also Table A-4).

The thermal rate constants were calculated using the temperatures measured during the experiments, with the small variations in temperature with time during the experiment being taken into account. The computer programs and modeling methods employed are discussed in more detail elsewhere (Carter et al, 1995c).

Atmospheric Reactivity Modeling Methods

To estimate the effects of styrene emissions on ozone formation under conditions more representative of polluted urban atmospheres, incremental reactivities were calculated for styrene, the mixture representing the VOCs emitted from all sources (the base ROG), and some other representative VOCs. The modeling approach and scenarios is the same as used in our previous studies of VOC reactivity, and is described in detail elsewhere (Carter, 1994a,b, Carter et al, 1993b). Therefore, it is only briefly summarized here.

Scenarios Used for Reactivity Assessment

The scenarios employed were those used by Carter (1994a,b) to develop various reactivity scales to quantify impacts of VOCs on ozone formation in various environments. These were based on a series of single-day EKMA box model scenarios (EPA, 1984) derived by the EPA for assessing how various ROG and NO_x control strategies would affect ozone nonattainment in various areas of the country (Baugues, 1990). The characteristics of these scenarios and the methods used to derive their input data are described in more detail elsewhere (Baugues, 1990; Carter, 1994b). Briefly, 39 urban areas in the United States were selected based on geographical representativeness of ozone nonattainment areas and data availability, and a representative

high ozone episode was selected for each. The initial non-methane organic carbon (NMOC) and NO_x concentrations, the aloft O_3 concentrations, and the mixing height inputs were based on measurement data for the various areas, the hourly emissions in the scenarios were obtained from the National Acid Precipitation Assessment Program emissions inventory (Baugues, 1990), and biogenic emissions were also included. Table 1 gives a summary of the urban areas represented and other selected characteristics of the scenarios.

Several changes to the scenario inputs were made based on discussions with the California ARB staff and others (Carter, 1994b). Two percent of the initial NO_x and 0.1% of the emitted NO_x in all the scenarios was assumed to be in the form of HONO. This change was made because HONO has been detected in ambient air at nighttime, and its rapid photolysis can provide a non-negligible source of radicals. The photolysis rates were calculated using solar light intensities and spectra calculated by Jeffries (1991) for 640 meters, the approximate mid-point of the mixed layer during daylight hours. The composition of the VOCs entrained from aloft was based on the analysis of Jeffries et al. (1989). The composition of the initial and emitted reactive organics (referred to as the "base ROG" mixture) was derived based on analyses of air quality data (Carter, 1994a, Jeffries et al, 1989). Complete listings of the input data for the scenarios are given elsewhere (Carter, 1994b).These are referred to as "base case" scenarios, to distinguish them from those where NO_x inputs are adjusted as discussed below.

In addition to these 39 base case scenarios, adjusted NO_x scenarios were developed to represent different conditions of NO_x availability. NO_x levels were found to be the most important factor affecting differences in relative ozone impacts among most VOCs (Carter and Atkinson, 1989; Carter, 1994a), and for such compounds the ranges of relative reactivities under various conditions can be reasonably well represented by ranges in relative reactivities in three "averaged conditions" scenarios representing three different NO_x conditions. These scenarios were derived by averaging the inputs to the 39 EPA scenarios, except for the NO_x emissions. Calculations were also carried out where the NO_x levels were varied, with three specific NO_x levels being of particular interest In the "Maximum Incremental Reactivity" (MIR) scenario, the NO_x inputs were adjusted such that the final O_3 level is most sensitive to changes in VOC emissions; in the "Maximum Ozone Incremental Reactivity" (MOIR) scenario the NO_x inputs were adjusted to yield the highest maximum O_3 concentration; and in the "Equal Benefit Incremental Reactivity" (EBIR) scenario the NO_x inputs were adjusted such that relative changes in VOC and NO_x emissions had equal effect on ozone formation. As discussed by Carter (1994a), these represent respectively the high, medium and low ranges of NO_x conditions which are of relevance when assessing VOC control strategies for reducing ozone.

The use of averaged conditions, adjusted NO_x scenarios in this work is slightly different than the approach used by Carter (1994a), where the MIR, MOIR, and EBIR scales were derived by adjusting NO_x conditions separately for each of the 39 base case scenarios, and then averaging the reactivities derived from them. However, Carter (1994a) showed that both approaches yield essentially the same results.

Table 1. Summary of the conditions of the scenarios used for atmospheric reactivity assessment.

	Scenario	Max O_3 (ppb)	Max 8-Hr Avg O_3 (ppb)	ROG / NO_x	NO_x / NO_x^{MO}	Height (kM)	Init., Emit ROG ($m.mol\ m^{-2}$)	O_3^{aloft} (ppb)
Adj'd	Max React	189	117	3.1	1.5	1.8	15	70
NOx	Max O3	242	164	4.5	1.0	1.8	15	70
	Equal Benefit	230	174	6.4	0.7	1.8	15	70
Base	Atlanta,GA	176	132	7.3	0.6	2.1	12	63
Case	Austin,TX	171	143	9.3	0.4	2.1	11	85
	Baltimore,MD	333	226	5.2	0.9	1.2	17	84
	Baton Rouge,LA	239	175	6.8	0.8	1.0	11	62
	Birmingham,AL	237	201	6.9	0.5	1.8	13	81
	Boston,MA	190	165	6.5	0.5	2.6	14	105
	Charlotte,NC	138	123	7.8	0.3	3.0	7	92
	Chicago,IL	266	221	11.6	0.5	1.4	25	40
	Cincinnati,OH	201	155	6.4	0.6	2.8	17	70
	Cleveland,OH	251	185	6.6	0.8	1.7	16	89
	Dallas,TX	221	153	4.7	1.0	2.3	18	75
	Denver,CO	208	146	6.3	1.0	3.4	29	57
	Detroit,MI	239	180	6.8	0.6	1.8	17	68
	El Paso,TX	186	140	6.6	0.9	2.0	12	65
	Hartford,CT	166	142	8.4	0.4	2.3	11	78
	Houston,TX	308	221	6.1	0.8	1.7	25	65
	Indianapolis,IN	210	151	6.6	0.7	1.7	12	52
	Jacksonville,FL	151	114	7.6	0.5	1.5	8	40
	Kansas City,MO	155	126	7.1	0.5	2.2	9	65
	Lake Charles,LA	272	203	7.4	0.5	0.5	7	40
	Los Angeles,CA	567	417	7.6	0.9	0.5	23	100
	Louisville,KY	210	157	5.5	0.7	2.5	14	75
	Memphis,TN	219	178	6.8	0.5	1.8	15	58
	Miami,FL	128	109	9.6	0.3	2.7	9	57
	Nashville,TN	162	135	8.0	0.4	1.6	7	50
	New York,NY	344	289	8.1	0.6	1.5	39	103
	Philadelphia,PA	242	173	6.2	0.8	1.8	19	53
	Phoenix,AZ	280	200	7.6	0.9	3.3	40	60
	Portland,OR	163	127	6.5	0.6	1.6	6	66
	Richmond,VA	234	175	6.2	0.7	1.9	16	64
	Sacramento,CA	204	146	6.6	0.7	1.1	7	60
	St Louis,MO	325	221	6.1	0.9	1.6	26	82
	Salt Lake City,UT	184	151	8.5	0.5	2.2	11	85
	San Antonio,TX	138	103	3.9	0.9	2.3	6	60
	San Diego,CA	193	153	7.1	0.8	0.9	8	90
	San Francisco,CA	255	138	4.8	1.7	0.7	25	70
	Tampa,FL	232	160	4.4	0.9	1.0	8	68
	Tulsa,OK	224	163	5.3	0.7	1.8	15	70
	Washington,DC	276	211	5.3	0.7	1.4	13	99

Quantification of Atmospheric Reactivity

The reactivity of a VOC in an airshed scenario is measured by the change in ozone caused by adding the VOC to the emissions, divided by the amount of VOC added, calculated for sufficiently small amounts of added VOC that the incremental reactivity is independent of the amount added[6]. The specific calculation procedure is discussed in detail elsewhere (Carter, 1994a,b). The incremental reactivities depend on how the amounts of VOC added and amounts of ozone formed are quantified. In this work, the amount of added VOC is quantified on a mass basis, since this is how VOCs are regulated. Two different ozone quantification methods were used, as follows:

- "Ozone Yield" incremental reactivities measure the effect of the VOC on the total amount of ozone formed in the scenario at the time of its maximum concentration. This is quantified as grams O_3 formed per gram VOC added. Most previous recent studies of incremental reactivity (Dodge, 1984; Carter and Atkinson, 1987, 1989, Chang and Rudy, 1990; Jeffries and Crouse, 1991) have been based on this quantification method.

- "Max 8 Hour Average" incremental measure the effect of the VOC on the average ozone concentration during the 8-hour period when the average ozone concentration was the greatest, which in these one-day scenarios was the last 8 hours of the simulation. This provides a measure of ozone impact which is more closely related to the new Federal ozone standard, which is given in terms of an 8 hour average.

Since ratios of reactivities are generally more relevant to control strategy applications and are usually less sensitive to scenario conditions, the calculated atmospheric reactivity results in this work are given in terms of relative reactivities. This is defined as the incremental reactivity of the VOC divided by the incremental reactivity of the base ROG mixture, i.e., the mixture used to represent VOC emissions from all sources in the scenarios. These relative reactivities can also be thought of as the relative effect on O_3 of controlling emissions of the particular VOC by itself, compared to controlling emissions from all VOC sources equally. Thus they are more meaningful in terms of control strategy assessment than absolute reactivities, which can vary greatly depending on the episode and local meteorology.

In previous reports, we have reported reactivities in terms of integrated O_3 over the previous Federal standard of 0.12 ppm, referred to as "IntO_3>0.12". This is the sum of the hourly ozone concentrations for the hours when ozone 0.12 ppm in the base case scenarios (Carter 1994a), and provides a measure of the effect of the VOC on exposure to unacceptable levels of ozone. This is replaced by the Max 8 Hour Average reactivities because (1) it is more representative of the new Federal ozone standard and (2) the IntO_3>0.12

[6] Note that the definition of incremental reactivity in this context differs from the that used for the environmental chamber experiments in that the experimental incremental reactivities are calculated for finite amounts of test compound added (see Equation I, above).

relative reactivities were found to be between the Ozone Yield and the Max 8 Hour Average relative for those VOCs where they were different. Therefore, presenting both ozone yield and maximum 8-hour average relative reactivities should be sufficient to provide information on how relative reactivities vary with ozone quantification method.

Chemical Models and Mechanisms Used

The chemical mechanisms used in the ambient simulations were the same as employed in the chamber simulations, except that the reactions representing chamber effects were removed, and the reactions for the full variety of VOCs emitted into the scenarios (Carter, 1994a) were included. Most of the emitted VOCs are not represented in the model explicitly, but are represented using lumped model species whose rate constants and product yield parameters are derived based on the mixture of compounds they represent. The rate constants and mechanistic parameters for the emitted species in the scenarios were the same as those used to calculate the MIR and other measures of reactivity of the species, as given by Carter (1998). The chemical mechanism used is given in Appendix A.

Note that when reviewing the available data on styrene's reaction products (see following section), the rate constant for the decomposition of PBzN was modified slightly. To permit the styrene reactivities calculated in this work to be comparable to the full set of reactivity data previously calculated with this mechanism (Carter, 1998), the PBzN rate constant was not changed when conducting the reactivity simulations. The effect of this change on calculated styrene reactivities was examined, and found to be negligible.

REACTIONS OF STYRENE AND REPRESENTATION IN THE MODEL

The major atmospheric reactions for styrene are expected to be with OH radicals, O_3 and NO_3 radicals, with the reaction with OH radicals estimated to be the most important loss process in the daytime (Marchello and Sterling, 1991). In addition, the reaction of styrene with $O(^3P)$ atoms may be non-negligible under the conditions of some of the environmental chamber experiments, and thus are also included in the model. Available information concerning these three loss processes, and how they are represented in the model simulations in this work, are summarized below. Following that, the reactions and model representation of the important styrene photooxidation products benzaldehyde and PBzN are discussed.

OH Radical Reaction

Atkinson (1989) reviewed the kinetic data concerning the OH radical reaction, and apparently no published studies of the kinetics of this reaction have been carried out since that time. Based on the relative rate constant determinations of Bignozzi et al (1981) and Atkinson and Aschmann (1988), which are in good agreement, Atkinson (1989) recommends

$$k_{OH + Styrene} = 5.8 \times 10^{-11} \text{ cm}^3 \text{ molec}^{-1} \text{ s}^{-1}$$

at 298K, with an estimated uncertainty of 25%. The temperature dependence of this rate constant has not been determined, but it is probably not large and is therefore ignored in the model simulations.

The reactions of OH radicals with styrene apparently occurs primarily at the double bond, since the major observed products are benzaldehyde and formaldehyde. Tuazon et al. (1993) report yields of 63±6% and 72±7%, for benzaldehyde and formaldehyde, respectively, and others report ~100% yields for benzaldehyde (Atkinson, 1994, and references therein). Tuazon et al. (1993) also report infrared bands suggesting formation of an organic nitrate ($RONO_2$) product, whose yield could not be quantified. This suggests an alkene-like mechanism, forming these products and HO_2 after one NO to NO_2 conversion (e.g., Atkinson, 1994; Carter, 1990), with some alkyl nitrate formation occurring in the peroxy + NO reaction:

$$OH + C_6H_5CH{=}CH_2 \rightarrow C_6H_5CH(\cdot)CHOH$$
$$C_6H_5CH(\cdot)CH_2OH + O_2 \rightarrow C_6H_5CH(OO\cdot)CH_2OH$$
$$C_6H_5CH(OO\cdot)CH_2OH + NO \rightarrow C_6H_5CH(ONO_2)CH_2OH \quad (1)$$
$$C_6H_5CH(OO\cdot)CH_2OH + NO \rightarrow C_6H_5CH(O\cdot)CH_2OH + NO_2 \quad (2)$$
$$C_6H_5CH(O\cdot)CH_2OH \rightarrow C_6H_5CHO + \cdot CH_2OH$$
$$\cdot CH_2OH + O_2 \rightarrow HCHO + HO_2$$

The current estimated mechanism incorporated in our atmospheric reactivity model assumes that 90% of the reaction yields benzaldehyde + formaldehyde after one NO to NO_2 conversion, and an estimated organic

nitrate yield ($k_1/[k_1+k_2]$) of 10%. However the data of Tuazon et al (1993) suggest that the organic nitrate yield may be as high as ~25-35%.

The nitrate yield estimate is highly uncertain, and assumptions concerning it can have significant effects on predictions of ozone reactivity (Carter and Atkinson, 1989; Carter, 1994a, 1995). The effects of making alternative assumptions concerning the nitrate yield were examined in the model simulations of the mini-surrogate reactivity experiments, and generally best fits are obtained if our initially estimated nitrate yield of 10% is retained. This therefore was used in all the model simulations presented in this report.

In terms of model species in the current mechanism, the overall effects of the above reactions can be represented as

$$OH + Styrene \rightarrow (1\text{-}y_N) \{RO2\text{-}R. + HCHO + BALD) + y_N\ RO2\text{-}N.$$

where y_N is the assumed overall nitrate yield ($k_1/[k_2+k_2]$), which is 10% in the estimated mechanism, HCHO and BALD are the model species for formaldehyde and benzaldehyde, respectively, and RO2-R. and RO2-N. are chemical "operators" representing the effects of forming peroxy radicals with react with NO to form NO_2 and HO_2 (for RO2-R.) or organic nitrates (for RO2-N.)[7]. This is used in the model simulations in this work, with the value of y_N being varied in the chamber simulations, but the "best fit" value of 0.1 being used in the mechanism for the atmospheric reactivity estimates, as shown in Appendix A. The reactions of the product species and chemical operators in the current version of the mechanism are also given in Appendix A.

Ozone Reaction

The most recent measurement of the rate constant for the reaction of ozone with styrene is reported by Tuazon et al (1993), who give

$$k_{O3 + Styrene} = 1.71 \times 10^{-17}\ cm^3\ molec^{-1}\ s^{-1}$$

at 296±2 K. This is reasonably consistent with the previous determinations of Atkinson et al (1982) and Bufalini and Altshuller (1965) and is used in the model simulations. The temperature dependence of this reaction is unknown and is neglected in the current mechanism.

The reaction with O_3 is expected to occur in a mechanism analogous to the reactions of$_3$O with simpler alkenes, as follows:

[7] Most of the discussion given by Carter (1990) for the chemical operators in the SAPRC-90 mechanism are still applicable for this version of the mechanism.

$$O_3 + C_6H_5CH{=}CH_2 \rightarrow \text{(ozonide)}$$

$$\text{(ozonide)} \rightarrow C_6H_5CHO + \cdot CH_2OO\cdot^* \quad (3)$$

$$\text{(ozonide)} \rightarrow C_6H_5CH(\cdot)OO\cdot^* + HCHO \quad (4)$$

$$\cdot CH_2OO\cdot^* \rightarrow \rightarrow \alpha\ HC(O)OH + \text{other products}$$

$$C_6H_5CH(\cdot)OO\cdot^* \rightarrow \rightarrow \text{unknown products, probably not } C_6H_5CHO$$

Here (ozonide) refers to the primary ozonide formed when O_3 adds across the double bond, and $\cdot CH_2OO\cdot^*$ and $C_6H_5CH(\cdot)OO\cdot^*$ refer to the excited Crigiee biradicals which are expected to be formed when the primary ozonide decomposes. Tuazon et al (1993) observed formation of formaldehyde (37±5% yield), benzaldehyde (41±5%) and formic acid (1-2% yield), and Grosjean and Grosjean (1996) reported formaldehyde and benzaldehyde yields of 34±5% and 64±7%, respectively. The data from these studies are reasonably consistent with this mechanism, but may not account for all the initial reaction pathways. Based on the data of Grosjean and Grosjean (1996), we assume that the primary ozonide fragments to benzaldehyde and $\cdot CH_2OO\cdot$ biradicals approximately 60% of the time, with the remaining 40% fragmenting to formaldehyde and $C_6H_5CH(\cdot)OO\cdot^*$, i.e., that $k_3/(k_3+k_4)=0.6$.

The available product data give no useful information concerning most of the reactions of the excited $\cdot CH_2OO\cdot^*$ and $C_6H_5CH(\cdot)OO\cdot^*$ biradicals, except that they apparently do not form either formaldehyde or benzaldehyde (or the yields of these products would be higher). Based on data for the ozone + ethene system, Atkinson (1997) recommends the following overall reaction pathways for $\cdot CH_2OO\cdot^*$,

$$\cdot CH_2OO\cdot^* \rightarrow 0.12\ \{HCO\cdot + OH\} + 0.13\ \{CO_2 + H_2\} + 0.38\ \{CO + H_2O\} + 0.37\ \cdot CH_2OO\cdot$$

where $\cdot CH_2OO\cdot$ refers to the stabilized biradical, which presumably reacts to form formic acid or other non-radical species. However, the $\cdot CH_2OO\cdot^*$ may have less energy when formed in the O_3 + styrene system than it does when formed from O_3 + ethene, and thus its reactions might result in relatively more stabilization and relatively less fragmentation forming radicals and other species.

Even less is known concerning the reactions of the excited $C_6H_5CH(\cdot)OO\cdot^*$. biradicals, which as indicated above are assumed to be formed ~40% of the time. The two most likely alternatives are stabilization to some unknown but presumably not highly reactive product (something other than benzaldehyde), or hydrogen shift followed by decomposition to OH and $C_6H_5CO\cdot$ radicals. (The subsequent reactions of the $C_6H_5CO\cdot$ radicals are discussed below.) In the previous versions of the SAPRc mechanism (Carter et al, 1997a) it was somewhat arbitrarily assumed that these two pathways were equally likely, but in the current mechanism we assume that only stabilization occurs.

As discussed below, the chamber data are best fit by models which assume that the reactions of O_3 with styrene result in no radical formation, which would be the case if both the $\cdot CH_2OO\cdot^*$ and the $C_6H_5CH(\cdot)OO\cdot^*$ biradicals were primarily stabilized. Thus in the standard "best fit" mechanism the overall process for the styrene + O_3 reaction is represented as

$$O3 + Styrene \rightarrow 0.6\ \{BALD + HCHO2\} + 0.4\ \{HCHO + RCHO2\}$$

where HCHO2 and RCHO2 refer to stabilized Crigiee biradicals which are assumed to form relatively low reactivity products whose subsequent reactions are not represented in the model.

To show the effects of alternative assumptions concerning the styrene + O_3 reactions on the model simulations of the chamber experiments, calculations carried out using an alternative, radical-forming O_3 + styrene mechanism are also shown. In this mechanism, the $\cdot CH_2OO\cdot$* is assumed to react with the same mechanism as believed to occur when it is formed in the O_3 + ethene system, but the $C_6H_5CH(\cdot)OO\cdot$*. biradical is still assumed to be primarily stabilized. In terms of model species, this mechanism is represented as

$$O3 + Styrene \rightarrow 0.6\ BALD + 0.072\ \{HO_2 + OH\} + 0.078\ CO_2 + 0.3\ CO + 0.4\ \{HCHO + RCHO2STAB\}$$

where the formation of H_2 and H_2O is ignored and the rapid reaction of HCO with O_2 to form HO_2 + CO is incorporated in the overall process. Higher overall radical yields could results if the $C_6H_5CH(\cdot)OO\cdot$* biradicals underwent non-negligible decompositions, and this possibility is discussed below in conjunction with the model simulations of the chamber experiments.

NO_3 Radical Reactions

The only reported data concerning the rate constant for the reaction of NO_3 radicals with styrene is from Atkinson and Aschmann (1988), who give

$$k_{NO3 + Styrene} = 1.5 \times 10^{-13}\ cm^3\ molec^{-1}\ s^{-1}$$

at 296±2 K. This is used in the model. The temperature dependence of this reaction is not known and is assumed not to be significant in the model calculations.

In the only reported product study of this reaction, Tuazon et al (1993) reported relatively low (~10%) yields of benzaldehyde and formaldehyde, and various unidentified stable and unstable products containing nitrate (ONO_2) and peroxynitrate (O_2NO_2) IR bands. As discussed by Atkinson (1991), the conditions of these experiments are not very representative of ambient conditions, and different products might be formed in the atmosphere or the chamber experiments. The reaction is expected to proceed by NO_3 adding to the double bond, probably primarily at the terminal position, giving rise to nitrate-containing peroxy radicals.

$$NO_3 + Styrene \xrightarrow{M} C_6H_5CH(\cdot)CH_2ONO_2$$
$$C_6H_5CH(\cdot)CH_2ONO_2 + O_2 \rightarrow C_6H_5CH(OO\cdot)CH_2ONO_2$$

Under the conditions of the product study, the $C_6H_5CH(OO\cdot)CH_2ONO_2$ would primarily react with NO_2 to form a nitrate-peroxynitrate species, which would eventually decompose, or react with other $C_6H_5CH(OO\cdot)CH_2ONO_2$ radicals to form the corresponding alkoxy radical or other products:

$$C_6H_5CH(OO\cdot)CH_2ONO_2 + NO_2 \rightleftharpoons C_6H_5CH(OONO_2)CH_2ONO_2$$

$$C_6H_5CH(OO\cdot)CH_2ONO_2 + C_6H_5CH(OO\cdot)CH_2ONO_2 \rightarrow O_2 + 2\ C_6H_5CH(O\cdot)CH_2ONO_2 \quad (5)$$

$$C_6H_5CH(OO\cdot)CH_2ONO_2 + C_6H_5CH(OO\cdot)CH_2ONO_2 \rightarrow O_2 + C_6H_5C(O)CH_2ONO_2 + C_6H_5CH(OH)CH_2ONO_2 \quad (6)$$

The alcohol and ketone formed in Reaction (6) are likely the stable products observed by Tuazon et al (1993), and the peroxynitrate is likely the unstable one. The alkoxy radical formed in Reaction (5) could either react with O_2 giving rise to HO_2 radicals and the same ketone-nitrate as formed in Reaction (5), or decompose, ultimately yielding formaldehyde, benzaldehyde, and NO_2.

$$C_6H_5CH(O\cdot)CH_2ONO_2 + O_2 \rightarrow HO_2 + C_6H_5C(O)CH_2ONO_2 \quad (7)$$

$$C_6H_5CH(O\cdot)CH_2ONO_2 \rightarrow HO_2 + C_6H_5CHO + \cdot CH_2ONO_2 \quad (8)$$

$$\cdot CH_2ONO_2 \rightarrow HCHO + NO_2$$

If we assume that Reactions (5) and (6) are the major ultimate loss process for the peroxy radicals under the conditions of the product study, and that these two reactions are about equally probable (as is the case for analogous reactions of simpler radicals (e.g., Atkinson et al, 1997), then the observed formation of 10-12% formaldehyde and benzaldehyde in the product study (Tuazon et al, 1993) suggests that decomposition (Reaction 8) may be occurring ~25% of the time. This is highly uncertain, however, especially in view of the fact that an unknown amount of the products may be tied up as peroxynitrate during the course of the experiments. The actual amount of decomposition could be higher, but probably is not lower.

Under conditions of photolysis in the atmosphere which are favorable for ozone formation, or in the chamber experiments in the presence of NO_x, the major sink for the peroxy radical would be reaction with NO, rather than the reactions above.

$$C_6H_5CH(OO\cdot)CH_2ONO_2 + NO \rightarrow C_6H_5CH(ONO_2)CH_2ONO_2 \quad (9)$$

$$C_6H_5CH(OO\cdot)CH_2ONO_2 + NO \rightarrow C_6H_5CH(O\cdot)CH_2ONO_2 \quad (10)$$

The relative importances of nitrate formation (Reaction 9) is unknown, but we estimate that it is approximately the same as assumed in the analogous reaction in the OH + styrene system, or ~10%. The alkoxy radical formed in Reaction (10) could then react via Reactions (7) or (8), as shown above.

Based on these considerations, under atmospheric photolysis conditions where reactions of the peroxy radical with NO should dominate, the overall process is represented as follows in terms of model species and operators in the current mechanism:

$$NO_3 + \text{Styrene} \rightarrow 0.1\ \{RO2\text{-}N.\ +\ XN\} + 0.9\ \alpha\ \{NO_2 + BALD + HCHO + R2O2.\} + 0.9\ (1\text{-}\alpha)\ \{RO2\text{-}R.\ +\ RNO3\}$$

where $\alpha = k_8/(k_7+k_8)$ represents the fraction of the alkoxy radical which decomposes to form benzaldehyde + formaldehyde + NO_2, R2O2. is the chemical operator representing NO to N_2O conversions caused by reactions of peroxy radicals, RNO3 is the generic organic nitrate model species, and RO2-N. and RO2-R. are as discussed above (see also Appendix A). Based on the results of the product study we estimate that $\alpha \approx 0.25$, though the possibility that it may be larger cannot be ruled out, and thus is examined in the model simulations of the chamber experiments.

Reaction with $O(^3P)$

Although probably not an important loss process in the atmosphere, reaction with ground-state oxygen atoms can be a non-negligible loss process for alkenes in environmental chamber experiments, where NO_2 levels, and therefore $O(^3P)$, tend to be higher than in the atmosphere. For that reason, this reaction is not neglected when modeling the environmental chamber experiments in this study. There is no information concerning the rate constant for the reactions of styrene with $O(^3P)$, but an estimate can be made based on assuming a correlation between $O(^3P)$ and OH radical rate constants. Since the OH radical rate constant for *cis*-2-butene is very similar to that of styrene ($k_{OH + cis\text{-}2\text{-}butene} = 6.4 \times 10^{-11}$ cm^3 $molec^{-1}$ s^{-1} at T=298K [Atkinson, 1997]), we assume that the $O(^3P)$ rate constants are also very similar. Since $k_{O3P + cis\text{-}2\text{-}butene} = 1.76 \times 10^{-11}$ cm^3 $molec^{-1}$ s^{-1} at room 298K (Atkinson, 1997), we therefore estimate that

$$k_{O3P + Styrene} \approx 1.76 \times 10^{-11} \text{ cm}^3 \text{ molec}^{-1} \text{ s}^{-1}$$

at ambient temperatures. The temperature dependence of this rate constant is expected to be small and is ignored.

As with other alkenes, the reaction is assumed to proceed by the $O(^3P)$ adding to the double bond, forming a vibrationally excited oxide, which can either be stabilized, rearrange to a carbonyl compound, or fragment to form radicals. Since fragmentation is expected to decrease with the size of the molecule and better fits to the chamber data for the higher alkenes are obtained if fragmentation is negligible for C_{4+} alkenes (Carter, 1999, report in preparation), we assume that fragmentation also is negligible in the $O(^3P)$ + styrene system. The products formed, which could be the stabilized oxide or methyl phenyl ketone, are represented in the model simulations by the generic higher non-aldehyde oxygenate product species PROD2.

Since the $O(^3P)$ + styrene reaction is estimated not to involve radical formation, it is not predicted to have a significant effect on the results of the simulations of the chamber experiments. On the other hand, if it did form radicals it would have a non-negligible effect on the simulations. However, the results of the simulations of the styrene experiments, discussed below, did not indicate a need to assume significant radical formation in this reaction, so this was not considered further.

Reactions of Benzaldehyde and PBzN

As discussed above, the major known primary oxidation products from the atmospheric reactions of styrene in the atmosphere are formaldehyde and benzaldehyde, though other compounds most presently unidentified, may be formed in lower yields. Formaldehyde is represented in the base mechanism (Carter, 1990; Carter 1999, report in preparation) and its atmospheric reactions are discussed in detail elsewhere (e.g., see Atkinson, 1990, Atkinson et al, 1997, NASA 1997). Although benzaldehyde is also in the base mechanism, its reactions are probably more important in affecting the reactivity of styrene than in affecting the reactivities of any other emitted VOC, and thus it is appropriate that information concerning it be discussed here.

Benzaldehyde is expected to be consumed in the atmosphere primarily by reaction with OH radicals and by direct photolysis, though reaction with NO_3 radicals may be non-negligible under some conditions. The OH rate constant of 1.29×10^{-11} cm^3 $molec^{-1}$ s^{-1}, recommended by Atkinson (1994) is assumed in the model. This is similar to the rate constant for the reaction of OH with other aldehydes, and is believed to occur primarily at the carbonyl group, ultimately giving rise to PBzN and products formed from phenoxy radicals.

$$OH + C_6H_5CHO \rightarrow C_6H_5C(O)\cdot + H_2O$$
$$C_6H_5C(O)\cdot + O_2 \rightarrow C_6H_5C(O)OO\cdot$$
$$C_6H_5C(O)OO\cdot + NO_2 \rightleftharpoons C_6H_5C(O)OONO_2 \text{ (PBzN)}$$
$$C_6H_5C(O)OO\cdot + NO \rightarrow C_6H_5C(O)O\cdot + NO_2$$
$$C_6H_5C(O)O\cdot \rightarrow C_6H_{5\cdot} + CO_2$$
$$C_6H_{5\cdot} + O_2 \rightarrow C_6H_5OO\cdot$$
$$C_6H_5OO\cdot + NO \rightarrow NO_2 + C_6H_5O\cdot$$

As indicated above, PBzN, like other PAN analogues, thermally decomposes back to its starting reactants NO_2 and the corresponding acyl peroxy radical.

The ultimate fate of the phenoxy radical is uncertain (it cannot react with O_2 and has no obvious decomposition route as do most other alkoxy radicals). It has been postulated to react with NO_2 to form nitrophenols, and this is assumed in the current mechanism (Carter, 1990; see Appendix A.) However, though this is not consistent with product data for the NO_3 + phenol reactions, where phenoxy is believed to be an intermediate (Atkinson, 1994, and references therein).

The reactions and rate constants used to represent these reactions in the current mechanism are given in Appendix A. The rate constants for the $C_6H_5C(O)OO\cdot + NO_x$ reactions and for PBzN decomposition are assumed to be the same for the other higher acyl peroxy and PAN analogues, which are based on those recommended by IUPAC (Atkinson et al., 1997) for $C_2H_5C(O)OO\cdot$ and PPN. The rate constant ratio for $C_2H_5C(O)OO\cdot + NO_2$ relative to reaction with NO have been measured by 0.63±0.02 by Kirchner et al (1992),

which is reasonably close to the ratio of 0.55 used in the model for all higher acyl peroxy radicals. The most recent determinations of the kinetics of the PBzN decomposition indicate that the decomposition rate constant is given by 7.9 x 10^{16} exp(-14000/T) sec^{-1}, which corresponds to 3.13 x 10^{4} sec^{-1} at 298K. This is approximately 30% lower than the 298K rate constant used for all higher PAN analogues in the present model. However, this rate constant was not changed in the base mechanism so that the styrene reactivities calculated in this work can be comparable with the complete set of updated VOC reactivity calculations presented previously (Carter, 1998). Test simulations indicate that using the PBzN decomposition rate expression of Kirchner et al (1992) results in essentially no change in the calculated concentration-time profiles for any measured species except for PBzN, which is changed only slightly.

Benzaldehyde may also react to some extent with NO_3 radicals, in a manner analogous to the reaction of NO_3 with other aldehydes,

$$NO_3 + C_6H_5CHO \rightarrow HNO_3 + C_6H_5C(O)\cdot$$

The rate constant was measured at 294 K to be 2.55 x 10^{-15} cm^3 $molec^{-1}$ s^{-1} by Atkinson et al (1984), and in the current mechanism the temperature dependence is estimated by assuming it has the same A factor as the reaction of NO_3 with acetaldehyde (see Appendix A). The reactions of the $C_6H_5C(O)\cdot$ radical are discussed above.

Benzaldehyde may also react by direct photolysis, and the absorption cross sections of Majer et al (1969) indicate that if the quantum yield is sufficiently high this could be significant loss process for benzaldehyde in the atmosphere. However, from modeling benzaldehyde loss rates in environmental chamber experiments in the SAPRC evacuable chamber Carter (1990) estimated that the overall quantum yield for formaldehyde loss by photolysis is no greater than ~5%. Since the spectrum of the light source in that chamber is reasonably similar to the solar spectrum and the spectrum of the light source in the CTC chamber used in this program, this indicates an overall quantum yield of 5% should be used in the both the chamber and ambient model simulations. It was also found that models could accurately predict the effects of benzaldehyde on ozone formation and other data in chamber experiments only if the models assume that benzaldehyde photolysis form only stable, non-radical products (Carter, 1990). The nature of these products are unknown, and they are assumed to be relatively unreactive in the current version of the mechanism.

Some exploratory experiments were carried out for this program to evaluate the assumed ~5% effective quantum yield for benzaldehyde and some of the other assumptions used for its mechanism. The results of these experiments suggest that perhaps a somewhat higher effective quantum yield should be used, but are consistent with the assumption that no radicals are formed in the photolysis reactions.

RESULTS AND DISCUSSION

Summary of Chamber Experiments and Characterization Results

Table 2 gives a chronological listing of all the experiments carried out for this program. In addition to the incremental reactivity experiments, actinometry experiments were conducted to measure light intensity trends, characterization experiments were carried out to measure chamber wall effects, and control runs were carried out to assure comparability of the data with the results of previous experiments.

The characterization experiments carried out for this program consisted of several NO_2 actinometry experiments, two n-butane - NO_x irradiations to measure the chamber radical source (Carter et al, 1982, 1995c,d), and two standard propene - NO_x experiments. The results of these experiments are summarized on Table 2. The results of the actinometry runs were consistent with the light intensity trend observed previously, though as discussed below the results of the base case surrogate - NO_x experiments suggest that they may be overestimating the actual light intensity inside the reaction bag. The results of the standard propene - NO_x experiments were within the range generally observed, though the model tended to somewhat underpredict the peak ozone yield in both cases. The results of the first n-butane - NO_x experiment indicated that the chamber radical source was about twice the default value used for this chamber, while the results of the second one indicated that the radical source was the same as the default value. For modeling the experiments for this program, a slightly higher radical source was used for the first set of experiments than was the default value for this chamber (see Table B-4 in Appendix B).

Results of the Base Case Experiments and Adjustments to the Assumed Light Intensities

As discussed above, most of the experiments for this program consist of conducting dual environmental chamber runs where a standard surrogate - NO_x mixture is irradiated in one of the reactors, with simultaneous irradiation of the same mixture with a test compound (styrene in this case) added. During the course of this and other similar programs in our laboratory a large number of replicate surrogate - NO_x experiments are carried out in this chamber. Because the same reactants, chamber, and run conditions are employed in all the experiments using a given type of surrogate - NO_x mixture, the results of these experiments over time should give an indication of long term trends in conditions affecting the results of these experiments, which would be expected to be determined primarily by trends in light intensity. These trends need be taken into account in the model representation of chamber conditions.

When conducting the initial model simulations of the base case experiments for this project, it was found that the results of the simulations of using the standard chamber model gave a consistent overprediction of NO oxidation rates and levels of O_3 formation for all the base case experiments carried out during this time period. This is shown on Figure 1, which gives plots of experimental and calculated 5-hour d(O_3-NO) carried

Table 2. Chronological listing of chamber experiments for this program, and associated characterization runs.

RunID	Date	Title	Comments
CTC244	9/14/98	n-Butane + NOx	Characterization run to measure the chamber radical source. NO oxidation rates were somewhat higher than predicted by the standard chamber model, but within the normal range. Results similar on both sides.
CTC245	9/15/98	Propene + NOx	Standard control run for comparison with previous propene - NO_x runs and side equivalency test run. Equivalent results obtained on both sides. Model gave good simulation of O_3 formation rate, but peak ozone yield somewhat higher than model predicted.
CTC246	9/16/98	Mini Surrogate + Styrene (A)	Addition of ~0.5 ppm styrene decreased both NO oxidation rate and OH radical levels. Conditions and results summarized on Table 3 and data plotted on Figure 4.
CTC247	9/17/98	NO2 Actinometry	Measured NO_2 photolysis rate was 0.198 min^{-1}, corresponding to an estimated NO_2 photolysis rate of 0.153 min^{-1} inside the reactors. This is consistent with the trend in light intensity indicated by the LiCor spectrl measurements during the runs.
CTC248	9/18/98	Full Surrogate + Styrene (B)	Addition of ~0.5 ppm styrene had relatively small effect on NO oxidation and O_3 formation, but decreased OH radical levels. Conditions and results summarized on Table 3 and data plotted on Figure 5.
CTC249	9/22/98	Low NOx Full Surrogate + Styrene (A)	Addition of ~0.5 ppm styrene decreased both final O_3 yield and OH radical levels. Conditions and results summarized on Table 3 and data plotted on Figure 8.
CTC250	9/23/98	Mini Surrogate + Styrene (B)	Addition of ~0.25 ppm styrene decreased both NO oxidation rate and OH radical levels. Conditions and results summarized on Table 3 and data plotted on Figure 3.

Table 2 (continued)

RunID	Date	Title	Comments
CTC251	9/24/98	Full Surrogate + Styrene (A)	Addition of ~0.7 ppm styrene slightly increased the O_3 formation rate but slightly decreased O_3 yield, and decreased OH radical levels. Conditions and results summarized on Table 3 and data plotted on Figure 6.
CTC252	9/25/98	n-Butane + NOx	Characterization run to measure the chamber radical source. NO oxidation rate was slightly higher on Side A but rates on both sides very close to prediction of standard chamber model.
CTC253	9/29/98	Low NOx Full Surrogate + Styrene (B)	Addition of ~0.3 ppm styrene decreased both final O3 yield and OH radical levels. Conditions and results summarized on Table 3 and data plotted on Figure 7.
CTC264	10/15/98	Propene + NOx	Standard control run for comparison with previous propene - NO_x runs and side equivalency test run. Equivalent results obtained on both sides, but ozone formation rate and final O_3 yields were somewhat greater than model predictions.
CTC265	10/16/98	NO2 Actinometry	Measured NO_2 photolysis rate was 0.211 min^{-1}, corresponding to an estimated NO2 photolysis rate of 0.163 min^{-1} inside the reactors. This is consistent with the trend in light intensity indicated by the LiCor spectrl measurements during the runs.
CTC266	12/3/98	Modified Mini-Surrogate + Benzaldehyde (A)	Approximately 0.15 ppm benzaldehyde added to a modified mini-surrogate mixture, where toluene and 1,3,5-trimethylbenzene was used instead of m-xylene. Benzaldehyde addition caused a decrease in NO oxidation and O_3 formation rates and radical levels. Conditions and results summarized on Table 3 and data plotted on Figure 9.
CTC267	12/4/98	Low NOx Full Surrogate + Benzaldehyde (B)	Addition of ~0.15 ppm benzaldehyde decreased both final O_3 yields and OH radical levels. Conditions and results summarized on Table 3 and data plotted on Figure 10.

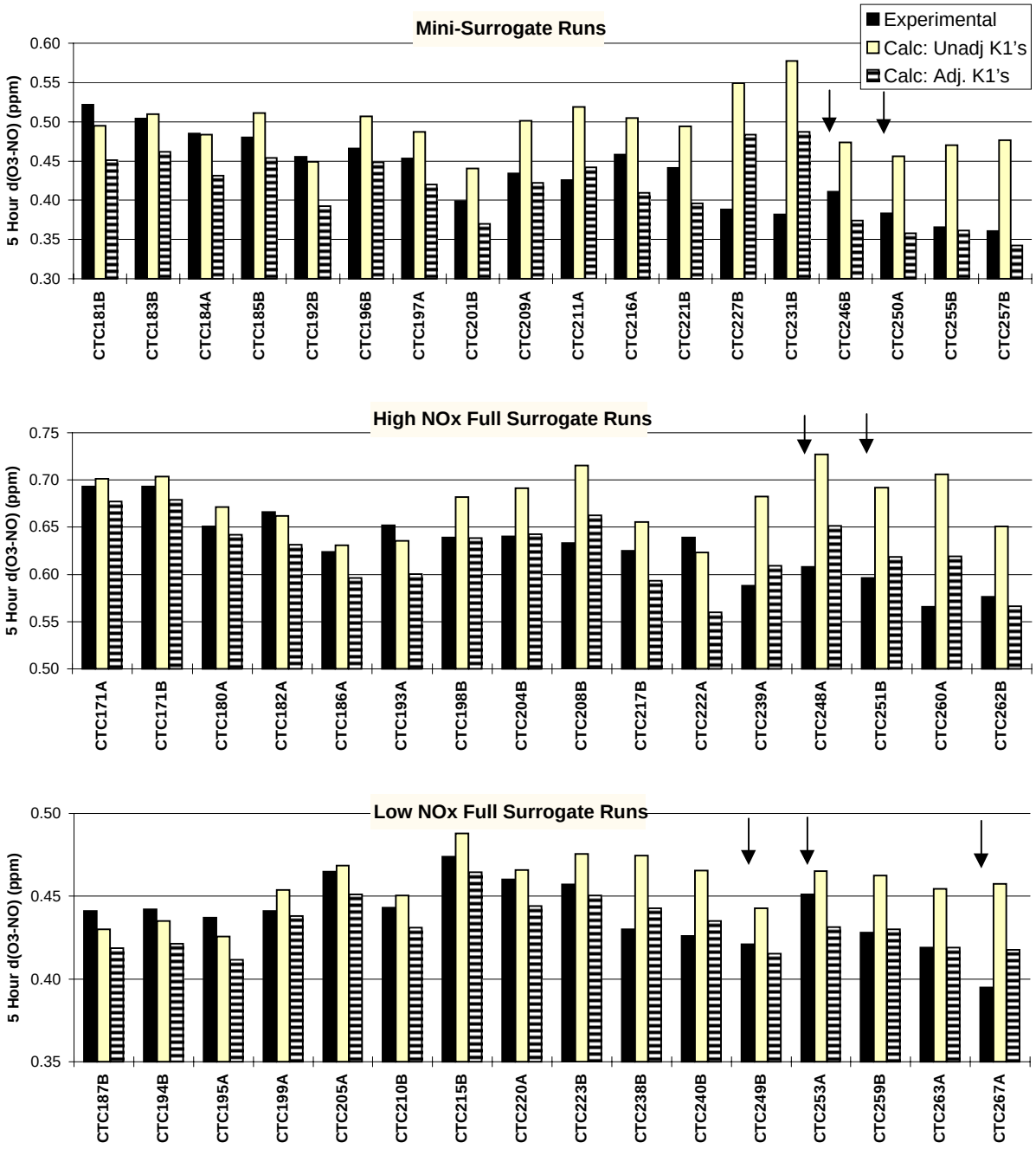

Figure 1. Plots of experimental and calculated 5-hour d(O3-NO) data for all the base case surrogate - NOx experiments carried out in the CTC since November, 1996. The arrows show the experiments carried out for this program. The "Unadjusted k1" calculations use the trend in NO2 photolysis rates derived from the actinometry and spectral radiometer results, while the "Adjusted k1" calculations used an NO2 photolysis rate trend adjusted to be consistent with these data.

out in this chamber since late 1996. Runs carried out for this program are indicated with arrows. The "Unadjusted k_1" calculations (where k_1 refers to the light intensity as measured by the NO_x photolysis rate) show trends in light intensity derived from the NO_2 actinometry experiments and the LiCor spectroradiometer data. It can be seen that although the these "unadjusted k_1" model simulations generally fit the data for the earlier time period, they consistently overpredicted d(O_3-NO) during the time period of the experiments for this program and the subsequent runs. Clearly, there is some trend causing a decline in overall reaction rates in these CTC experiments which is not accounted for with the standard chamber model and the light intensity trends derived from the NO_2 actinometry and LiCor data.

This decline in overall reactivity cannot be accounted for by a decrease in the chamber radical source, since the n-butane - NO_x experiments, which are much more sensitive to this effect than these surrogate runs, indicate no such trend. Tracking the initial measured and injected reactant concentrations also indicate no trend which can account for this decline. Also there is no such unexplained decline of reactivity of surrogate runs in our other, blacklight-irradiated, environmental chamber.

The only reasonable explanation for this result is that the actual light intensity in the reaction bag is declining at a greater rate than has been assumed in our chamber characterization model. This possibility was investigated by carrying out "Adjusted k_1" model calculations where the light intensity trend was adjusted to minimize the bias in the d(O_3-NO) simulations of these experiments[8]. The results of these calculations are shown on Figure 1, where they can be compared with the data and the results of the initial, unadjusted model simulations. It can be seen that although this adjustment does not cause perfect fits to all the data for all the runs, the bias in the overall trends has been eliminated. More significantly, the same adjustment eliminated the bias for all three of the types of surrogate runs, despite the fact that the three types of runs have different sensitivities to changes in light intensity, initial reactant concentrations, and other types of chamber effects.

These results indicate possible problems with the method we have used for deriving light intensity trends when modeling runs in this chamber. The data used to derive these trends are shown on Figure 2, which plots results of various types of actinometry experiments carried out in the CTC since mid-1995 through the time of the preparation of this report (late 1998). These include relative trend results obtained using the quartz tube method and the LiCor data, and absolute light intensity measurements made using the n-butane

[8]This adjustment was carried out as follows: The k_1 was assumed to vary linearly with CTC run number, and the slope and intercept of the k_1 vs run number line was optimized to minimize the least squares error between the observed 5-hour d(O_3-NO) for all the base case experiments surrogate - NO_x experiments shown on Figure 1 and the estimated 5-hour d(O_3-NO) for the light intensity. (The 5-hour data were used instead of the final, 6-hour data because some experiments did not have 6-hour data.) The estimated 5-hour d(O_3-NO) data were derived for each type of surrogate experiment by determining the average initial concentrations for that type of run, calculating the 5-hour d(O_3-NO) as a function of light intensity, and fitting these to a straight line as a function of k_1 so they can be estimated for a given k_1..

Figure 2. Plot of trends in NO_2 photolysis rates in the CTC, as derived by various methods.

+ Cl_2 method (Carter et al, 1997a). (Data using the $NO/NO_2/O_3$ steady state method are not shown because such experiments have not been carried out recently, and give thus give no information about trends.) The relative trend data were placed on an absolute basis by adjusting them to agree with average absolute measurements carried out using the n-butane + Cl_2 method and the $NO/NO_2/O_3$ steady state method in early-mid 1995, as discussed by Carter et al. (1997a). The solid line shows the trend which was fit to the LiCor data, which has been the trend used as the for estimating the photolysis rates for modeling experiments carried out for previous programs because of its precision and consistency with the trend obtained from the quartz tube results. The dashed line shows the trend which gave the best fits to the trend in $d(O_3\text{-}NO)$ data when modeling the surrogate - NO_x experiments, as discussed above. (The shorter dashes are extrapolations to the time period before the experiments used to derive this trend.) It is interesting to note that although the adjusted trend line declines faster than indicated by the LiCor or quartz tube data, it is in good agreement with the trend indicated by the results of the Cl_2 + n-butane actinometry experiments. These Cl_2 + n-butane data have not been used previously when deriving light trend estimates for modeling because of the greater scatter of the data, but they appear to be more consistent with the results of the base case surrogate runs.

The apparent difference in light intensity trends as measured by the LiCor and quartz tube and as derived from the Cl_2 + n-butane experiments and modeling the surrogate runs can be explained if there were a tendency for the light transmission through the FEP Teflon film walls to decline gradually with time. The reaction bags have not been changed during the entire period of data shown on Figures 1 and 2. The NO_2

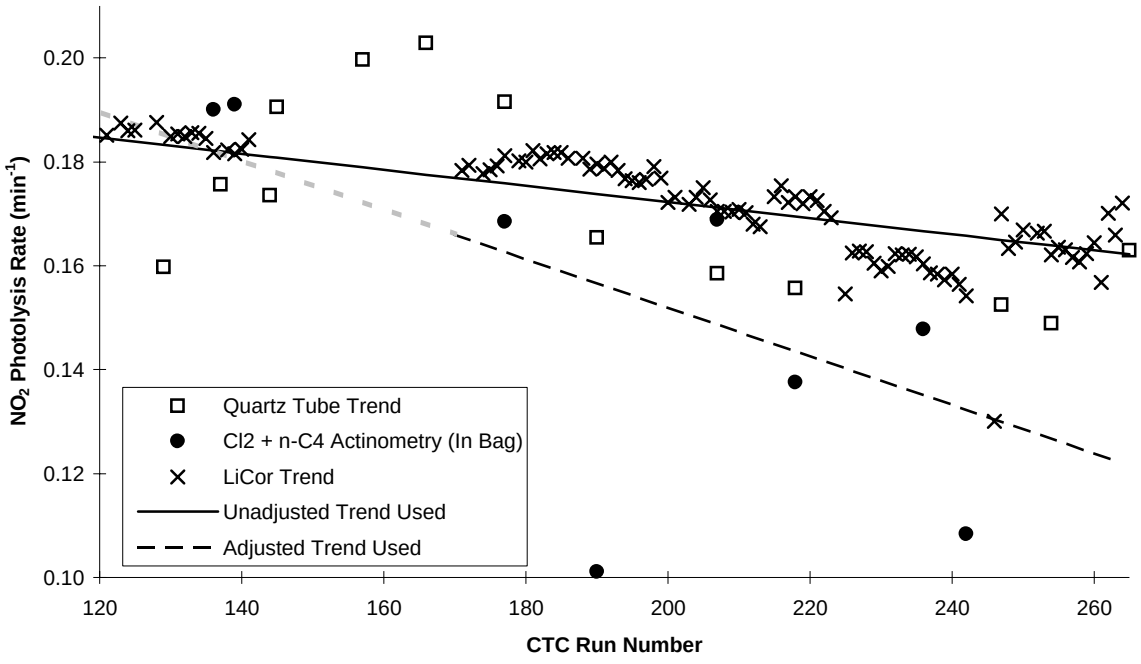

Figure 2. Plots of trends in NO_2 photolysis rates in the CTC, as derived by various methods.

actinometry tube and the LiCor spectroradiometer are both located immediately outside the reaction bag, and thus measure the intensity of the light before it passes through the chamber walls, while the Cl_2 + n-butane and the surrogate - NO_x experiments measure light intensity inside the chamber. Experiments and measurements to evaluate this have not yet been carried out.

Note that the evaluation of the styrene mechanism is based on comparing experimental and model predictions of the effect of styrene on *changes* in d(O_3-NO) and other experimental measures, so any biases in model simulations of the surrogate - NO_x base case experiment would also be present in the simulations of the surrogate - NO_x + styrene test experiment would, to a first-order approximation, cancel out when calculating the change. However having a consistent bias in the simulation of the base case experiment is still not desirable because it may also cause biases in the prediction of the change, which would affect the evaluation of the styrene mechanism. For that reason, it is important that the bias in the base case mechanism be removed when using these data to evaluate the styrene mechanism, even if the cause of the bias has not been fully verified. Therefore, all the model simulations used for evaluating the styrene mechanism discussed in the following sections were carried out using the adjusted light intensity trends as shown by the dashed line in Figure 2.

Results of The Reactivity Experiments

A total of eight reactivity experiments were carried out for this program, six for styrene and two for benzaldehyde, styrene's main photooxidation product. The styrene runs included two each using the mini-surrogate, the high NO_x full surrogate, and the low NO_x full surrogate, and the benzaldehyde runs included one each using a modified mini-surrogate and the low NO_x full surrogate. Table 3 summarizes the conditions and selected results of these experiments, and plots of the major results for each experiment are given in separate figures, discussed below. Results of model simulations are also shown on those figures.

The results of the two mini-surrogate + styrene experiments are shown on Table 3 and Figures 3 and 4. It can be seen that the addition of styrene inhibits rates of NO oxidation and O_3 formation and overall OH radical levels in the conditions of those experiments. The addition of styrene caused measurable formation of benzaldehyde and detectable levels of PBzN in run CTC250; these products were probably also formed in run CTC246 but data are not available. Note that the rate of consumption of styrene was relatively slow in the initial stages of the experiment, but increased around the time when ozone formation began. Although formaldehyde is the other major product expected from the photooxidation of styrene, the addition of benzaldehyde in these experiments actually caused a slight decrease in the formaldehyde levels. This is probably because the suppression of OH levels and O_3 by the added styrene caused a decrease in the rate of formation of formaldehyde from the components of the base case surrogate (primarily ethylene), which was apparently more than enough to counteract the formaldehyde formed from styrene's direct reactions.

Table 3. Summary of conditions and results of the incremental reactivity experiments.

Run	Initial Reactants (ppm)			t=3 d(O3-NO) (ppm)			t=6 d(O3-NO) (ppm)			t=6 IntOH (10-6 min)		
	NOx	Surg [a]	Test VOC	Base	Test	IR [b]	Base	Test	IR [b]	Base	Test	IR [b]
Mini-Surrogate +Styrene												
CTC-250 (B)	0.23	5.3	0.23	0.17	0.09	-0.33	0.50	0.29	-0.87	15	5	-46
CTC-246 (A)	0.31	5.6	0.51	0.17	0.09	-0.17	0.53	0.30	-0.45	14	4	-20
Full Surrogate + Styrene												
CTC-248 (B)	0.33	6.2	0.50	0.46	0.49	0.06	0.66	0.61	-0.10	23	14	-17
CTC-251 (A)	0.35	6.1	0.73	0.44	0.48	0.05	0.66	0.58	-0.11	24	13	-16
Low NOx Full Surrogate + Styrene												
CTC-253 (B)	0.16	6.2	0.30	0.44	0.38	-0.20	0.45	0.36	-0.30	21	14	-24
CTC-249 (A)	0.17	6.1	0.51	0.41	0.32	-0.17	0.42	0.28	-0.27	20	9	-20
Modified Mini-Surrogate + Benzaldehyde [c]												
CTC-266 (A)	0.23	5.7	0.14	0.22	0.09	-0.95	0.53	0.30	-1.66	21	9	-87
Low NOx Full Surrogate + Benzaldehyde												
CTC-267 (B)	0.16	5.9	0.13	0.39	0.34	-0.36	0.39	0.35	-0.36	21	17	-30

[a] Total base ROG surrogate in ppmC.

[b] Incremental Reactivity = (Test-Base)/(Styrene Added).

[c] The ~0.12 ppm m-xylene in the mini-surrogate was replaced by 0.18 ppm toluene and 0.05 ppm 1,3,5-trimethyl benzene.

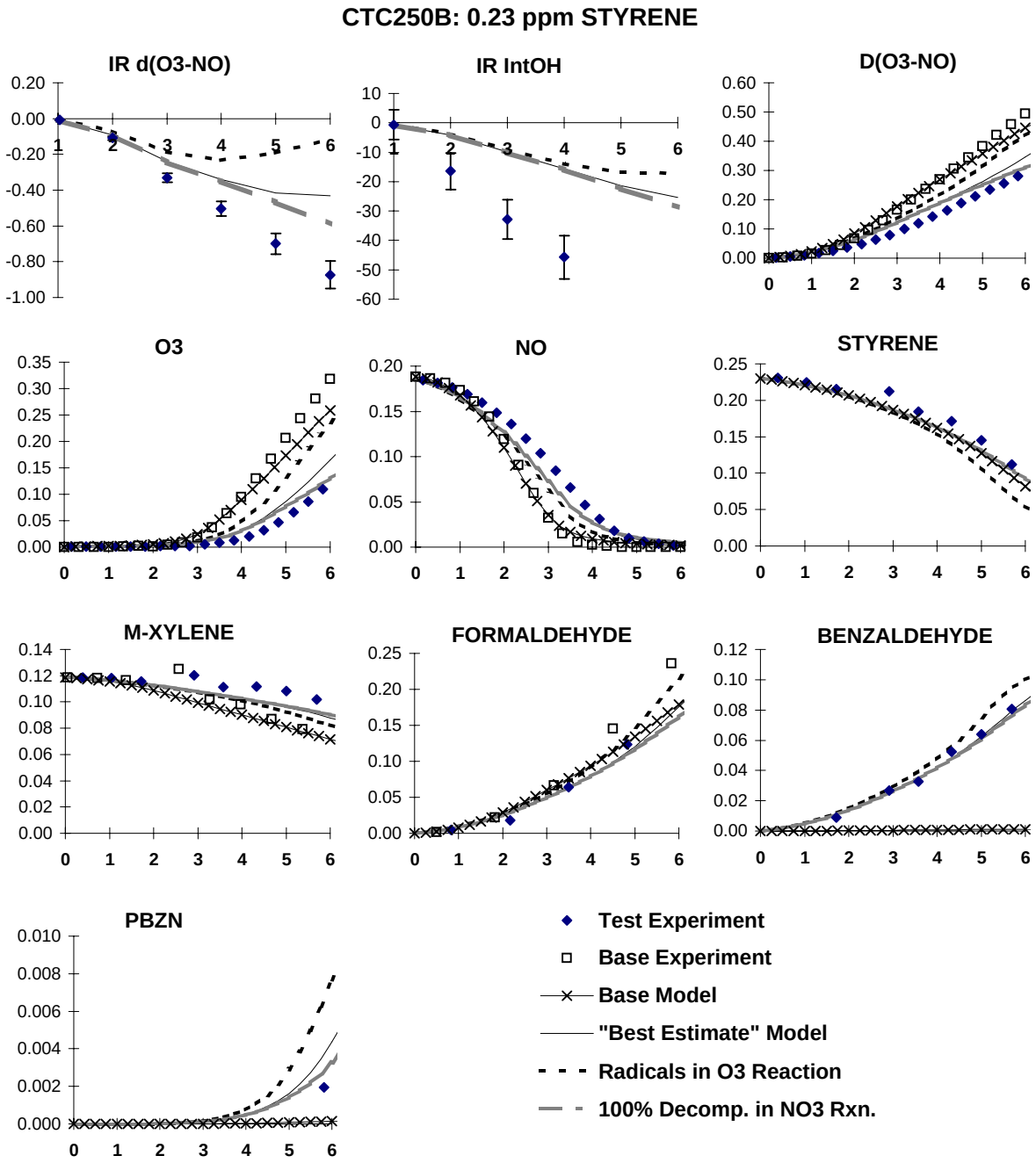

Figure 3. Plots of experimental and calculated d(O_3-NO) and IntOH incremental reactivities and concentration-time plots for selected species for the mini-surrogate + styrene experiment CTC250. Units in this and the following figures are as follows: Time: hours; concentrations: ppm; IR d(O3-NO): mole O3 per mole VOC added; IR IntOH: ppt-min OH per ppm VOC added.

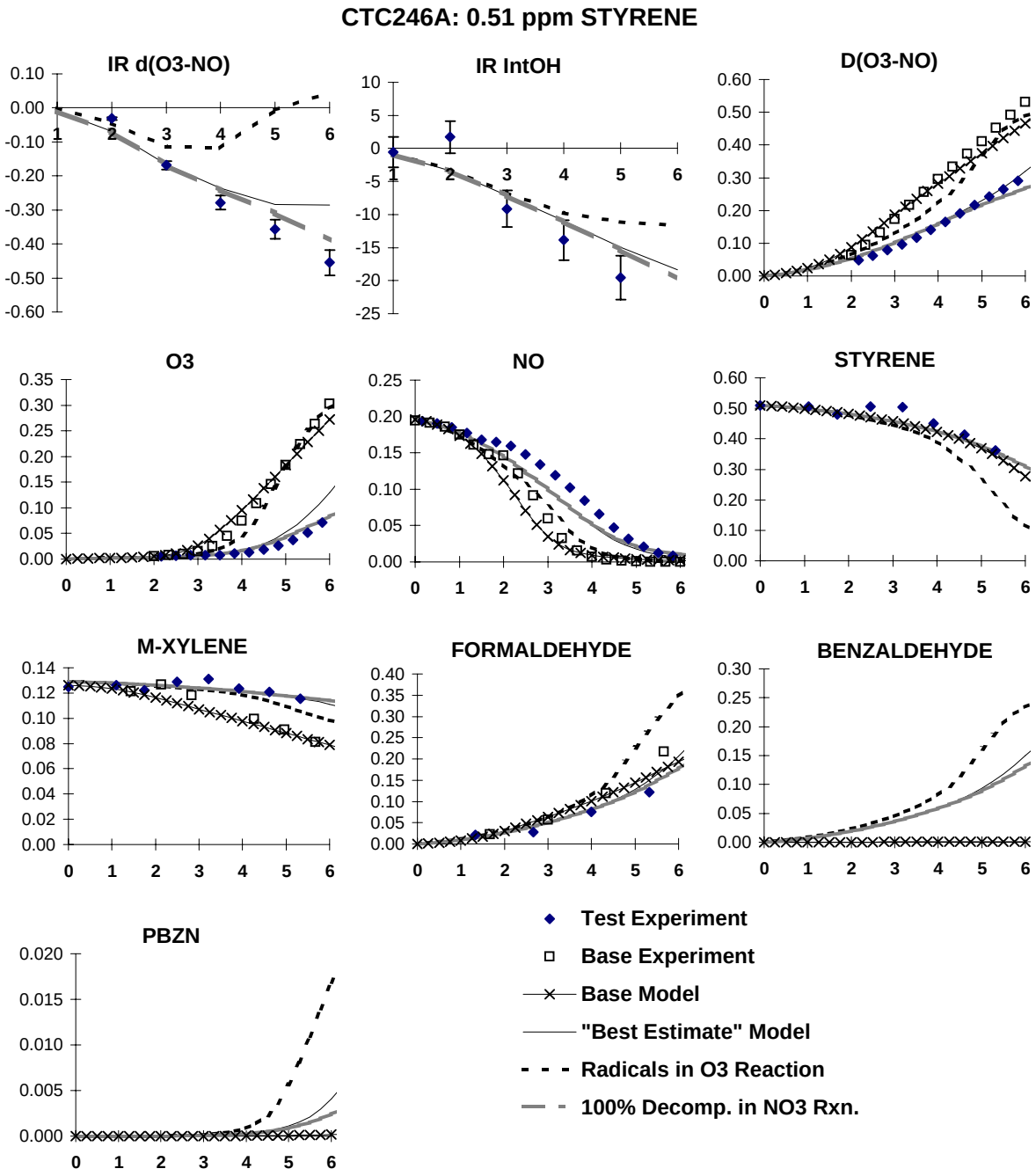

Figure 4. Plots of experimental and calculated d(O_3-NO) and IntOH incremental reactivities and concentration-time plots for selected species for the mini-surrogate + styrene experiment CTC246.

The results of the two higher NO_x full surrogate + styrene experiments are shown on Table 3 and Figures 5 and 6. The effects of the added styrene were quite different in these experiments than they were in the mini-surrogate runs. Although styrene inhibited both rates of both NO consumption and O_3 formation in the mini-surrogate runs, in these runs the styrene had no measurable effect on NO consumption rates, tended to slightly enhance the initial rate of ozone formation, but then slightly suppressed ozone at the end of the experiment, though to a much lesser extent than was the case in the mini-surrogate runs. Although styrene inhibited OH radical levels in these experiments, it did so to much less an extent than was the case in the full surrogate experiments. This is consistent with results of reactivity experiments with other VOCs, where VOCs with radial-inhibiting characteristics were found to have much greater inhibiting effects on mini-surrogate runs than on full surrogate experiments (Carter et al, 1995b). The styrene, benzaldehyde, formaldehyde and PBzN results were similar to those in the low NO_x full surrogate experiments, discussed below.

The results of the two low NO_x full surrogate + styrene experiments are shown on Table 3 and Figures 7 and 8. The addition of styrene slightly decreased the rates of NO oxidation and tended to inhibit ozone levels throughout the experiment, with the inhibiting effect being greater on the ultimate ozone yields than on the ozone formation rates. The styrene also inhibited OH radical levels, to a greater extent than in the higher NO_x full surrogate runs, but to a lesser extent than in the mini-surrogate experiments. Note that in general VOCs tend to have greater inhibiting effects on radicals in the full surrogate experiments with the lower NO_x levels than in the runs with higher NO_x (Carter et al, 1995b), so in this respect these results are consistent with data obtained from other VOCs.

In all four of the full surrogate experiments the added styrene had completely reacted by the end of the 6-hour irradiation, and significant formation of benzaldehyde and significantly enhanced formation of formaldehyde is observed. PBzN was also formed with measured yields which were an order of magnitude higher than observed in the mini-surrogate run with PBzN data. The higher PBzN yield can be explained in part by the fact that more styrene had reacted, but mainly by the fact that NO levels were relatively high throughout most of the mini-surrogate + benzaldehyde experiment, and the presence of NO inhibits the formation of PBzN and other PAN analogues because the reaction of NO with the acetyl peroxy radical precursor competes with its reaction with NO_2 to form the PAN analogue. The fact that styrene had a large positive effect on formaldehyde in the full surrogate experiments but slightly inhibited it in the mini-surrogate runs can be explained by the facts that the styrene had less of an inhibiting effect on OH radical levels in the full surrogate runs, and also that there somewhat less formaldehyde formation (i.e., increase above the initial formaldehyde) in the base case full surrogate runs than is the case for runs using the mini-surrogate. Similar behavior has been observed with other formaldehyde precursor compounds which tend to be radical inhibitors (e.g., see Carter et al, 1997b).

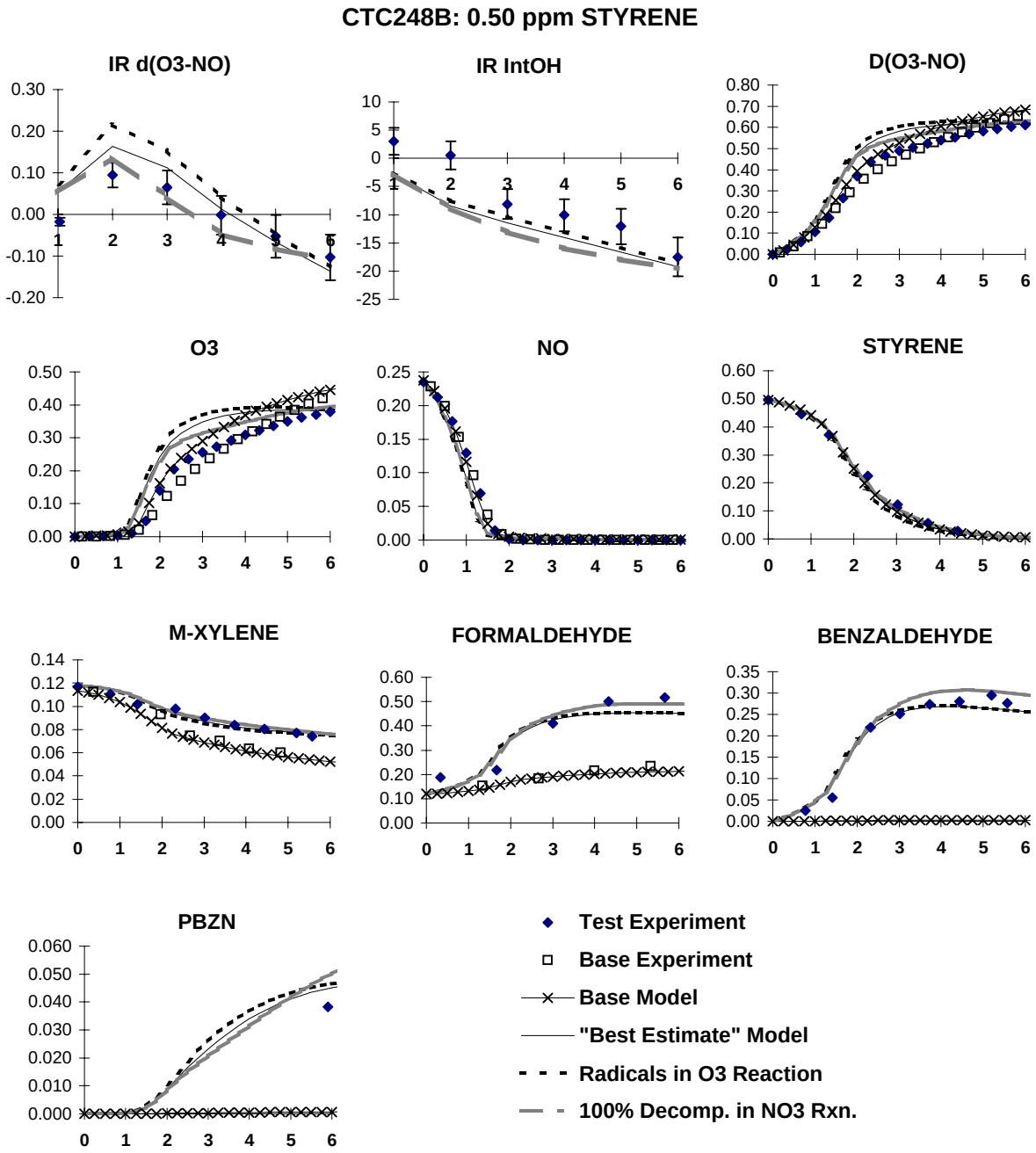

Figure 5. Plots of experimental and calculated d(O_3-NO) and IntOH incremental reactivities and concentration-time plots for selected species for the full surrogate + styrene experiment CTC248.

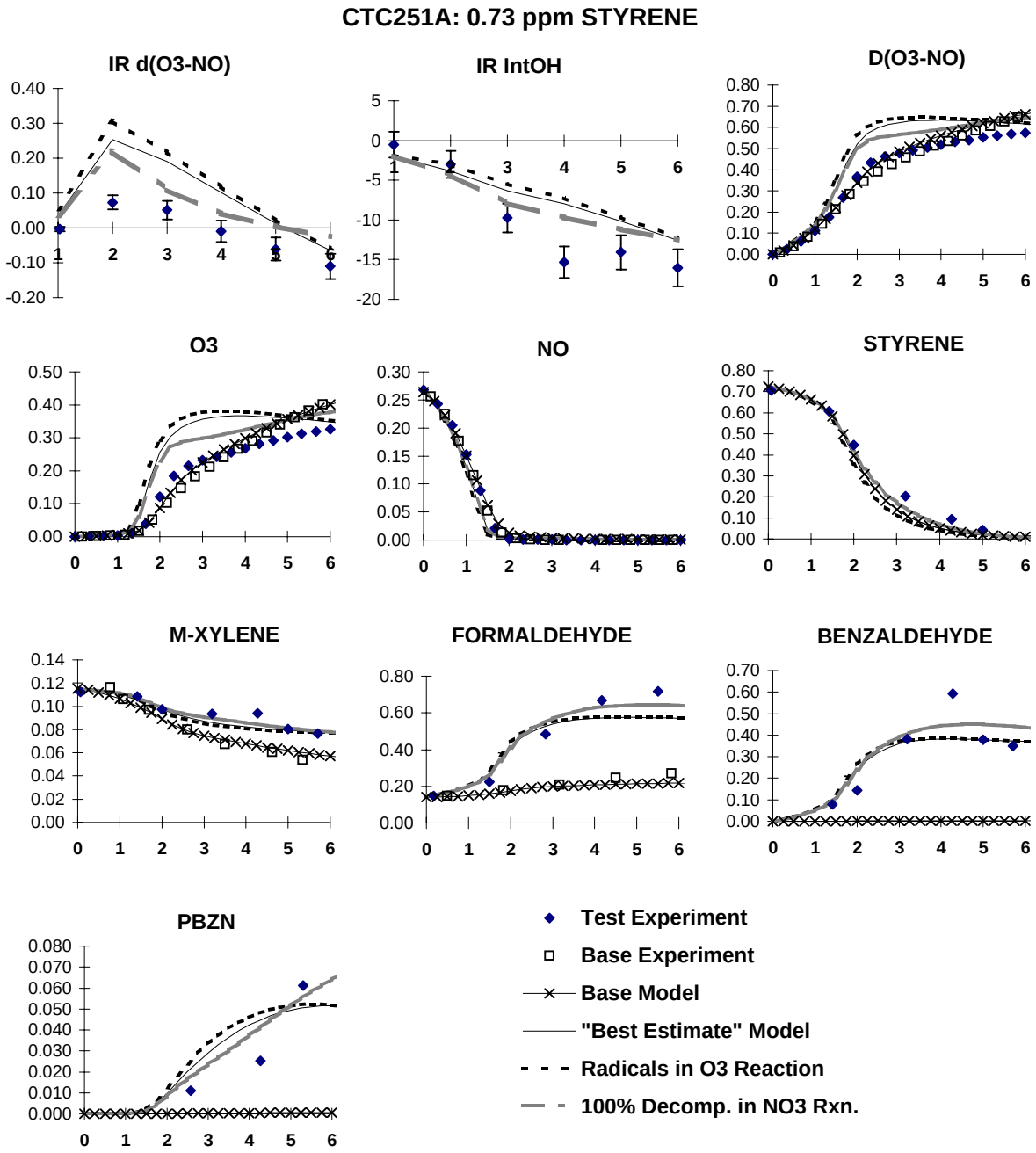

Figure 6. Plots of experimental and calculated d(O_3-NO) and IntOH incremental reactivities and concentration-time plots for selected species for the full surrogate + styrene experiment CTC251.

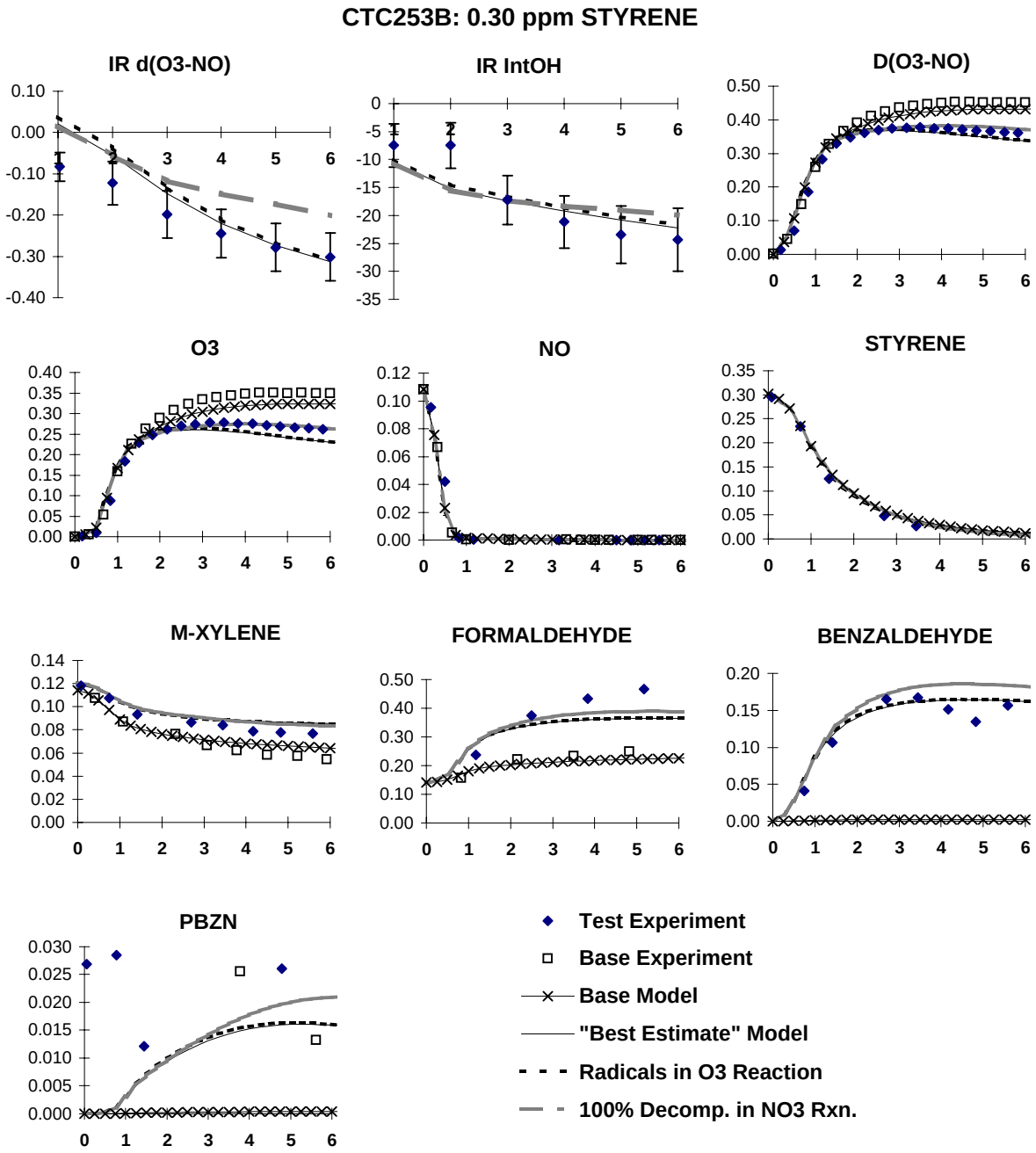

Figure 7. Plots of experimental and calculated d(O_3-NO) and IntOH incremental reactivities and concentration-time plots for selected species for the low NO_x full surrogate + styrene experiment CTC253.

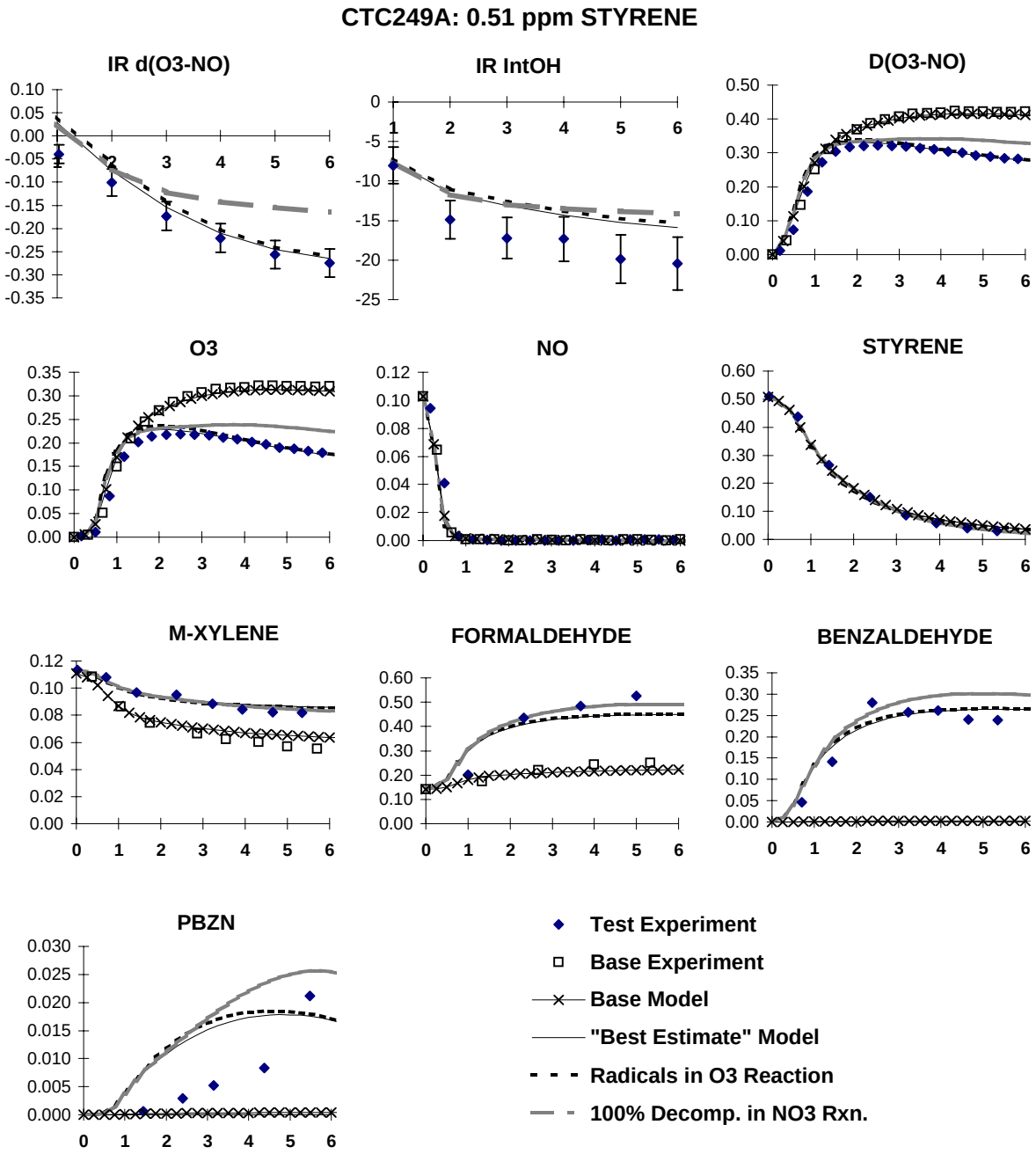

Figure 8. Plots of experimental and calculated d(O_3-NO) and IntOH incremental reactivities and concentration-time plots for selected species for the low NO_x full surrogate + styrene experiment CTC249.

Two experiments were carried out added benzaldehyde because benzaldehyde is a major styrene photooxidation product for which there have been inadequate mechanism evaluation data. The results of these experiments are shown on Table 3 and the data for the modified mini-surrogate experiment are shown on Figures 9 and the data for the full surrogate experiments are shown on Figure 10. The modified mini-surrogate employed toluene + 1,3,5-trimethylbenzene was used in place of m-xylene, but is expected to have similar reactivity characteristics to the standard full surrogate used in the styrene runs[9]. As expected, the addition of benzaldehyde was found to inhibit NO oxidation, O_3 formation and OH radical levels in both these experiments, and to a greater extent than the inhibition observed with styrene. For example, the magnitude of the negative 6-hour d(O_3-NO) and IntOH reactivities were for benzaldehyde were approximately a factor of two greater for benzaldehyde than was observed for styrene in run CTC560, which had the same amount of added test compound. The inhibition of d(O_3-NO) and IntOH by styrene was less in the low NO_x full surrogate run, and the differences between styrene and benzaldehyde were somewhat less.

Approximately half of the added benzaldehyde was consumed in the low NO_x full surrogate experiment, with a much lower amount reacting in the mini-surrogate runs. Attempts were made to monitor aromatic products such as phenol or nitrophenol by GC-FID with Tenax trapping, but significant yields were not observed in either the styrene or added benzaldehyde experiments. The only product observed in the added benzaldehyde runs was PBzN, in levels which were comparable to those in corresponding runs with added styrene. In contrast with the added styrene runs the added benzaldehyde caused a slight suppression of formaldehyde formation in the mini-surrogate run, and a large suppression in the mini-surrogate experiment. This consistent with the fact that formaldehyde is not expected to be formed in the photooxidation of benzaldehyde, so the effect on formaldehyde formation would be entirely due to its inhibiting effect on the reactions of OH radicals and O_3 with the base ROG surrogate components.

Mechanism Evaluation Results Figures 3-10 show the results of the model simulations of the added styrene or added benzaldehyde reactivity experiments, where they can be compared with the experimental data. The methods and mechanisms used in the model calculations were discussed above. Three alternative styrene mechanisms were used in the simulations of the added styrene experiments, based on differing assumptions concerning uncertain aspects of the mechanisms for the reaction of styrene with O_3 or with NO_3 radicals. These are as follows:

---

[9] This modified mini-surrogate is being investigated as an alternative to the standard mini-surrogate because the IntOH levels can be monitored with greater precision using 1,3,5-trimethylbenzene as the radical tracer rather than m-xylene, because of its more rapid rate of reaction with OH radicals. Modeling and experimental tests with other VOCs indicate that adding test VOCs to this surrogate has similar effects to adding them to the standard mini-surrogate employed previously (unpublished results from this laboratory). However, as discussed below, the current mechanism needs to be refined before it can satisfactorily simulate the base case experiment with this surrogate.

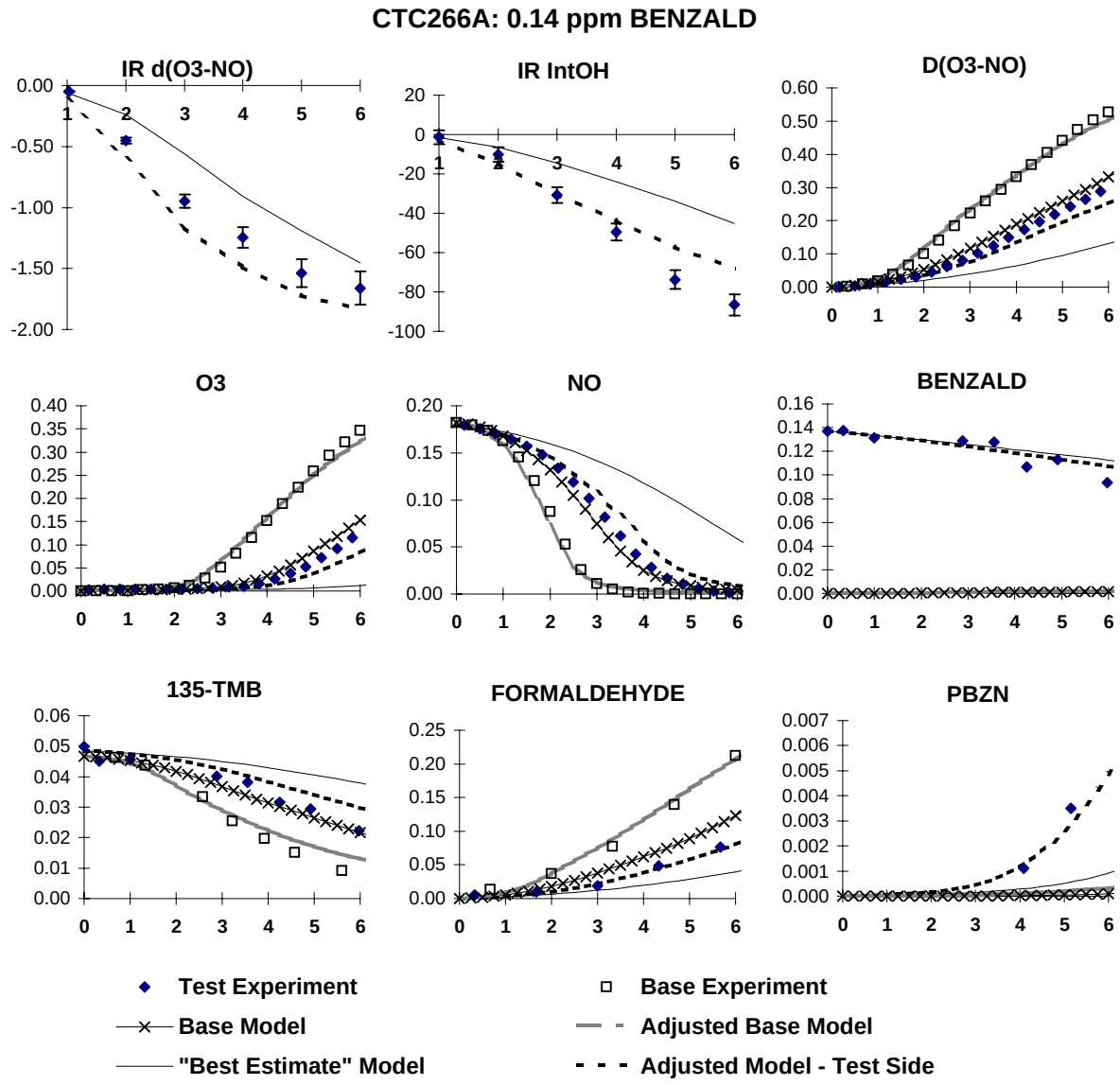

Figure 9. Plots of experimental and calculated d(O_3-NO) and IntOH incremental reactivities and concentration-time plots for selected species for the modified mini- surrogate + benzaldehyde experiment CTC266.

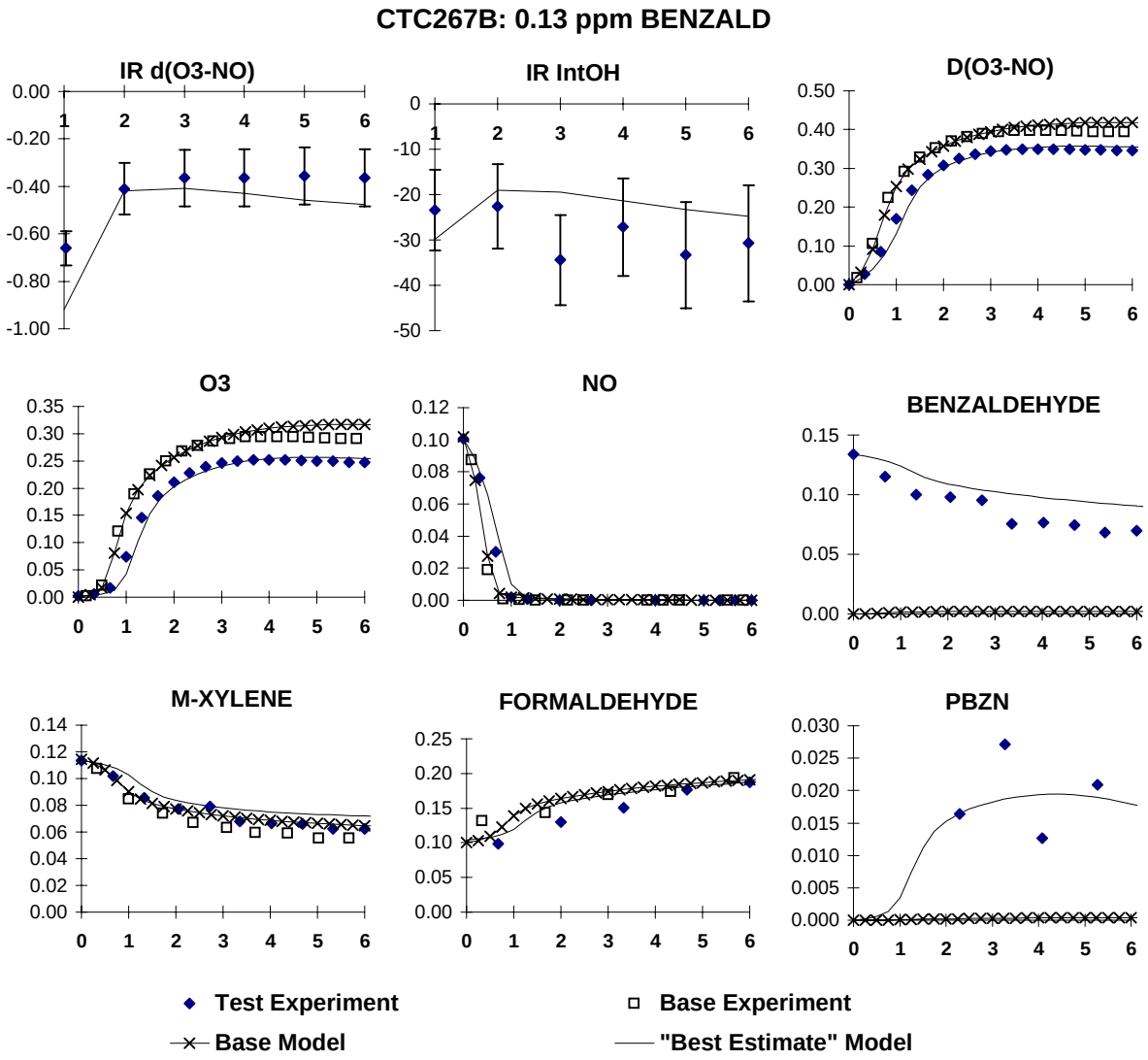

Figure 10. Plots of experimental and calculated d(O_3-NO) and IntOH incremental reactivities and concentration-time plots for selected species for the low NO_x full surrogate + benzaldehyde experiment CTC267.

The "Best Estimate" model is so designated because as shown on the figures it gives the best fits to the chamber data obtained in this study. It is based on assuming that there is no radical formation in the O_3 + styrene reaction, and that the parameter α in the NO_3 + styrene mechanism (which represents the fraction of the alkoxy radical formed in the NO_3 + styrene reaction which decomposes to benzaldehyde + formaldehyde + NO_2) is equal to its estimated (and also estimated lower limit) value of 25%. This is referred to as "Model A" in the atmospheric reactivity calculations discussed in the following section.

The "Radicals in O_3 Reaction" model assumes that the styrene + O_3 reaction involves about 7% fragmentation to form radical products, based on the assumption that the $HCHO_2$ Crigiee biradical formed in this system reacts in the same way as assumed when it is formed in the ethene system. The NO_3 + styrene mechanism is the same as used in the Best Estimate model. Note that this styrene mechanism is actually closer to the styrene mechanism used in the latest version of the SAPRC mechanism prior to this study, except that that mechanism assumed even higher radical yields in the styrene + O_3 reaction. Because this model was judged not to be consistent with the chamber data (see below), it was not used in the atmospheric reactivity calculations discussed below.

The "100% Decomposition in NO_3 Reaction" model is like the Best Estimate model in that no radicals are assumed to be formed in the styrene + O_3 reaction, but it assumes that decomposition of the alkoxy radical formed in the NO_3 + styrene system decomposes 100% of the time to benzaldehyde + formaldehyde + NO_2 (i.e., $\alpha \approx 1$). This alternative was examined to investigate the sensitivity of these results to uncertainties in the NO_3 + styrene mechanism. This is referred to as "Model B" in the atmospheric reactivity calculations discussed in the following section.

Figures 3 and 4 show that the "Radicals in O_3 Reaction" model significantly underpredicts the tendency of styrene to inhibit d(O_3-NO) and IntOH levels in the mini-surrogate experiments, though its performance in simulating the full surrogate experiments is not nearly as bad. The tendency for this model to underpredict styrene inhibition in the mini-surrogate experiments can be reduced by assuming higher organic nitrate yields in the OH radical reactions (i.e., higher values of $y_N = k_1/(k_1+k_2)$, above), but adjusting this to fit mini-surrogate results results in incorrect predictions of O_3 profiles in the full surrogate runs. Satisfactory simulations of the mini-surrogate data without significantly degrading the model performance in the full surrogate runs can only be obtained if no radical formation is assumed to occur in the styrene + O_3 reaction. Apparently if $\cdot HCHO_{2\cdot *}$ biradicals are formed in the styrene system they react with a different mechanism than what is believed to be the case when they are formed in the O_3 + ethene system, perhaps because they are formed with less excitation energy. The phenyl-substituted biradical which is also expected to be formed in the styrene + O_3 reaction also apparently do not decompose to a significant extent to form radicals as well.

Figures 3 and 4 show that the Best Estimate mechanism has a slight tendency to underpredict the inhibition of ozone in the latter stages of the mini-surrogate experiments, and that the mechanism assuming 100% decomposition in the NO_3 reaction performs slightly better in this regard. Both these mechanisms underpredict the inhibition of IntOH in one of these experiments but fit the IntOH reactivity data in the other reasonably well. All the mechanisms overpredict the effect of styrene on enhancing O_3 levels in the middle stages of the higher NO_x full surrogate experiments, but fit the effect on final O_3 levels and the observed IntOH reactivities reasonably well. Again, the "100% decomposition in NO_3 mechanism" (Model B) performs slightly better in this regard, while the "radicals in O_3 mechanism" performs slightly worse.

Figures 7 and 8 show that the Best Estimate (Model A) and "radicals in O_3" mechanisms give essentially the same predictions in the low NO_x mini-surrogate experiments, and both give good fits to the effects of styrene on O_3 and d(O_3-NO) and acceptable fits to its effects on IntOH. In contrast with the other experiments, the "100% decomposition in NO_3" mechanism (Model B) does not perform as satisfactorily in simulating these low NO_x full surrogate runs, consistently underpredicting the inhibiting effect of styrene on final ozone yields. In other words, Model A performs somewhat better in simulating styrene's effect on O_3 under low NO_x conditions, while Model B is somewhat better in simulating higher NO_x experiments where ozone yields are affected primarily by effects on O_3 formation rates. Thus the data are ambiguous concerning the relative predictive capabilities of these two mechanisms.

Except for the simulations of mini-surrogate runs by the "radicals in O_3" mechanism, where the model grossly overpredicts the overall reactivity in the added styrene runs, all the models give good fits to the observed consumption rates of styrene in these experiments, give good fits to the observed effects of styrene on benzaldehyde and formaldehyde levels, and fit the observed PBzN yields to within the scatter and probable uncertainty of the data. This indicates that the current mechanism probably represents the appropriate yields of these products in styrene's major reactions. Note that the uncertainty in the NO_3 mechanism has only a relatively small effect on the predicted benzaldehyde and formaldehyde yields, because most of the styrene is reacting either with OH radicals or with ozone. However, the effect of the uncertainty in the NO_3 reaction on the yields of these products are not totally negligible, though they are less than its effect on the overall ozone yield.

Figures 9 and 10 show the results of the model simulations of the added benzaldehyde experiments. Because the uncertainty concerning the styrene + O_3 and NO_3 reactions are not applicable in this case, the model simulations where these are varied would give the same results as the "best estimate" model and thus are not shown. Figure 10 shows that the model gives excellent simulations of the effects of benzaldehyde on O_3, IntOH and PBzN levels in the low NO_x full surrogate experiment, though the consumption rate of benzaldehyde is somewhat underpredicted. The latter could be fit if the overall quantum yield for benzaldehyde photolysis to unreactive products were set at ~12%, rather than the ~5% used in the present

model. Making this adjustment affects only the simulation of the formaldehyde consumption rate, and does not significantly affect model predictions for the other species measured in this experiment.

The model simulations of the modified mini-surrogate + benzaldehyde experiment CTC266 (figure 9) is complicated by the fact that the current mechanism significantly underpredicts the overall reactivity in the base case experiment. For this reason, the model significantly underpredicts the PBzN yields in the added benzaldehyde experiment, and this may also contribute to the model's underprediction of d(O_3-NO) and IntOH reactivities of benzaldehyde. If the yields of the unknown photoreactive products in the 1,3,5-trimethylbenzene oxidation mechanism (see Carter, 1990; Carter et al, 1997b) so the model satisfactorily fits the overall reactivity observed in the base case experiment (shown as the "Adjusted Model" calculations on Figure 9), the model gives much better simulations of the effect of benzaldehyde on d(O_3-NO) and IntOH, and surprisingly good simulations of the data for PBzN. The effect of benzaldehyde on inhibiting formaldehyde is also well simulated. Although the adjustment of the 1,3,5-trimethylbenzene mechanism is arbitrary and probably will not result in satisfactory model simulations of other experiments with this compound, the data for this run indicate that if the base mechanism gives a good simulation of the base case reactants at least under the conditions of this experiment, it will also give a good simulation of the effect of benzaldehyde on this experiment, thus tending to validate at least the benzaldehyde portion of the mechanism, which is the objective of this experiment.

Atmospheric Reactivity Calculations

As discussed above, the environmental chamber data obtained in this program indicate that the "Best Estimate" (Model A) and "100% decomp. in NO_3" (Model B) give fair to good fits to the effects of styrene on O_3 formation and radical levels in the chamber experiments for this program, and good fits to the yields of the major products which were observed. These two mechanisms can then be used as a basis for estimating styrene's effects on ozone formation in the atmosphere, with any differences between the predictions of these mechanisms indicating the effect of the uncertainty in the styrene + NO_3 reaction mechanism.

The relative ozone impacts of styrene, ethane, and toluene are shown on Table 4. Ethane is shown for comparison because it is the compound the EPA has traditionally used as the standard for determining "negligible" reactivity for VOC exemption purposes (Dimitriades, 1996), and toluene is shown because it is a chemically similar compound which is emitted in large quantities, and because toluene has been proposed as defining a borderline between "reactive" and "highly reactive" VOCs (Dimitriades, 1996). The impacts are given as relative reactivities (see above), derived in terms of ozone formed per unit mass of VOC emitted, relative to ozone formed per unit mass for the total (or weighted average) of all VOC emissions into the scenarios. The ozone impacts are quantified both in terms of peak ozone (ozone yield) and in terms of maximum 8-hour average ozone. Since the ozone impacts are shown relative to the ozone impact caused by increasing the mass emissions of all VOCs, the numbers on the table can be considered to be an estimate of the relative effects of controlling emissions of styrene or ethane, compared to controlling emissions of VOCs

Table 4. Summary of calculated incremental reactivities (gram basis) for ethane, toluene, and the two styrene models, relative to the average of all VOC emissions.

Scenario		O3 Yield Relative Reactivities				Max 8 Hour Avg Relative. Reactivities			
		Ethane	Toluene	Styrene		Ethane	Toluene	Styrene	
				A	B			A	B
Adj'd NOx	Max React	0.09	1.06	0.61	0.61	0.07	0.97	0.65	0.65
	Max Ozone	0.16	0.78	-0.47	-0.48	0.10	0.90	0.23	0.22
	Equal Benefit	0.21	0.32	-2.19	-2.19	0.12	0.73	-0.56	-0.56
Base Case	**Average**	**0.21**	**0.21**	**-2.72**	**-2.72**	**0.12**	**0.69**	**-0.90**	**-0.91**
	St.Dev	**0.06**	**0.65**	**2.24**	**2.24**	**0.03**	**0.21**	**1.06**	**1.06**
	Maximum	**0.40**	**0.95**	**0.58**	**0.59**	**0.20**	**0.97**	**0.62**	**0.62**
	ATL GA	0.21	0.48	-2.34	-2.34	0.12	0.79	-0.72	-0.72
	AUS TX	0.25	-0.01	-4.41	-4.42	0.15	0.50	-1.93	-1.95
	BAL MD	0.18	0.45	-0.95	-0.95	0.10	0.80	0.12	0.12
	BAT LA	0.19	0.51	-1.78	-1.77	0.10	0.85	-0.47	-0.47
	BIR AL	0.28	-0.55	-5.17	-5.20	0.16	0.30	-2.29	-2.30
	BOS MA	0.26	0.15	-3.02	-3.03	0.16	0.55	-1.34	-1.34
	CHA NC	0.26	0.02	-4.78	-4.81	0.18	0.43	-2.74	-2.75
	CHI IL	0.40	-2.74	-12.40	-12.42	0.17	-0.12	-3.93	-3.95
	CIN OH	0.23	0.32	-2.40	-2.40	0.13	0.69	-0.67	-0.68
	CLE OH	0.18	0.40	-1.62	-1.63	0.10	0.77	-0.18	-0.19
	DAL TX	0.15	0.95	-0.26	-0.26	0.10	0.97	0.17	0.17
	DEN CO	0.12	0.73	-0.57	-0.58	0.07	0.90	0.26	0.26
	DET MI	0.24	0.21	-2.56	-2.55	0.13	0.69	-0.72	-0.71
	ELP TX	0.13	0.78	-0.84	-0.84	0.08	0.90	0.04	0.04
	HAR CT	0.25	0.07	-4.09	-4.08	0.16	0.56	-1.94	-1.94
	HOU TX	0.22	0.33	-1.65	-1.65	0.12	0.72	-0.40	-0.41
	IND IN	0.19	0.49	-1.92	-1.91	0.11	0.84	-0.46	-0.46
	JAC FL	0.21	0.39	-3.21	-3.22	0.11	0.81	-1.15	-1.15
	KAN MO	0.23	0.45	-2.50	-2.50	0.14	0.74	-0.93	-0.93
	LAK LA	0.32	-0.69	-5.97	-5.91	0.15	0.47	-2.50	-2.47
	LOS CA	0.15	-0.01	-1.84	-1.76	0.08	0.66	-0.30	-0.31
	LOU KY	0.23	0.56	-1.71	-1.70	0.14	0.81	-0.60	-0.60
	MEM TN	0.26	-0.02	-3.47	-3.46	0.14	0.60	-1.23	-1.23
	MIA FL	0.25	-0.12	-5.97	-5.98	0.15	0.54	-2.70	-2.72
	NAS TN	0.29	-0.04	-5.39	-5.40	0.20	0.43	-3.58	-3.59
	NEW NY	0.25	-1.27	-3.96	-4.00	0.10	0.42	-0.50	-0.51
	PHI PA	0.22	0.39	-1.90	-1.91	0.12	0.76	-0.36	-0.37
	PHO AZ	0.16	0.45	-1.50	-1.51	0.09	0.79	-0.26	-0.27
	POR OR	0.23	0.50	-2.50	-2.52	0.14	0.80	-1.02	-1.03
	RIC VA	0.23	0.18	-2.50	-2.50	0.12	0.68	-0.52	-0.52
	SAC CA	0.20	0.60	-1.90	-1.91	0.11	0.88	-0.62	-0.63
	SAI MO	0.17	0.41	-1.17	-1.17	0.09	0.78	0.04	0.03
	SAL UT	0.21	0.14	-3.32	-3.33	0.11	0.65	-1.11	-1.13
	SAN TX	0.17	0.92	-0.64	-0.65	0.11	0.94	-0.06	-0.06
	SDO CA	0.16	0.51	-1.74	-1.79	0.10	0.81	-0.42	-0.44
	SFO CA	0.05	0.94	0.58	0.59	0.05	0.88	0.62	0.62
	TAM FL	0.18	0.73	-0.80	-0.79	0.10	0.90	0.04	0.03
	TUL OK	0.23	0.46	-1.57	-1.55	0.12	0.78	-0.21	-0.20
	WAS DC	0.24	0.18	-2.24	-2.24	0.13	0.63	-0.67	-0.67

from all sources equally. In other words, if the number on the table is 1, it means that the impact of the VOC in that scenario and ozone quantification method is the same as the average of all VOC emissions. The data are shown for each of the 39 "base case" EKMA scenarios, together with the corresponding averages and standard deviations, and for the three adjusted NO_x scenarios.

To examine the extent to which variations in NO_x conditions explain the differences in styrene relative reactivities among the various scenarios, Figure 11 shows a plot of the best estimate (Model A) relative styrene reactivities against relative NO_x levels in the various scenarios. The latter is quantified by the ratio of NO_x inputs (sum of initially present and emitted NO_x) in the scenarios divided by the NO_x inputs which give the highest peak ozone concentrations, i.e., the NO_x inputs of the corresponding MOIR scenario (referred to as NO_x^{MO}). This quantity is believed to be a good indicator of relative NO_x levels in scenarios as they affect VOC reactivity (Carter, 1994a). The points on the plot show the results of the calculations for the individual base case scenarios, while the lines show the results of calculations using the "average conditions" scenario wither the NO_x inputs are continuously varied. The scatter in the base case points, and the differences between these points and the "averaged conditions" lines give an indication of the effects of other scenario conditions besides relative NO_x levels.

The data on Table 4 show that there are only very small differences between the styrene reactivities calculated using Mechanisms A and B. This indicates that the calculated ozone impacts are much less sensitive to uncertainties in the NO_3 + styrene mechanism than is the case for impacts in the environmental chamber experiments. This greater sensitivity in the chamber experiments to the NO_3 reaction mechanism may be a consequence of the use of the blacklight light source, which has a much lower intensity in the longer (visible) wavelengths which affect the photolysis of NO_3 radicals than is the case for sunlight in the lower atmosphere. Since photolysis is an important removal process for NO_3 radicals in the daytime, this would result in higher NO_3 concentrations in the chamber than under comparable chemical conditions in the atmosphere, with consequent higher sensitivities to mechanisms of NO_3 reactions. Although apparently it does not make a significant difference whether Model A or B is used, for atmospheric modeling purposes we recommend use of Model A. This is our "best estimate" NO_3 radical mechanism because it is derived from our assessment of the available (albeit limited and ambiguous) laboratory data. Furthermore, it performs better simulating the chamber experiments with the higher ROG/NO_x conditions which are more characteristic of most of the base case scenarios.

It can be seen from Table 4 and Figure 11 that the ozone impacts of styrene are highly dependent on environmental conditions, particularly conditions of NO_x availability. The reactivities are the highest under the relatively high NO_x maximum incremental reactivity (MIR) condition, where styrene is calculated to have about ten times more ozone impact than ethane (the informal standard of "negligible" reactivity) and 60-65% of the ozone impact of toluene and the average of all reactive organic emissions. The high NO_x or MIR

Figure 11. Plots of calculated relative reactivities for styrene against the NO_x / NO_x^{MO} ratio for the base case and the adjusted NO_x averaged conditions scenarios.

reactivity is about the same regardless of whether ozone impacts are quantified effects on by peak ozone yield or on the maximum 8-hour average.

The reactivities for the adjusted NO_x scenarios shown on Table 4 and the plots of reactivities against relative NO_x conditions on Figure 11 show that the ozone impacts of styrene decrease as relative NO_x levels are reduced, and become negative (in some cases highly so) when NO_x levels become sufficiently low. Although the styrene reactivities under the higher NO_x (MIR) conditions are about the same regardless of how O_3 impacts are quantified, the reactivities derived from effects on peak O_3 yields decline much more rapidly as NO_x is reduced than reactivities derived from effects on 8-hour average ozone. This behavior is similar to what is seen for other VOCs whose reactivities are highly dependent on NO_x conditions, as discussed by Carter (1994a)[10], and can be seen to be the case for toluene as well, though to a much lesser degree than is the case for styrene. For example, although the current mechanism predicts that toluene has a positive ozone impact in the maximum ozone (MOIR) scenarios regardless of how ozone is quantified (albeit lower for ozone yield impacts), in the case of styrene the impact for maximum ozone scenarios is negative if quantified by ozone yield but positive if quantified by effect on the maximum eight hour average. However, as the NO_x is reduced to below MOIR levels, the ozone impact becomes negative regardless of how ozone is quantified.

[10] Carter (1994) did not calculate reactivities relative to maximum 8-hour average ozone, but for one day scenarios, these would correlate closely to the reactivities given relative to integrated ozone.

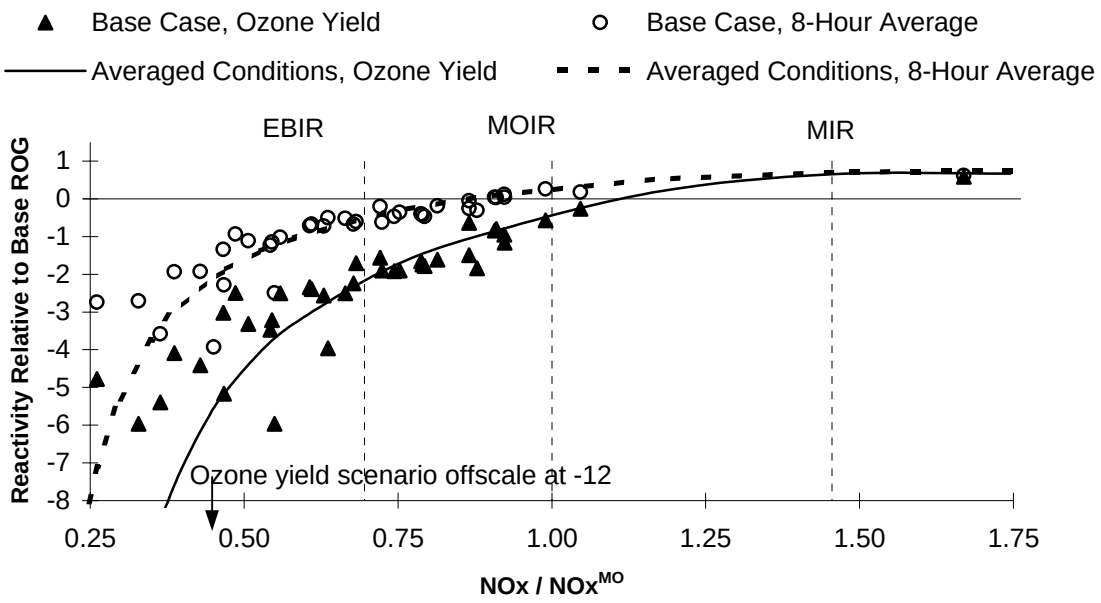

Figure 11. Plots calculated relative reactivities for styrene against the NO_x / NO_x^{MO} ratio for the base case and the adjusted NO_x averaged conditions scenarios.

Discussion of Factors Affecting Styrene's Ozone Reactivities

The variability of reactivities with environmental conditions is caused by the fact that there are various mechanistic factors which affect a VOC's ozone impact, and the relative importance of these factors differ with environmental conditions and also with how ozone impacts are quantified. Mechanistic factors which affect the rates of ozone formation are important in affecting the ozone impacts of VOCs under the relatively high NO_x conditions where the maximum possible ozone yields have not been achieved, and where ozone levels are thus determined by how rapidly ozone is formed. Factors affecting rates of ozone formation also affect ozone reactivities in lower NO_x scenarios (all else being equal), but the relative importance of these factors decrease as NO_x levels are reduced to and below the MOIR levels. These factors are also relatively more important in affecting integrated ozone levels (and thus longer term averages) than peak ozone in the lower NO_x scenarios, since if the ozone formation begins sooner the long term average may be higher even if the peak ozone is the same or even slightly lower. This explains the fact that reactivities relative to effects on integrated or long-term average ozone levels tend vary less strongly with NO_x conditions than do reactivities relative to peak ozone yields.

The two major factors which determine the effect of a VOC on ozone formation rate is its effect of the VOC on overall radical levels, and the number of NO to NO_2 conversions resulting from the VOC's reactions. Styrene has both positive and negative reactivity characteristics in this regard. The experimental IntOH reactivity data clearly indicate that styrene tends to have a relatively high negative effect on radical levels. This is explained in the mechanism by two processes: the ~10% formation of organic nitrates in the OH reaction, and also by the formation of high yields benzaldehyde, whose subsequent relatively rapid reaction with OH radicals is believed to nearly 100% radical terminating. (The assumed radical terminating characteristics is validated by the fact that the model assuming this benzaldehyde mechanism gives good fits to its effects of added benzaldehyde in the reactivity experiments with this compound.) This explains the negative reactivities of styrene in the mini-surrogate experiments, which tend to be highly sensitive to radical inhibition effects (Carter et al, 1995b).

On the other hand, styrene's mechanism also has positive effects on ozone formation, in that its reactions with OH radicals (and also the reactions of benzaldehyde and formaldehyde, it's major products) form peroxy radicals which convert NO to NO_2, the process directly responsible for ozone formation. Thus there is a balance between the negative effect due to the radical terminating processes and the positive effect due to the NO to NO_2 conversions. This affects ultimate ozone yields as well as ozone formation rates. Its importance relative to radical inhibition depend not only on NO_x levels, but also on other conditions under which the styrene is reacting, such as the nature of the other VOCs which are reacting. The balance is clearly on the side of the radical inhibition effects in the mini-surrogate experiments where styrene's d(O_3-NO) reactivities are highly negative, but is more on the positive side in the higher NO_x full surrogate experiments, where the d(O_3-NO) reactivities of styrene are slightly positive. The balance is also clearly on the positive side in the atmospheric reactivity MIR scenarios, where positive reactivities are also observed. Note that the

overall radical levels in the atmosphere tend to be higher than in these experiments, making the atmospheric scenarios somewhat less sensitive to radical inhibiting effects. However, the calculated MIR for styrene is still relatively low considering it's relatively high rates of OH reaction, and this can be attributed to the negative contribution caused by styrene (and benzaldehyde's) radical termination characteristics.

The other major mechanistic factor affecting a VOC's ozone reactivity is the effect of the reactions of the VOC on overall NO_x levels. Since NO_x is required for ozone formation, reactions which increase the rate of NO_x consumption will tend to reduce the ultimate amount of ozone which can be formed in scenarios which are NO_x limited. Although this has no effect on ozone levels in higher NO_x scenarios where ozone is not NO_x limited, it becomes important as NO_x is reduced to or below the MOIR levels, and becomes increasingly important and dominant as NO_x is reduced further.

The current mechanism for the reactions of benzaldehyde (whose predictions tend to be verified by the experiments carried out for this study) predict that the relatively rapid reaction of a benzaldehyde molecule with OH will always cause at least one molecule of NO_x to be removed, either in the form of BPzN (following the reactions of the benzoyl peroxy radical with NO_2), or in the form of compounds represented by nitrophenols (following formation of phenoxy radicals in the reaction of benzoyl peroxy with NO or the decomposition of PBzN). This represents an unusually strong NO_x sink which would cause highly negative reactivities in low NO_x scenarios. Since benzaldehyde is formed in large yields from styrene and reacts relatively rapidly, this would clearly contribute to the negative $d(O_3\text{-}NO)$ reactivities for styrene observed in the low NO_x full surrogate experiments, and to the large negative styrene reactivities calculated in the low NO_x airshed scenarios.

In addition to the formation of benzaldehyde as a major product, the ~10% nitrate formation reaction in the OH reaction and the formation of nitrates in the NO_3 reactions would also act as NO_x sinks and contribute to negative reactivities in low NO_x scenarios. However, the higher molecular weight alkanes have even higher nitrate yields and their reactivities tend not to be as consistently or highly negative in the low NO_x scenarios as is the case for styrene (Carter et al, 199?). The NO_3 reaction is probably even less important, given the similarity in the reactivity predictions for Models A and B, which have significantly different assumptions concerning NO_x removal in that reaction. Therefore, it is almost certainly the benzaldehyde formation which is the major reason for styrene's highly negative reactivities in the low NO_x scenarios.it does not make a significant difference whether Model A or B is used, for atmospheric modeling purposes we recommend use of Model A. This is our "best estimate" NO_3 radical mechanism because it is derived from our assessment of the available (albeit limited and ambiguous) laboratory data. Furthermore, it performs better simulating the chamber experiments with the higher ROG/NO_x conditions which are more characteristic of most of the base case scenarios.

It can be seen from Table 4 and Figure 11 that the ozone impacts of styrene are highly dependent on environmental conditions, particularly conditions of NO_x availability. The reactivities are the highest under the relatively high NO_x maximum incremental reactivity (MIR) condition, where styrene is calculated to have about ten times more ozone impact than ethane (the informal standard of "negligible" reactivity) and 60-65% of the ozone impact of toluene and the average of all reactive organic emissions. The high NO_x or MIR reactivity is about the same regardless of whether ozone impacts are quantified effects on by peak ozone yield or on the maximum 8-hour average.

The reactivities for the adjusted NO_x scenarios shown on Table 4 and the plots of reactivities against relative NO_x conditions on Figure 11 show that the ozone impacts of styrene decrease as relative NO_x levels are reduced, and become negative (in some cases highly so) when NO_x levels become sufficiently low.

CONCLUSIONS

This program has achieved its objective in providing data needed to improve our confidence in the ability of airshed models to estimate the atmospheric impacts of styrene emissions. The data obtained indicated that a mechanism based on our current understanding can successfully predict the consumption rates of styrene under simulated atmospheric conditions, and its impact on the formation of benzaldehyde, formaldehyde, and PBzN, its major known photooxidation products. The data confirmed model predictions that styrene may have a positive effect on O_3 under high NO_x conditions when reacting in the presence of surrogates representing ambient VOC mixtures, but that it has negative effects on ozone when NO_x is limited. On the other hand, the data obtained indicated that the styrene mechanism used prior to this work needed to be modified to successfully predict the effect of styrene on experiments which are sensitive to effects of VOCs on radical levels. In particular, these data indicated that the reaction of styrene with ozone does not result in the significant formation of radical levels, contrary to what was previously estimated. This will result in some revisions to the mechanism recommended for use when modeling styrene's effects on ozone formation in the atmosphere.

Consistent with previous predictions, the results of this work indicate that styrene is considerably more reactive than ethane under high NO_x, MIR conditions where ozone is most sensitive to VOC emissions. Thus styrene would not be considered to be a negligibly reactive compound under the criteria which has been used by the EPA in this regard (Dimitriades, 1996). On the other hand, in none of the airshed scenarios examined in this work did styrene have a reactivity greater than ~65% of the average of all reactive VOC emissions (on a mass basis), indicating that even in the scenarios where it has the most positive effect on ozone it has less of an effect on ozone than the average of all emissions. Therefore, it could not be appropriately classified as "highly reactive" under schemes such as that proposed by Dimitriades (1996). Indeed, ozone formation in much of the atmosphere is NO_x limited, and under those conditions styrene is calculated to cause reduced ozone levels. A discussion of the regulatory implications of this is beyond the scope of this report.

This relative MIR for styrene of 0.61 calculated in this work is not greatly different from the 0.70 value calculated previously (Carter, 1994a) using the SAPRC-90 (Carter, 1990) mechanism, which was incorporated in the California Clean Fuels-Low Emissions Vehicle regulations (CARB, 1993). The slight (~12%) reduction could be attributed in part to the change in the O_3 + styrene mechanism, since the previous mechanism assumed that radicals were formed in that reaction, while in this work the chamber data were found to be more consistent to the assumption that no radicals are formed, giving a less reactive mechanism. The other modifications made to the mechanism as a result of this work are expected to be relatively minor in terms of overall styrene impact predictions. The main contribution of this work was not to improve the reactivity predictions of the current styrene mechanisms, but to significantly reduce their overall level of

uncertainty. This would have implications in reactivity based regulatory schemes which take uncertainty into account, such as the proposed consumer products regulations being considered in California.

Nevertheless, uncertainties remain in the details of the styrene photooxidation mechanism which may affect predictions of its ultimate fate in the environment. The known products in the ozone reaction account for less than 60% of the reacting carbon, and the model assumes that the rest are relatively unreactive species whose reactions can be ignored. The nature of these products, which may include organic acids, are unknown, and any impacts they have on the environment would not be represented in the current model. The products formed in the NO_3 reaction, which may be a major nighttime sink for styrene, are also unknown, and their representation in the model as a mixture of benzaldehyde and alkyl-nitrate-like model species may be inappropriate. Furthermore, the fate of the phenoxy radicals formed in the decomposition of PBzN (or when benzaldehyde reacts in the presence of excess NO) is unknown. It is represented in the model as forming nitrocresols, but in fact the relatively high yields of nitrocresols predicted by this model are not observed. Therefore, although the data obtained in this work indicate that the representation in the current mechanism is probably reasonably accurate in its predictions of the effects of styrene on formations of ozone, benzaldehyde, formaldehyde, PBzN, and overall radical levels, it may not be correctly accounting for the full environmental fate of the reacting styrene in the atmosphere. More information is needed concerning the products formed in the reactions of styrene with ozone and NO_3 radicals, and concerning the atmospheric fate of phenoxy radicals, are needed before models can be used with any confidence in this regard. This will probably require development of improved analytical methods for detecting and quantifying the types of products which may be formed.

Based on the results of this work, recommended mechanism for airshed model simulations of the atmospheric impacts of styrene, given terms of model species in the current (SAPRC-98) mechanism, is as follows:

Rctnt	Products	k (cm^3 $molec^{-1}$ s^{-1})
OH	0.9 {RO2-R. + HCHO + BALD) + 0.1 RO2-N.	5.8×10^{-11}
O3	0.6 {BALD + HCHO2-STAB} + 0.4 {HCHO + RCHO2-STAB}	1.71×10^{-17}
NO_3	0.1 {RO2-N. + XN} + 0.225 {NO_2 + BALD + HCHO + R2O2.} + 0.675 {RO2-R. + RNO3}	1.5×10^{-13}
$O(^3P)$	(can be neglected in ambient simulations)	1.76×10^{-11}

It is probably not necessary to represent the $O(^3P)$ reaction, though it may occur at non-negligible rates in high NO_x-containing plumes, because the chamber data indicate that it does not form significant amounts of radical initiating products. The appropriate representation of benzaldehyde (BALD) is critical in view of its significant contribution to styrene's reactivity, both in terms of its relatively low MIR compared to its relatively high reaction rate constants, and its highly negative low NO_x reactivities. Unfortunately, neither the Carbon

Bond (Gery et al, 1998) nor the RADM-2 (Stockwell et al, 1990) mechanism contain a model species for benzaldehyde. The mechanism for benzaldehyde as given in Appendix A, whici is based on that given by Carter (1990), appears to perform well in simulating the effects of this compound. Note that use of a generic aldehyde model species, which are generally based on reactions of acetaldehyde or propionaldehyde, would not be satisfactory in this regard because of their significantly different reactivity characteristics. Therefore, a model species for benzaldehyde would have to be added for models using these mechanisms to even approximately predict styrene's atmospheric impacts.

REFERENCES

Atkinson, R. (1989): "Kinetics and Mechanisms of the Gas-Phase Reactions of the Hydroxyl Radical with Organic Compounds," J. Phys. Chem. Ref. Data, Monograph no 1.

Atkinson, R. (1990): "Gas-Phase Tropospheric Chemistry of Organic Compounds: A Review," Atmos. Environ., 24A, 1-24.

Atkinson, R. (1991): "Kinetics and Mechanisms of the Gas-Phase Reactions of the NO_3 Radical with Organic Compounds," J. Phys. Chem. Ref. Data, 20, 459-507.

Atkinson, R. (1994): "Gas-Phase Tropospheric Chemistry of Organic Compounds," J. Phys. Chem. Ref. Data, Monograph No. 2.

Atkinson, R. (1997): "Gas Phase Tropospheric Chemistry of Volatile Organic Compounds: 1. Alkanes and Alkenes," J. Phys. Chem. Ref. Data, 26, 215-290.

Atkinson, R., S. M. Aschmann, D. R. Fitz, A. M. Winer and J. N. Pitts, Jr. (1982): Int J. Chem. Kinet. 14, 13-18.

Atkinson, R. C. N. Plum, W. P. L. Carter, A. M. Winer and J. N. Pitts, Jr. (1984): Int. J. Chem. Kinet. 16, 887.

Atkinson, R. and S. M. Aschmann (1988): Int J. Chem. Kinet. 20, 513.

Atkinson, R., D. L. Baulch, R. A. Cox, R. F. Hampson, Jr., J. A. Kerr, M. J. Rossi, and J. Troe (1997): "Evaluated Kinetic, Photochemical and Heterogeneous Data for Atmospheric Chemistry: Supplement V., IUPAC Subcommittee on Gas Kinetic Data Evaluation for Atmospheric Chemistry," J. Phys. Chem. Ref. Data, 26, 521-1011.

Baugues, K. (1990): "Preliminary Planning Information for Updating the Ozone Regulatory Impact Analysis Version of EKMA," Draft Document, Source Receptor Analysis Branch, Technical Support Division, U. S. Environmental Protection Agency, Research Triangle Park, NC, January.

Bignozzi, C. A., A. Maldotti, C. Chiorboli, C. Bartocci, and V. Carasiti (1981): Int. J. Chem. Kinet. 13, 1235.

Bufalini, J. J. and A. P. Altshuller (1965): Can. J. Chem, 43, 2243-2250.

CARB (1993): "Proposed Regulations for Low-Emission Vehicles and Clean Fuels — Staff Report and Technical Support Document," California Air Resources Board, Sacramento, CA, August 13, 1990. See also Appendix VIII of "California Exhaust Emission Standards and Test Procedures for 1988 and Subsequent Model Passenger Cars, Light Duty Trucks and Medium Duty Vehicles," as last amended September 22, 1993. Incorporated by reference in Section 1960.1 (k) of Title 13, California Code of Regulations.

Carter, W. P. L. (1990): "A Detailed Mechanism for the Gas-Phase Atmospheric Reactions of Organic Compounds," Atmos. Environ., 24A, 481-518.

Carter, W. P. L. (1994a): "Development of Ozone Reactivity Scales for Volatile Organic Compounds," J. Air & Waste Manage. Assoc., 44, 881-899.

Carter, W. P. L. (1994b): "Calculation of Reactivity Scales Using an Updated Carbon Bond IV Mechanism," Report Prepared for Systems Applications International Under Funding from the Auto/Oil Air Quality Improvement Research Program, April 12.

Carter, W. P. L. (1995): "Computer Modeling of Environmental Chamber Measurements of Maximum Incremental Reactivities of Volatile Organic Compounds," Atmos. Environ., 29, 2513-2517.

Carter, W. P. L. (1995): "Updated Maximum Incremental Reactivity Scale for Regulatory Applications," Preliminary Report to California Air Resources Board Contract No. 95-308. (This report is available at http://cert.ucr.edu/~carter/r98tab.htm.)

Carter, W. P. L. (1999): "Development and Application of an Updated Photochemical Mechanism for VOC Reactivity Assessment," Final report to CARB Contract 92-329, in preparation.

Carter, W. P. L., R. Atkinson, A. M. Winer, and J. N. Pitts, Jr. (1982): "Experimental Investigation of Chamber-Dependent Radical Sources," Int. J. Chem. Kinet., 14, 1071.

Carter, W. P. L. and R. Atkinson (1987): "An Experimental Study of Incremental Hydrocarbon Reactivity," Environ. Sci. Technol., 21, 670-679

Carter, W. P. L. and R. Atkinson (1989): "A Computer Modeling Study of Incremental Hydrocarbon Reactivity", Environ. Sci. Technol., 23, 864.

Carter, W. P. L., and F. W. Lurmann (1990): "Evaluation of the RADM Gas-Phase Chemical Mechanism," Final Report, EPA-600/3-90-001.

Carter, W. P. L., and R. Atkinson (1985): "Atmospheric Chemistry of Alkanes", J. Atmos. Chem., 3, 377-405, 1985.

Carter, W. P. L. and F. W. Lurmann (1991): "Evaluation of a Detailed Gas-Phase Atmospheric Reaction Mechanism using Environmental Chamber Data," Atm. Environ. 25A, 2771-2806.

Carter, W. P. L., J. A. Pierce, I. L. Malkina, and D. Luo (1992): "Investigation of the Ozone Formation Potential of Selected Volatile Silicone Compounds," Final Report to Dow Corning Corporation, Midland, MI, November.

Carter, W. P. L., J. A. Pierce, I. L. Malkina, D. Luo and W. D. Long (1993a): "Environmental Chamber Studies of Maximum Incremental Reactivities of Volatile Organic Compounds," Report to Coordinating Research Council, Project No. ME-9, California Air Resources Board Contract No. A032-0692; South Coast Air Quality Management District Contract No. C91323, United States Environmental Protection Agency Cooperative Agreement No. CR-814396-01-0, University

Corporation for Atmospheric Research Contract No. 59166, and Dow Corning Corporation. April 1. (This report is available at http://cert.ucr.edu/~carter/bycarter.htm.)

Carter, W. P. L, D. Luo, I. L. Malkina, and J. A. Pierce (1993b): "An Experimental and Modeling Study of the Photochemical Ozone Reactivity of Acetone," Final Report to Chemical Manufacturers Association Contract No. KET-ACE-CRC-2.0. December 10. (This report is available at http://cert.ucr.edu/~carter/bycarter.htm.)

Carter, W. P. L., J. A. Pierce, D. Luo, and I. L. Malkina (1995a): "Environmental Chamber Study of Maximum Incremental Reactivities of Volatile Organic Compounds," Atmos. Environ. 29, 2499-2511.

Carter, W. P. L., D. Luo, I. L. Malkina, and J. A. Pierce (1995b): "Environmental Chamber Studies of Atmospheric Reactivities of Volatile Organic Compounds. Effects of Varying ROG Surrogate and NO_x," Final report to Coordinating Research Council, Inc., Project ME-9, California Air Resources Board, Contract A032-0692, and South Coast Air Quality Management District, Contract C91323. March 24. (This report is available at http://cert.ucr.edu/~carter /bycarter.htm.)

Carter, W. P. L., D. Luo, I. L. Malkina, and D. Fitz (1995c): "The University of California, Riverside Environmental Chamber Data Base for Evaluating Oxidant Mechanism. Indoor Chamber Experiments through 1993," Report submitted to the U. S. Environmental Protection Agency, EPA/AREAL, Research Triangle Park, NC., March 20. (This report is available at http://cert. ucr.edu/~carter/bycarter.htm.)

Carter, W. P. L., D. Luo, I. L. Malkina, and J. A. Pierce (1995d): "Environmental Chamber Studies of Atmospheric Reactivities of Volatile Organic Compounds. Effects of Varying Chamber and Light Source," Final report to National Renewable Energy Laboratory, Contract XZ-2-12075, Coordinating Research Council, Inc., Project M-9, California Air Resources Board, Contract A032-0692, and South Coast Air Quality Management District, Contract C91323, March 26. (This report is available at http://cert.ucr.edu/~carter/bycarter.htm.)

Carter, W. P. L., D. Luo, and I. L. Malkina (1996a): "Investigation of Atmospheric Ozone Formation Potentials of C_{12} - C_{16} n-Alkanes," Report to the Aluminum Association, October 28. (This report is available at http://cert.ucr.edu/~carter/bycarter.htm.)

Carter, W. P. L., D. Luo, and I. L. Malkina (1997a): "Environmental Chamber Studies for Development of an Updated Photochemical Mechanism for VOC Reactivity Assessment," Draft final report to California Air Resources Board Contract 92-345, Coordinating Research Council Project M-9, and National Renewable Energy Laboratory Contract ZF-2-12252-07. March 10. (This report is available at http://cert.ucr.edu/~carter/bycarter.htm.)

Carter, W. P. L., D. Luo, and I. L. Malkina (1997b): "Investigation of the Atmospheric Ozone Formation Potential of t-Butyl Acetate," Report to ARCO Chemical Corporation, July 2. (This report is available at http://cert.ucr.edu/~carter/bycarter.htm.)

Carter, W. P. L., D. Luo and I. L. Malkina (1999): "Investigation of the Atmospheric Reactivities of Selected Stationary Source VOCs," Final Report for California Air Resources Board Contract 95-308, in preparation.

Chang, T. Y. and S. J. Rudy (1990): "Ozone-Forming Potential of Organic Emissions from Alternative-Fueled Vehicles," Atmos. Environ., 24A, 2421-2430.

Dimitriades, B. (1996): "Scientific Basis for the VOC Reactivity Issues Raised by Section 183(e) of the Clean Air Act Amendments of 1990," J. Air Waste Manage. Assoc. 46, 963-970.

Dodge, M. C. (1984): "Combined effects of organic reactivity and NMHC/NOx ratio on photochemical oxidant formation -- a modeling study," Atmos. Environ., 18, 1657.

EPA (1984): "Guideline for Using the Carbon Bond Mechanism in City-Specific EKMA," EPA-450/4-84-005, February.

Gery, M. W., G. Z. Whitten, and J. P. Killus (1988): "Development and Testing of the CBM-IV For Urban and Regional Modeling,", EPA-600/ 3-88-012, January.

Grosjean, E. and D. Grosjean (1996): "Carbonyl Products of the Gas-Phase Reaction of Ozone with 1-Alkenes," Atmos. Environ., 30, 4107-4113.

Johnson, G. M. (1983): "Factors Affecting Oxidant Formation in Sydney Air," in "The Urban Atmosphere -- Sydney, a Case Study." Eds. J. N. Carras and G. M. Johnson (CSIRO, Melbourne), pp. 393-408.

Jeffries, H. E. (1991): "UNC Solar Radiation Models," unpublished draft report for EPA Cooperative Agreements CR813107, CR813964 and CR815779". Undated.

Jeffries, H. E., K. G. Sexton, J. R. Arnold, and T. L. Kale (1989): "Validation Testing of New Mechanisms with Outdoor Chamber Data. Volume 2: Analysis of VOC Data for the CB4 and CAL Photochemical Mechanisms," Final Report, EPA-600/3-89-010b.

Jeffries, H. E. and R. Crouse (1991): "Scientific and Technical Issues Related to the Application of Incremental Reactivity. Part II: Explaining Mechanism Differences," Report prepared for Western States Petroleum Association, Glendale, CA, October.

Kirchner, F., F. Zabel and K. H. Becker (1992): "Kinetic Behavior of Benzoylperoxy Radicals in the Presence of NO and NO_2," Chem. Phys. Lett. 191, 169-174.

Majer, J. R., Naman, S-A. M. A., and Robb, J. C. (1969): "Photolysis of Aromatic Aldehydes," Trans. Faraday Soc. 65, 1846-1853.

Marchello, J. M. and D. A. Sterling (1991): "Fate of Styrene in Air," Final Report to Styrene Information and Research Center, November 1.

NASA (1997): "Chemical Kinetics and Photochemical Data for Use in Stratospheric Modeling, Evaluation Number 12," JPL Publication 97-4, Jet Propulsion Laboratory, Pasadena, California, January.

Pitts, J. N., Jr., E. Sanhueza, R. Atkinson, W. P. L. Carter, A. M. Winer, G. W. Harris, and C. N. Plum (1984): "An Investigation of the Dark Formation of Nitrous Acid in Environmental Chambers," Int. J. Chem. Kinet., 16, 919-939.

Stockwell, W. R., P. Middleton, J. S. Chang, and X. Tang (1990): "The Second Generation Regional Acid Deposition Model Chemical Mechanism for Regional Air Quality Modeling," J. Geophys. Res. 95, 16343- 16376.

Tuazon, E. C., R. Atkinson, C. N. Plum, A. M. Winer, and J. N. Pitts, Jr. (1983): "The Reaction of Gas-Phase N_2O_5 with Water Vapor," Geophys. Res. Lett. 10, 953-956.

Tuazon, E. C., J. Arey, R. Atkinson, and S. M. Aschmann (1993): "Gas-Phase Reactions of 2-Vinylpyridine and Styrene with OH and NO_3 Radicals and O_3," Environ. Sci. Technol. 27, 1832-1841.

Zafonte, L., P. L. Rieger, and J. R. Holmes (1977): "Nitrogen Dioxide Photolysis in the Los Angeles Atmosphere," Environ. Sci. Technol. 11, 483-487.

APPENDIX A
LISTING OF THE CHEMICAL MECHANISM

The chemical mechanism used in the environmental chamber and atmospheric model simulations discussed in this report is given in Tables A-1 through A-4. Table A-1 lists the species used in the mechanism, Table A-2 gives the reactions and rate constants, Table A-3 gives the parameters used to calculate the rates of the photolysis reactions, and Table A-4 gives the values and derivations of the chamber-dependent parameters used when modeling the environmental chamber experiments. Footnotes to Table A-2 indicate the format used for the reaction listing.

Table A-1. List of species in the chemical mechanism used in the model simulations for this study.

Name	Description
Constant Species.	
O2	Oxygen
M	Air
H2O	Water
HV	Light
Active Inorganic Species.	
O3	Ozone
NO	Nitric Oxide
NO2	Nitrogen Dioxide
NO3	Nitrate Radical
N2O5	Nitrogen Pentoxide
HONO	Nitrous Acid
HNO3	Nitric Acid
HNO4	Peroxynitric Acid
HO2H	Hydrogen Peroxide
Active Radical Species and Operators.	
HO.	Hydroxyl Radicals
HO2.	Hydroperoxide Radicals
C-O2.	Methyl Peroxy Radicals
RO2.	Operator to Calculate Total Higher Organic Peroxy Radicals
CCO-O2.	Acetyl Peroxy Radicals
RCO3.	Operator to Calculate Total Higher Acetyl Peroxy Radicals
Active Reactive Organic Product Species.	
CO	Carbon Monoxide
HCHO	Formaldehyde
CCHO	Acetaldehyde
RCHO	Lumped C3+ Aldehydes

Table A-1, (continued)

Name	Description
ACET	Acetone
MEK	Ketones and other non-aldehyde oxygenated products which react with OH radicals slower than 5 x 10^{-12} cm^3 $molec^{-1}$ s^{-1}
PROD2	Ketones and other non-aldehyde oxygenated products which react with OH radicals faster than 5 x 10^{-12} cm^3 $molec^{-1}$ s^{-1}
PHEN	Phenol
CRES	Cresols
BALD	Aromatic aldehydes (e.g., benzaldehyde)
GLY	Glyoxal
MGLY	Methyl Glyoxal
BACL	Biacetyl or other lumped α-dicarbonyls, including α-keto esters
DCB1	Reactive Aromatic Fragmentation Products represented by 2-butene 1,3-dial.
DCB2	Reactive Aromatic Fragmentation Products which photolyze with a-dicarbonyl-like action spectrum.
DCB3	Reactive Aromatic Fragmentation Products which photolyze with acrolein action spectrum.
DCB4	Reactive Aromatic Fragmentation Products which do not photolyze rapidly.
NPHE	Nitrophenols
ACROLEIN	Acrolein
METHACRO	Methacrolein
MVK	Methyl Vinyl Ketone
ISOPROD	Lumped isoprene product species
MEOH	Methanol
ETOH	Ethanol
COOH	Methyl Hydroperoxide
ROOH	Lumped higher organic hydroperoxides
RNO3	Organic Nitrates
PAN	Peroxy Acetyl Nitrate
PAN2	PPN and other higher alkyl PAN analogues
GPAN	PAN analogue formed from Glyoxal
PBzN	PAN analogues formed from Aromatic Aldehydes
MA-PAN	PAN analogue formed from Methacrolein
Non-Reacting Species	
CO2	Carbon Dioxide
XC	"Lost Carbon"
XN	"Lost Nitrogen"
H2	Hydrogen
Low Reactivity Compounds or Unknown Products Represented as Unreactive	
HCOOH	Formic Acid
CCO-OH	Acetic Acid
RCO-OH	Higher organic acids
CCO-OOH	Peroxy Acetic Acid
RCO-OOH	Higher organic peroxy acids
COH	Methanol (when formed in some peroxy + peroxy radical operator reactions)
ROH	Higher alcohols (when formed in some peroxy + peroxy radical operator reactions)
CONO2	Methyl Nitrate
HCHO2-STAB	Stabilization products from the $HCHO_2$ Crigiee biradical
CCHO2-STAB	Stabilization products from the CH_3CHO_2 Crigiee biradical

Table A-1, (continued)

Name	Description
RCHO2-STAB	Stabilization products from Other Crigiee biradicals
NROG	Unspecified Unreactive Carbon
NOX-Wall	NOx absorbed on the chamber walls (used as counter species in chamber model only)
General Steady State Radical Species	
O3P	Ground State Oxygen Atoms
O*1D2	Excited Oxygen Atoms
C-O.	Methoxy Radicals
TBU-O.	t-Butoxy Radicals
BZ-O.	Phenoxy Radicals
BZ(NO2)-O.	Nitro-substituted Phenoxy Radical
HOCOO.	Radical formed when Formaldehyde reacts with HO_2
(HCOCHO2)	Crigiee Biradicals formed from the reaction of O3 with unsaturated carbonyls with HCO-CH_2= groups
(C2(O2)CHO)	Crigiee Biradicals formed from the reaction of O3 with other unsaturated carbonyls.
Steady State Peroxy Radical Species or Operators	
RO2-R.	Peroxy Radical Operator representing NO to NO2 conversion with HO2 formation.
RO2-N.	Peroxy Radical Operator representing NO consumption with organic nitrate formation.
RO2-XN.	Peroxy Radical Operator representing NO consumption with formation of organic nitrates which are represented as unreactive.
RO2-NP.	Peroxy Radical Operator representing NO consumption with nitrophenol formation
R2O2.	Peroxy Radical Operator representing NO to NO2 conversion.
RCO-O2.	Peroxy Propionyl and higher peroxy acyl Radicals
HCOCO-O2.	Peroxyacyl radical formed from Glyoxal
BZCO-O2.	Peroxyacyl radical formed from Aromatic Aldehydes
MA-RCO3.	Peroxyacyl radicals formed from methacrolein and other acroleins.
[*radical*]	One such operator for each of the above steady state peroxy radical species or operators: Operator used to represent the reactions of the radical after its contribution to RO2. or RCO3. formation has already been taken into account.
Primary Organics Represented explicitly	
CH4	Methane
ETHANE	Ethane
N-C4	n-Butane
N-C6	n-Hexane
N-C8	n-Octane
TOLUENE	Toluene
M-XYLENE	m-Xylene
135-TMB	1,3,5-Trimethyl Benzene
ETHENE	Ethene
PROPENE	Propene
T-2-BUTE	trans-2-Butene
STYRENE	Styrene
Biogenic Compounds in the EKMA Simulations	
ISOP	Isoprene
APIN	α-Pinene
UNKN	Unknown biogenics.

Table A-1, (continued)

Name	Description
Lumped species used to represent the Base ROG mixture in the EKMA model simulations.	
ALK1	Alkanes and other saturated compounds with kOH < 10^4 ppm^{-1} min^{-1}.
ALK2	Alkanes and other saturated compounds with kOH ≥ 10^4 ppm^{-1} min^{-1}.
ARO1	Aromatics with kOH < $2x10^4$ ppm^{-1} min^{-1}.
ARO2	Aromatics with kOH ≥ $2x10^4$ ppm^{-1} min^{-1}.
OLE2	Alkenes (other than ethene) with kOH < $7x10^4$ ppm^{-1} min^{-1}.
OLE3	Alkenes with kOH ≥ $7x10^4$ ppm^{-1} min^{-1}.
ALD1	Lumped higher aldehydes which are emitted.

Table A-2. List of reactions in the chemical mechanism used in the model simulations for this study.

Rxn. Label	Kinetic Parameters [a] k(300)	A	Ea	B	Reactions [b]
Inorganic Reactions					
1	(Phot. Set = NO2)				NO2 + HV = NO + O3P
2	5.91E-34	5.91E-34	0.00	-2.80	O3P + O2 + M = O3 + M
3	8.34E-15	8.00E-12	4.09	0.00	O3P + O3 = 2 O2
4	1.00E-31	1.00E-31	0.00	-1.60	O3P + NO + M = NO2 + M
5	9.70E-12	6.50E-12	-0.24	0.00	O3P + NO2 = NO + O2
6	1.79E-12	(Falloff Kinetics)			O3P + NO2 = NO3 + M
	k0 =	9.00E-32	0.00	-2.00	
	kINF =	2.20E-11	0.00	0.00	
		F= 0.80	n= 1.00		
8	1.87E-14	1.80E-12	2.72	0.00	O3 + NO = NO2 + O2
9	3.72E-17	1.40E-13	4.91	0.00	O3 + NO2 = O2 + NO3
10	2.60E-11	1.80E-11	-0.22	0.00	NO + NO3 = 2 NO2
11	1.93E-38	3.30E-39	-1.05	0.00	NO + NO + O2 = 2 NO2
12	1.53E-12	(Falloff Kinetics)			NO2 + NO3 = N2O5
	k0 =	2.80E-30	0.00	-3.50	
	kINF =	2.00E-12	0.00	0.20	
		F= 0.45	n= 1.00		
13	6.74E-02	(Falloff Kinetics)			N2O5 = NO2 + NO3
	k0 =	1.00E-03	21.86	-3.50	
	kINF =	9.70E+14	22.02	0.10	
		F= 0.45	n= 1.00		
14	2.60E-22	(No T Dependence)			N2O5 + H2O = 2 HNO3
14a	0.00E+00	(No T Dependence)			N2O5 + H2O + H2O = 2 HNO3 + H2O
17	6.75E-16	4.50E-14	2.50	0.00	NO2 + NO3 = NO + NO2 + O2
18	(Phot. Set = NO3NO)				NO3 + HV = NO + O2
19	(Phot. Set = NO3NO2)				NO3 + HV = NO2 + O3P
20	(Phot. Set = O3O3P)				O3 + HV = O3P + O2
21	(Phot. Set = O3O1D)				O3 + HV = O*1D2 + O2
22	2.20E-10	(No T Dependence)			O*1D2 + H2O = 2 HO.
23	2.87E-11	2.09E-11	-0.19	0.00	O*1D2 + M = O3P + M
24	7.31E-12	(Falloff Kinetics)			HO. + NO = HONO
	k0 =	7.00E-31	0.00	-2.60	
	kINF =	3.60E-11	0.00	-0.10	
		F= 0.60	n= 1.00		
25	(Phot. Set = HONO-NO)				HONO + HV = HO. + NO
26	(Phot. Set = HONO-NO2)				HONO + HV = HO2. + NO2
27	6.42E-12	2.70E-12	-0.52	0.00	HO. + HONO = H2O + NO2
28	8.81E-12	(Falloff Kinetics)			HO. + NO2 = HNO3
	k0 =	2.43E-30	0.00	-3.10	
	kINF =	1.67E-11	0.00	-2.10	
		F= 0.60	n= 1.00		
29	2.00E-11	(No T Dependence)			HO. + NO3 = HO2. + NO2
30	1.44E-13	5.45E-15	-1.95	0.00	HO. + HNO3 = H2O + NO3
31	(Phot. Set = HNO3)				HNO3 + HV = HO. + NO2
32A	1.30E-13	(No T Dependence)			HO. + CO = HO2. + CO2
32B	3.19E-33	(No T Dependence)			HO. + CO + M = HO2. + CO2 + M
33	6.78E-14	1.90E-12	1.99	0.00	HO. + O3 = HO2. + O2
34	8.36E-12	3.40E-12	-0.54	0.00	HO2. + NO = HO. + NO2
35	1.37E-12	(Falloff Kinetics)			HO2. + NO2 = HNO4
	k0 =	1.80E-31	0.00	-3.20	
	kINF =	4.70E-12	0.00	0.00	
		F= 0.60	n= 1.00		
36	9.61E-02	(Falloff Kinetics)			HNO4 = HO2. + NO2
	k0 =	4.10E-05	21.16	0.00	
	kINF =	5.70E+15	22.20	0.00	
		F= 0.50	n= 1.00		
37	(Phot. Set = HO2NO2)				HNO4 + HV = 0.61 "HO2. + NO2" + 0.39 "HO. + NO3"
38	4.98E-12	1.50E-12	-0.72	0.00	HNO4 + HO. = H2O + NO2 + O2
39	1.89E-15	1.40E-14	1.19	0.00	HO2. + O3 = HO. + 2 O2
40A	1.63E-12	2.20E-13	-1.19	0.00	HO2. + HO2. = HO2H + O2
40B	3.48E-30	3.08E-34	-5.56	0.00	HO2. + HO2. + H2O = HO2H + O2 + H2O
40C	4.85E-32	1.85E-33	-1.95	0.00	HO2. + HO2. + M = HO2H + O2 + M
40D	0.00E+00	0.00E+00	-6.32	0.00	HO2. + HO2. + M + H2O = HO2H + O2 + M + H2O
41	4.00E-12	(No T Dependence)			NO3 + HO2. = HO. + NO2 + O2
42	2.41E-16	8.50E-13	4.87	0.00	NO3 + NO3 = 2 NO2 + O2
43	(Phot. Set = H2O2)				HO2H + HV = 2 HO.
44	1.70E-12	2.90E-12	0.32	0.00	HO2H + HO. = HO2. + H2O
45	1.10E-10	4.80E-11	-0.50	0.00	HO. + HO2. = H2O + O2
HNN3	0.00E+00	(No T Dependence)			NO3 + HONO = HNO3 + NO2
HNO3	0.00E+00	(No T Dependence)			O3 + HONO = HNO3 + O2

Table A-2 (continued)

Rxn. Label	Kinetic Parameters [a] k(300)	A	Ea	B	Reactions [b]
General Organic Radical Reactions					
MER1	7.50E-12	2.90E-12	-0.57	0.00	C-O2. + NO = NO2 + C-O.
MER4	5.12E-12	3.80E-13	-1.55	0.00	C-O2. + HO2. = COOH + O2
MEN3	0.00E+00	(No T Dependence)			C-O2. + NO3 = C-O. + NO2 + O2
MER5	2.60E-13	2.45E-14	-1.41	0.00	C-O2. + C-O2. = MEOH + HCHO + O2
MER6	1.08E-13	5.90E-13	1.01	0.00	C-O2. + C-O2. = 2 C-O. + O2
MER7	1.97E-15	7.20E-14	2.15	0.00	C-O. + O2 = HCHO + HO2.
MER8	1.24E-11	(Falloff Kinetics)			C-O. + NO2 = CONO2
	k0 =	2.80E-29	0.00	-4.50	
	kINF =	2.00E-11	0.00	0.00	
		F= 0.22 n= 1.00			
TBON	2.40E-11	(No T Dependence)			TBU-O. + NO2 = RNO3 + -2 XC
TBOD	1.18E+03	7.50E+14	16.20	0.00	TBU-O. = ACET + C-O2.
Reactions of Peroxy Radical Operators					
LPNO	8.96E-12	2.70E-12	-0.72	0.00	RO2. + NO = NO
LPH2	1.45E-11	1.90E-13	-2.58	0.00	RO2. + HO2. = HO2.
LPN3	(Same k as Reaction MEN3)				RO2. + NO3 = NO3
LPME	2.00E-13	(No T Dependence)			RO2. + C-O2. = C-O2.
LPAP	1.00E-11	(No T Dependence)			RO2. + CCO-O2. = CCO-O2.
LPP2	1.00E-11	(No T Dependence)			RO2. + RCO3. =
LPR2	3.00E-14	(No T Dependence)			RO2. + RO2. =
R2XX	(Fast)				R2O2. = [R2O2] + RO2.
R2NO	(Same k as Reaction LPNO)				[R2O2] + NO = NO2
R2H2	(Same k as Reaction LPH2)				[R2O2] + HO2. = HO2.
R2ME	(Same k as Reaction LPME)				[R2O2] + C-O2. = C-O2.
R2N3	(Same k as Reaction MEN3)				[R2O2] + NO3 = NO2
R2AP	(Same k as Reaction LPAP)				[R2O2] + CCO-O2. = CCO-O2.
R2P2	(Same k as Reaction LPP2)				[R2O2] + RCO3. = RCO3.
R2R2	(Same k as Reaction LPR2)				[R2O2] + RO2. = RO2.
RRXX	(Fast)				RO2-R. = [RO2-R] + RO2.
RRNO	(Same k as Reaction LPNO)				[RO2-R] + NO = NO2 + HO2.
RRH2	(Same k as Reaction LPH2)				[RO2-R] + HO2. = ROOH + O2 + -3 XC
RRME	(Same k as Reaction LPME)				[RO2-R] + C-O2. = 0.5 C-O. + 0.25 "HCHO + COH"
RRN3	(Same k as Reaction MEN3)				[RO2-R] + NO3 = NO2 + HO2.
RRAP	(Same k as Reaction LPAP)				[RO2-R] + CCO-O2. = 0.5 "C-O2. + CO2 + CCO-OH"
RRP2	(Same k as Reaction LPP2)				[RO2-R] + RCO3. = RCO3.
RRR2	(Same k as Reaction LPR2)				[RO2-R] + RO2. = RO2.
RNXX	(Fast)				RO2-N. = [RO2-N] + RO2.
RNNO	(Same k as Reaction LPNO)				[RO2-N] + NO = RNO3
RNH2	(Same k as Reaction LPH2)				[RO2-N] + HO2. = ROOH + 2 XC
RNME	(Same k as Reaction LPME)				[RO2-N] + C-O2. = 0.5 "C-O. + MEK + HO2." + 0.25 "HCHO + MEOH + MEK + ROH" + O2 + 1.25 XC
RNN3	(Same k as Reaction MEN3)				[RO2-N] + NO3 = NO2 + HO2. + MEK + XC
RNAP	(Same k as Reaction LPAP)				[RO2-N] + CCO-O2. = 0.5 "C-O2. + CO2 + HO2. + CCO-OH" + MEK + O2 + XC
RNP2	(Same k as Reaction LPP2)				[RO2-N] + RCO3. = RCO3. + MEK + 0.5 HO2. + XC
RNR2	(Same k as Reaction LPR2)				[RO2-N] + RO2. = RO2. + 0.5 "MEK + HO2. + ROH" + O2 + 1.5 XC
RXXX	(Fast)				RO2-XN. = [RO2-XN] + RO2.
RXNO	(Same k as Reaction LPNO)				[RO2-XN] + NO = XN
RXH2	(Same k as Reaction LPH2)				[RO2-XN] + HO2. = ROOH + -3 XC
RXME	(Same k as Reaction LPME)				[RO2-XN] + C-O2. = 0.5 C-O. + 0.25 "HCHO + COH"
RXN3	(Same k as Reaction MEN3)				[RO2-XN] + NO3 = NO2 + HO2.
RXAP	(Same k as Reaction LPAP)				[RO2-XN] + CCO-O2. = 0.5 "C-O2. + CO2 + CCO-OH"
RXP2	(Same k as Reaction LPP2)				[RO2-XN] + RCO3. = RCO3.
RXR2	(Same k as Reaction LPR2)				[RO2-XN] + RO2. = RO2.
RPXX	(Fast)				RO2-NP. = [RO2-NP] + RO2.
RPNO	(Same k as Reaction LPNO)				[RO2-NP] + NO = NPHE
RPH2	(Same k as Reaction LPH2)				[RO2-NP] + HO2. = PHEN
RPME	(Same k as Reaction LPME)				[RO2-NP] + C-O2. = C-O. + BZ-O.
RPN3	(Same k as Reaction MEN3)				[RO2-NP] + NO3 = NO2 + BZ-O.
RPAP	(Same k as Reaction LPAP)				[RO2-NP] + CCO-O2. = C-O2. + CO2 + BZ-O.
RPP2	(Same k as Reaction LPP2)				[RO2-NP] + RCO3. = RCO3. + BZ-O.
RPR2	(Same k as Reaction LPR2)				[RO2-NP] + RO2. = RO2. + 0.5 "BZ-O. + PHEN"

Table A-2 (continued)

Rxn. Label	Kinetic Parameters [a] k(300)	A	Ea	B	Reactions [b]
Reactions of Acyl Peroxy Radicals and Acyl Peroxy Radical Operators and PANs					
APN2	1.04E-11	(Falloff Kinetics)			CCO-O2. + NO2 = PAN
	k0 =	2.57E-28	0.00	-7.10	
	kINF =	1.20E-11	0.00	-0.90	
		F= 0.30 n= 1.00			
DPAN	7.04E-04	(Falloff Kinetics)			PAN = CCO-O2. + NO2
	k0 =	4.90E-03	24.05	0.00	
	kINF =	4.00E+16	27.03	0.00	
		F= 0.30 n= 1.00			
APNO	2.18E-11	(No T Dependence)			CCO-O2. + NO = C-O2. + CO2 + NO2
APH2	1.38E-11	4.30E-13	-2.07	0.00	CCO-O2. + HO2. = 0.75 "CCO-OOH +O2" + 0.25 "CCO-OH + O3"
APME	1.26E-11	5.10E-12	-0.54	0.00	CCO-O2. + C-O2. = 0.15 "C-O2. + CO2 + C-O." + 0.85 "CCO-OH + HCHO" + O2
APAP	1.64E-11	2.80E-12	-1.05	0.00	CCO-O2. + CCO-O2. = 2 "C-O2. + CO2" + O2
LAN2	1.20E-11	1.20E-11	0.00	-0.90	RCO3. + NO2 = NO2
LANO	(Same k as Reaction APNO)				RCO3. + NO = NO
LAH2	(Same k as Reaction APH2)				RCO3. + HO2. = HO2.
LAME	(Same k as Reaction APME)				RCO3. + C-O2. = C-O2.
LAAP	(Same k as Reaction APAP)				RCO3. + CCO-O2. = CCO-O2.
LALA	(Same k as Reaction APAP)				RCO3. + RCO3. =
PPXX	(Fast)				RCO-O2. = [RCO-O2] + RCO3.
PPN2	(Same k as Reaction LAN2)				[RCO-O2] + NO2 = PAN2
PPNO	(Same k as Reaction APNO)				[RCO-O2] + NO = NO2 + CCHO + RO2-R. + CO2
PPH2	(Same k as Reaction APH2)				[RCO-O2] + HO2. = RCO-OOH + O2
PPME	(Same k as Reaction APME)				[RCO-O2] + C-O2. = 0.15 "CCHO + RO2-R. + CO2 + C-O." + 0.85 "RCO-OH + HCHO" + O2
PPAP	(Same k as Reaction APAP)				[RCO-O2] + CCO-O2. = 2 CO2 + C-O2. + CCHO + RO2-R. + O2
PPR2	(Same k as Reaction LPAP)				[RCO-O2] + RO2. = RO2. + 0.5 "RCO-OH + CCHO + RO2-R. + CO2"
PPLA	(Same k as Reaction APAP)				[RCO-O2] + RCO3. = RCO3. + CCHO + RO2-R. + CO2
PAN2	5.90E-04	2.00E+15	25.44	0.00	PAN2 = RCO-O2. + NO2
GPXX	(Fast)				HCOCO-O2. = [HCOCO-O2] + RCO3.
GPN2	(Same k as Reaction LAN2)				[HCOCO-O2] + NO2 = GPAN
GPNO	(Same k as Reaction APNO)				[HCOCO-O2] + NO = NO2 + CO2 + CO + HO2.
GPH2	(Same k as Reaction APH2)				[HCOCO-O2] + HO2. = RCO-OOH + O2
GPME	(Same k as Reaction APME)				[HCOCO-O2] + C-O2. = 0.15 "HO2. + CO + CO2 + C-O." + 0.85 "RCO-OH + HCHO" + O2
GPAP	(Same k as Reaction APAP)				[HCOCO-O2] + CCO-O2. = 2 CO2 + C-O2. + HO2. + CO + O2
GPR2	(Same k as Reaction LPAP)				[HCOCO-O2] + RO2. = RO2. + 0.5 "RCO-OH + HO2. + CO + CO2"
GPLA	(Same k as Reaction APAP)				[HCOCO-O2] + RCO3. = RCO3. + HO2. + CO + CO2
GPAN	(Same k as Reaction PAN2)				GPAN = HCOCO-O2. + NO2
BPXX	(Fast)				BZCO-O2. = [BZCO-O2] + RCO3.
BPN2	(Same k as Reaction LAN2)				[BZCO-O2] + NO2 = PBZN
BPNO	(Same k as Reaction APNO)				[BZCO-O2] + NO = NO2 + CO2 + BZ-O. + R2O2.
BPH2	(Same k as Reaction APH2)				[BZCO-O2] + HO2. = RCO-OOH + O2
BPME	(Same k as Reaction APME)				[BZCO-O2] + C-O2. = 0.15 "BZ-O. + R2O2. + CO2 + C-O." + 0.85 "RCO-OH + HCHO" + O2
BPAP	(Same k as Reaction APAP)				[BZCO-O2] + CCO-O2. = 2 CO2 + C-O2. + BZ-O. + R2O2.
BPR2	(Same k as Reaction LPAP)				[BZCO-O2] + RO2. = RO2. + 0.5 "RCO-OH + BZ-O. + R2O2. + CO2"
BPLA	(Same k as Reaction APAP)				[BZCO-O2] + RCO3. = RCO3. + BZ-O. + R2O2. + CO2
BPAN	(Same k as Reaction PAN2)				PBZN = BZCO-O2. + NO2
MPXX	(Fast)				MA-RCO3. = [MA-RCO3] + RCO3.
MPN2	(Same k as Reaction LAN2)				[MA-RCO3] + NO2 = MA-PAN
MPNO	(Same k as Reaction APNO)				[MA-RCO3] + NO = NO2 + CO2 + HCHO + CCO-O2.
MPH2	(Same k as Reaction APH2)				[MA-RCO3] + HO2. = RCO-OOH + O2 + XC
MPME	(Same k as Reaction APME)				[MA-RCO3] + C-O2. = 0.15 "HCHO + CCO-O2. + CO2 + C-O." + 0.85 "RCO-OH + HCHO + XC" + O2
MPAP	(Same k as Reaction APAP)				[MA-RCO3] + CCO-O2. = 2 CO2 + C-O2. + HCHO + CCO-O2. + O2
MPR2	(Same k as Reaction LPAP)				[MA-RCO3] + RO2. = RO2. + 0.5 "RCO-OH + HCHO + CCO-O2. + CO2 + XC"
MPLA	(Same k as Reaction APAP)				[MA-RCO3] + RCO3. = RCO3. + HCHO + CCO-O2. + CO2
MPPN	4.79E-04	1.60E+16	26.80	0.00	MA-PAN = MA-RCO3. + NO2
Reactions of Organic Product Species					
FAHV	(Phot. Set = HCHO_R)				HCHO + HV = 2 HO2. + CO
FAVS	(Phot. Set = HCHO_M)				HCHO + HV = H2 + CO
FAOH	9.19E-12	8.60E-12	-0.04	0.00	HCHO + HO. = HO2. + CO + H2O

Table A-2 (continued)

Rxn. Label	Kinetic Parameters [a] k(300)	A	Ea	B	Reactions [b]
FAH2	7.79E-14	9.70E-15	-1.24	0.00	HCHO + HO2. = HOCOO.
FAHR	1.77E+02	2.40E+12	13.91	0.00	HOCOO. = HO2. + HCHO
FAHN	(Same k as Reaction MER1)				HOCOO. + NO = HCOOH + NO2 + HO2.
FAN3	6.07E-16	2.00E-12	4.83	0.00	HCHO + NO3 = HNO3 + HO2. + CO
AAOH	1.57E-11	5.60E-12	-0.62	0.00	CCHO + HO. = CCO-O2. + H2O
AAHV	(Phot. Set = CCHO_R)				CCHO + HV = CO + HO2. + C-O2.
AAN3	2.84E-15	1.40E-12	3.70	0.00	CCHO + NO3 = HNO3 + CCO-O2.
PAOH	2.00E-11	(No T Dependence)			RCHO + HO. = 0.034 RO2-R. + 0.001 RO2-N. + 0.965 RCO-O2. + 0.034 CO + 0.034 CCHO + -0.003 XC
PAHV	(Phot. Set = C2CHO)				RCHO + HV = CCHO + RO2-R. + CO + HO2.
PAN3	(Same k as Reaction AAN3)				NO3 + RCHO = HNO3 + RCO-O2.
K3OH	2.22E-13	2.80E-12	1.51	0.00	ACET + HO. = HCHO + CCO-O2. + R2O2.
K3HV	(Phot. Set = ACETONE)				ACET + HV = CCO-O2. + C-O2.
K4OH	1.16E-12	2.92E-13	-0.82	2.00	HO. + MEK = 0.374 RO2-R. + 0.042 RO2-N. + 0.609 R2O2. + 0.491 CCO-O2. + 0.093 RCO-O2. + 0.109 HCHO + 0.483 CCHO + 0.374 RCHO + 0.332 XC
K4HV	(Phot. Set = KETONE)				MEK + HV + #(0.1) = CCO-O2. + CCHO + RO2-R.
K6OH	9.64E-12	(No T Dependence)			HO. + PROD2 = 0.521 RO2-R. + 0.044 RO2-N. + 0.342 HO2. + 0.082 CCO-O2. + 0.011 RCO-O2. + 0.439 HCHO + 0.945 RCHO + 1.308 XC
K6HV	(Phot. Set = KETONE)				PROD2 + HV + #(0.1) = RO2-R. + 0.015 R2O2. + CCO-O2. + 0.038 HCHO + 0.988 RCHO + -0.003 XC
MeOH	9.54E-13	5.41E-13	-0.34	2.00	HO. + MEOH = 0.85 HO2. + 0.15 C-O. + 0.85 HCHO
EtOH	3.27E-12	5.56E-13	-1.06	2.00	HO. + ETOH = 0.05 RO2-R. + 0.078 HCHO + 0.961 CCHO + 0.95 HO2.
MER9	5.46E-12	2.90E-12	-0.38	0.00	COOH + HO. = H2O + 0.35 "HCHO + HO." + 0.65 C-O2.
MERA	(Phot. Set = COOH)				COOH + HV = C-O. + HO.
LPR9	1.10E-11	(No T Dependence)			ROOH + HO. = H2O + RCHO + 0.34 RO2-R. + 0.66 HO.
LPRA	(Phot. Set = COOH)				ROOH + HV = RCHO + HO2. + HO.
RNOH	2.99E-12	(No T Dependence)			HO. + RNO3 = 0.505 RO2-R. + 0.111 RO2-N. + 0.708 R2O2. + 0.004 HCHO + 0.393 CCHO + 0.455 RCHO + 0.032 MEK + 0.034 PROD2 + 0.136 XC + 0.251 XN + 0.365 RNO3 + 0.384 NO2
RNHV	(Phot. Set = IC3ONO2)				RNO3 + HV = 0.868 RO2-R. + 0.132 HO2. + 0.031 CCHO + 0.031 RCHO + 0.132 MEK + 0.838 PROD2 + -0.706 XC + NO2
GLHV	(Phot. Set = GLY_R)				GLY + HV = 2 "CO + HO2."
GLVM	(Phot. Set = GLY_ABS)				GLY + HV + 0.006 = HCHO + CO
GLOH	1.14E-11	(No T Dependence)			GLY + HO. = 0.63 HO2. + 1.26 CO + 0.37 HCOCO-O2.
GLN3	(Same k as Reaction AAN3)				GLY + NO3 = HNO3 + 0.63 HO2. + 1.26 CO + 0.37 HCOCO-O2.
MGHV	(Phot. Set = MGLY_ADJ)				MGLY + HV = HO2. + CO + CCO-O2.
MGOH	1.50E-11	(No T Dependence)			MGLY + HO. = CO + CCO-O2.
MGN3	(Same k as Reaction AAN3)				MGLY + NO3 = HNO3 + CO + CCO-O2.
BAHV	(Phot. Set = BACL_ADJ)				BACL + HV = 2 CCO-O2.
PHOH	2.63E-11	(No T Dependence)			HO. + PHEN = 0.24 BZ-O. + 0.76 RO2-R. + 0.23 GLY + 4.1 XC
PHN3	3.78E-12	(No T Dependence)			NO3 + PHEN = HNO3 + BZ-O.
CROH	4.20E-11	(No T Dependence)			HO. + CRES = 0.24 BZ-O. + 0.76 RO2-R. + 0.23 MGLY + 4.87 XC
CRN3	1.37E-11	(No T Dependence)			NO3 + CRES = HNO3 + BZ-O. + XC
BZOH	1.29E-11	(No T Dependence)			BALD + HO. = BZCO-O2.
BZHV	(Phot. Set = BZCHO)				BALD + HV + #(0.05) = 7 XC
BZNT	2.71E-15	1.40E-12	3.72	0.00	BALD + NO3 = HNO3 + BZCO-O2.
BRN2	3.79E-11	2.30E-11	-0.30	0.00	BZ-O. + NO2 = NPHE
BRH2	(Same k as Reaction LPH2)				BZ-O. + HO2. = PHEN
BRXX	1.00E-03	(No T Dependence)			BZ-O. = PHEN
NPN3	(Same k as Reaction PHN3)				NPHE + NO3 = HNO3 + BZ(NO2)-O.
BNN2	(Same k as Reaction BRN2)				BZ(NO2)-O. + NO2 = 2 XN + 6 XC
BNH2	(Same k as Reaction LPH2)				BZ(NO2)-O. + HO2. = NPHE
BNXX	(Same k as Reaction BRXX)				BZ(NO2)-O. = NPHE
D1OH	5.00E-11	(No T Dependence)			DCB1 + HO. = RCHO + RO2-R. + CO

Table A-2 (continued)

Rxn. Label	Kinetic Parameters [a] k(300)	A	Ea	B	Reactions [b]
D1HV	(Phot. Set = ACROLEIN)				DCB1 + HV + #(3.4E-3) = HO2. + 2 CO + RO2-R. + GLY + R2O2.
D1O3	2.00E-18	(No T Dependence)			DCB1 + O3 = GLY + (HCOCHO2)
ZAC	(Fast)				(HCOCHO2) = 0.12 "HO2. + HO." + 0.24 CO + 0.74 XC + 0.51 "CO2 + HCHO"
D2OH	5.00E-11	(No T Dependence)			DCB2 + HO. = R2O2. + RCHO + CCO-O2.
D2HV	(Phot. Set = MGLY_ABS)				DCB2 + HV + #(0.365) = RO2-R. + 0.5 "CCO-O2. + HO2." + CO + R2O2. + 0.5 "GLY + MGLY + XC"
D3OH	5.00E-11	(No T Dependence)			DCB3 + HO. = R2O2. + RCHO + CCO-O2.
D3HV	(Phot. Set = ACROLEIN)				DCB3 + HV + #(7.28) = RO2-R. + 0.5 "CCO-O2. + HO2." + CO + R2O2. + 0.5 "GLY + MGLY + XC"
D4OH	5.00E-11	(No T Dependence)			DCB4 + HO. = RCHO + RO2-R. + CO + 2 XC
D4O3	2.00E-18	(No T Dependence)			DCB4 + O3 = 0.5 "MGLY + (HCOCHO2) + GLY + (C2(O2)CHO)" + XC
RMAZ	(Fast)				(C2(O2)CHO) = HO. + R2O2. + HCHO + HCOCO-O2.
ACOH	1.99E-11	(No T Dependence)			HO. + ACROLEIN = 0.25 RO2-R. + 0.167 CO +0.083 HCHO + 0.167 RCHO + 0.083 GLY +0.75 MA-RCO3. + -.917 XC
ACO3	3.07E-19	1.36E-15	5.01	0.00	O3 + ACROLEIN = 0.32 RO2-R. + 0.32 HO. +0.77 CO + 0.135 CO2 + 0.57 HCHO + 0.5 GLY +0.185 HCHO2-STAB + 0.17 RCHO2-STAB + -0.17 XC
ACN3	1.15E-14	(No T Dependence)			NO3 + ACROLEIN = 0.964 RO2-R. + 0.036 RO2-N. +0.964 CO + 0.964 RCHO + -1.036 XC + XN
ACOP	4.32E-12	(No T Dependence)			O3P + ACROLEIN = RCHO
ACHV	(Phot. Set = ACROLEIN)				ACROLEIN + HV + #(3.3E-3) = 1.01 HO2. + 0.172 RO2-R. + 0.172 HO. + 1.182 CO + 0.046 CO2 + 0.512 HCHO + 0.33 MA-RCO3. + -.284 XC + 0.112 CCHO2-STAB +0.046 NROG
MAOH	3.33E-11	1.86E-11	-0.35	0.00	HO. + METHACRO = 0.5 RO2-R. + 0.416 CO +0.084 HCHO + 0.416 MEK + 0.084 MGLY +0.5 MA-RCO3. + -0.416 XC
MAO3	1.19E-18	1.36E-15	4.20	0.00	O3 + METHACRO = 0.008 HO2. + 0.1 RO2-R. +0.208 HO. + 0.1 RCO-O2. + 0.45 CO + 0.117 CO2 +0.2 HCHO + 0.9 MGLY + 0.333 HCHO2-STAB +-0.1 XC
MAN3	4.76E-15	1.50E-12	3.43	0.00	NO3 + METHACRO = 0.5 "HNO3 + RO2-R. + CO +MA-RCO3." + 1.5 XC + 0.5 XN
MAOP	1.69E-11	(No T Dependence)			O3P + METHACRO = RCHO + XC
MAHV	(Phot. Set = ACROLEIN)				METHACRO + HV +#(4.1E-3) = 0.34 HO2. + 0.33 RO2-R. +0.33 HO. + 0.67 CCO-O2. + 0.67 CO + 0.67 HCHO +0.33 MA-RCO3. + -0 XC
MVOH	1.87E-11	4.14E-12	-0.90	0.00	HO. + MVK = 0.3 RO2-R. + 0.025 RO2-N. +0.675 R2O2. + 0.675 CCO-O2. + 0.3 HCHO +0.675 RCHO + 0.3 MGLY + -0.7 XC
MVO3	4.74E-18	7.51E-16	3.02	0.00	O3 + MVK = 0.064 HO2. + 0.05 RO2-R. + 0.164 HO. + 0.05 RCO-O2. + 0.475 CO + 0.124 CO2 + 0.1 HCHO + 0.95 MGLY + 0.351 HCHO2-STAB + -0.05 XC
MVN3	1.15E-14	(No T Dependence)			NO3 + MVK = 0.08 RO2-XN. + 0.92 R2O2. +0.92 CCO-O2. + 0.92 RCHO + -0.602 XC + XN
MVOP	4.32E-12	(No T Dependence)			O3P + MVK = 0.45 RCHO + 0.55 MEK + 0.45 XC
MVHV	(Phot. Set = ACROLEIN)				MVK + HV + #(2.1E-3) = 0.3 RO2-R. + 0.7 CO + 0.3 HCHO + 0.7 PROD2 + 0.3 MA-RCO3. + -2.4 XC
IPOH	6.19E-11	(No T Dependence)			HO. + ISOPROD = 0.705 RO2-R. + 0.006 RO2-N. + 0.357 CO + 0.056 HCHO + 0.148 RCHO + 0.159 MEK + 0.353 PROD2 + 0.159 GLY + 0.179 MGLY + 0.289 MA-RCO3. + -.949 XC
IPO3	4.18E-18	(No T Dependence)			O3 + ISOPROD = 0.132 HO2. + 0.11 RO2-R. + 0.289 HO. + 0.048 RCO-O2. + 0.402 CO + 0.065 CO2 + 0.155 HCHO + 0.047 RCHO + 0.211 MEK + 0.023 GLY + 0.742 MGLY + 0.1 HCHO2-STAB + 0.443 RCHO2-STAB + -.748 XC
IPN3	1.00E-13	(No T Dependence)			NO3 + ISOPROD = 0.15 HNO3 + 0.85 RO2-R. + 0.608 CO + 0.242 HCHO + 0.234 RCHO + 0.608 RNO3 + 0.008 MGLY + 0.15 MA-RCO3. + -.517 XC + 0.242 XN
IPHV	(Phot. Set = ACROLEIN)				ISOPROD + HV + #(4.1E-3) = 1.234 RO2-R. + 0.466 CCO-O2. + 0.3 RCO-O2. + 1.234 CO + 0.3 HCHO + 0.466 RCHO + 0.234 MEK + -1 XC
Reactions of Primary VOC Species Represented Explicitly					
c1OH	6.41E-15	2.30E-12	3.51	0.00	CH4 + HO. = H2O + C-O2.
c2OH	2.60E-13	1.37E-12	0.99	2.00	HO. + ETHANE = RO2-R. + CCHO

Table A-2 (continued)

Rxn. Label	Kinetic Parameters [a] k(300)	A	Ea	B	Reactions [b]
c4OH	2.46E-12	1.52E-12	-0.29	2.00	HO. + N-C4 = 0.93 RO2-R. + 0.07 RO2-N. +0.386 R2O2. + 0.575 CCHO + 0.127 RCHO +0.516 MEK + 0.058 XC
c6OH	5.49E-12	1.38E-12	-0.82	2.00	HO. + N-C6 = 0.787 RO2-R. + 0.213 RO2-N. +0.777 R2O2. + 0.014 CCHO + 0.128 RCHO +0.691 PROD2 + 0.375 XC
c8OH	8.74E-12	2.48E-12	-0.75	2.00	HO. + N-C8 = 0.652 RO2-R. + 0.348 RO2-N. +0.788 R2O2. + 0.022 RCHO + 0.63 PROD2 +2.414 XC
tlOH	5.91E-12	1.81E-12	-0.70	0.00	HO. + TOLUENE = 0.758 RO2-R. + 0.234 HO2. +0.234 CRES + 0.008 RO2-NP. + 0.116 GLY +0.135 MGLY + 0.085 BALD + 0.135 DCB1 +0.160 DCB2 + 0.054 DCB3 + 0.325 DCB4 + 0.528 XC
xyOH	2.36E-11	(No T Dependence)			HO. + M-XYLENE = 0.782 RO2-R. + 0.210 HO2. +0.210 CRES + 0.008 RO2-NP. + 0.107 GLY +0.335 MGLY + 0.037 BALD + 0.295 DCB2 +0.109 DCB3 + 0.342 DCB4 + 0.940 XC
tmOH	5.75E-11	(No T Dependence)			HO. + 135-TMB = 0.804 RO2-R. + 0.186 HO2. +0.186 CRES + 0.010 RO2-NP. + 0.621 MGLY +0.025 BALD + 0.152 DCB3 + 0.627 DCB4 + 1.078 XC
etOH	8.43E-12	1.96E-12	-0.87	0.00	HO. + ETHENE = RO2-R. + 1.567 HCHO +0.216 RCHO + -0.216 XC
etO3	1.68E-18	9.14E-15	5.13	0.00	O3 + ETHENE = 0.12 RO2-R. + 0.12 HO. + 0.5 CO +0.13 CO2 + HCHO + 0.37 HCHO2-STAB
etN3	2.18E-16	4.39E-13	4.53	2.00	NO3 + ETHENE = RO2-R. + RCHO + -1 XC + XN
etOP	7.42E-13	1.04E-11	1.57	0.00	O3P + ETHENE = 0.5 HO2. + 0.2 RO2-R. +0.3 C-O2. + 0.491 CO + 0.191 HCHO + 0.25 CCHO +0.009 GLY + 0.25 XC + 0.25 NROG
prOH	2.60E-11	4.85E-12	-1.00	0.00	HO. + PROPENE = RO2-R. + HCHO + CCHO
prO3	1.05E-17	5.51E-15	3.73	0.00	O3 + PROPENE = 0.06 RO2-R. + 0.26 C-O2. +0.32 HO. + 0.51 CO + 0.135 CO2 + 0.5 HCHO +0.5 CCHO + 0.185 HCHO2-STAB + 0.17 CCHO2-STAB +0.07 XC + 0.07 NROG
prN3	9.74E-15	4.59E-13	2.30	0.00	NO3 + PROPENE = 0.964 RO2-R. + 0.036 RO2-XN. + 3 XC + XN
prOP	4.01E-12	1.18E-11	0.64	0.00	O3P + PROPENE = 0.45 RCHO + 0.55 MEK + -0.55 XC
tbOH	6.32E-11	1.01E-11	-1.09	0.00	HO. + T-2-BUTE = 0.964 RO2-R. + 0.036 RO2-N. +1.927 CCHO + -0.036 XC
tbO3	1.95E-16	6.64E-15	2.10	0.00	O3 + T-2-BUTE = 0.52 C-O2. + 0.52 HO. + 0.52 CO +0.14 CO2 + CCHO + 0.34 CCHO2-STAB + 0.14 XC +0.14 NROG
tbN3	3.93E-13	1.10E-13	-0.76	2.00	NO3 + T-2-BUTE = 0.701 NO2 + 0.219 RO2-R. +0.08 RO2-N. + 0.701 R2O2. + 1.402 CCHO +0.219 RNO3 + -0.299 XC + 0.08 XN
tbOP	2.18E-11	(No T Dependence)			O3P + T-2-BUTE = MEK
Reactions of Biogenic Species Represented in the Ambient Simulations					
ISOH	9.73E-11	2.50E-11	-0.81	0.00	HO. + ISOP = 0.909 RO2-R. + 0.091 RO2-N. + 0.079 R2O2. + 0.626 HCHO + 0.23 METHACRO + 0.32 MVK + 0.359 ISOPROD + -0.076 XC
ISO3	1.34E-17	7.86E-15	3.80	0.00	O3 + ISOP = 0.066 RO2-R. + 0.134 R2O2. + 0.266 HO. + 0.275 CO + 0.122 CO2 + 0.6 HCHO + 0.1 PROD2 + 0.39 METHACRO + 0.16 MVK + 0.2 MA-RCO3. + 0.204 HCHO2-STAB + 0.15 RCHO2-STAB + -0.25 XC
ISN3	6.81E-13	3.03E-12	0.89	0.00	NO3 + ISOP = 0.19 NO2 + 0.76 RO2-R. + 0.05 RO2-N. + 0.19 R2O2. + 0.95 ISOPROD + 0.81 XN
ISOP	3.60E-11	(No T Dependence)			O3P + ISOP = 0.25 RO2-R. + 0.25 R2O2. + 0.5 HCHO + 0.75 PROD2 + 0.25 MA-RCO3. + -1 XC
APOH	5.31E-11	1.21E-11	-0.88	0.00	HO. + APIN = 0.75 RO2-R. + 0.25 RO2-N. + 0.5 R2O2. + 0.75 RCHO + 6.5 XC
APO3	8.80E-17	1.01E-15	1.46	0.00	O3 + APIN = 0.183 RO2-N. + 0.667 R2O2. + 0.85 HO. + 0.631 CCO-O2. + 0.036 RCO-O2. + 0.036 HCHO + 0.631 RCHO + 0.15 RCHO2-STAB + 5.336 XC
APN3	6.10E-12	1.19E-12	-0.97	0.00	NO3 + APIN = 0.75 NO2 + 0.25 RO2-N. + 0.75 R2O2. + 0.75 RCHO + 6.5 XC + 0.25 XN
APOP	3.20E-11	(No T Dependence)			O3P + APIN = PROD2 + 4 XC
UBOH	0.00E+00	(No T Dependence)			HO. + UNKN = 0.75 RO2-R. + 0.25 RO2-N. + 0.5 R2O2. + 0.375 HCHO + 0.375 RCHO + 0.375 PROD2 + 5 XC

Table A-2 (continued)

Rxn. Label	Kinetic Parameters [a] k(300)	A	Ea	B	Reactions [b]
UBO3	0.00E+00	(No T Dependence)			O3 + UNKN = 0.045 RO2-R. + 0.121 RO2-N. + 0.39 R2O2. + 0.6 HO. + 0.316 CCO-O2. + 0.119 RCO-O2. + 0.185 CO + 0.048 CO2 + 0.148 HCHO + 0.316 RCHO + 0.37 PROD2 + 0.137 HCHO2-STAB + 0.075 RCHO2-STAB + 5 XC
UBN3	0.00E+00	(No T Dependence)			NO3 + UNKN = 0.375 NO2 + 0.375 RO2-R. + 0.25 RO2-N. + 0.75 R2O2. + 0.375 RCHO + 0.375 RNO3 + 6.5 XC + 0.625 XN
UBOP	0.00E+00	(No T Dependence)			O3P + UNKN = 0.2 RCHO + 0.8 PROD2 + 5.1 XC
Reactions of Lumped Species Represented in the Ambient Simulations [c]					
A1OH	3.45E-12	2.29E-12	-0.25	1.00	ALK1 + HO. = 0.0244 HO. + 0.0120 HO2. + 0.7909 RO2-R. + 0.0904 RO2-N. + 0.0059 RO2-XN. + 0.7135 R2O2. + 0.0054 C-O2. + 0.0627 TBU-O. + 0.0081 CCO-O2. + 0.0005 RCO-O2. + 0.0281 HCHO + 0.3864 CCHO + 0.2112 RCHO + 0.3192 ACET + 0.1698 MEK + 0.0796 PROD2 + 0.0233 CO + 0.0245 GLY + 0.0001 MGLY + 0.0120 NROG + 0.3933 XC
A2OH	9.19E-12	4.06E-12	-0.49	1.00	ALK2 + HO. = 0.6700 RO2-R. + 0.9956 R2O2. + 0.3277 RO2-N. + 0.0021 RO2-XN. + 0.0001 CCO-O2. + 0.0441 HCHO + 0.1146 CCHO + 0.2439 RCHO + 0.0857 ACET + 0.1014 MEK + 0.4051 PROD2 + 0.0001 CO + 2.5828 XC
A3OH	5.91E-12	5.91E-12	0.00	1.00	ARO1 + HO. = 0.2246 HO2. + 0.7641 RO2-R. + 0.0114 RO2-NP. + 0.0587 PROD2 + 0.1173 GLY + 0.1201 MGLY + 0.0161 PHEN + 0.2084 CRES + 0.0583 BALD + 0.1723 DCB1 + 0.1098 DCB2 + 0.0488 DCB3 + 0.3170 DCB4 + 0.9719 XC
B1OH	2.63E-11	9.76E-12	-0.59	1.00	ARO2 + HO. = 0.8044 RO2-R. + 0.1868 HO2. + 0.0087 RO2-NP. + 0.0970 GLY + 0.2866 MGLY + 0.0871 BACL + 0.1868 CRES + 0.0503 BALD + 0.0272 DCB1 + 0.0901 DCB2 + 0.0973 DCB3 + 0.5399 DCB4 + 0.9708 XC
O1OH	3.23E-11	2.72E-12	-1.48	1.00	OLE1 + HO. = 0.9239 RO2-R. + 0.1015 R2O2. + 0.0002 RO2-XN. + 0.0760 RO2-N. + 0.8352 HCHO + 0.2938 CCHO + 0.5705 RCHO + 0.0050 ACET + 0.0596 PROD2 + 1.2688 XC
O1O3	1.10E-17	9.80E-16	2.68	1.00	OLE1 + O3 = 0.1549 HO. + 0.0255 HO2. + 0.0531 RO2-R. + 0.0764 C-O2. + 0.5000 HCHO + 0.1537 CCHO + 0.3637 RCHO + 0.0012 ACET + 0.3449 CO + 0.0856 CO2 + 0.1850 HCHO2-STAB + 0.3346 RCHO2-STAB + 0.0500 CCHO2-STAB + 0.0206 NROG + 1.4595 XC
O1N3	1.13E-14	1.71E-14	0.25	1.00	OLE1 + NO3 = 0.8297 RO2-R. + 0.4891 R2O2. + 0.0115 RO2-XN. + 0.4903 XN + 0.0105 CCHO + 0.0400 RCHO + 0.0238 ACET + 0.1589 RO2-N. + 0.5097 RNO3 + 1.6017 XC
O1OP	4.32E-12	3.89E-12	-0.06	1.00	OLE1 + O3P = 0.4500 RCHO + 0.4367 MEK + 0.1133 PROD2 + 1.3803 XC
O2OH	6.32E-11	6.59E-12	-1.35	1.00	OLE2 + HO. = 0.9181 RO2-R. + 0.0079 R2O2. + 0.0255 ISOPROD + 0.0819 RO2-N. + 0.2473 HCHO + 0.7162 CCHO + 0.5081 RCHO + 0.1265 ACET + 0.0755 MEK + 0.0623 BALD + 0.0246 ACROLEIN + 0.4946 XC
O2O3	1.05E-16	1.84E-16	0.34	1.00	OLE2 + O3 = 0.4142 HO. + 0.0388 RO2-R. + 0.1907 C-O2. + 0.1630 CCO-O2. + 0.0078 RCO-O2. + 0.1737 R2O2. + 0.0069 RO2-N. + 0.0255 ACROLEIN + 0.0069 BZ-O. + 0.3150 HCHO + 0.4553 CCHO + 0.2946 RCHO + 0.0249 ACET + 0.0230 MEK + 0.0064 PROD2 + 0.0277 BALD + 0.2776 CO + 0.0718 CO2 + 0.0402 HCHO2-STAB + 0.1247 CCHO2-STAB + 0.3015 RCHO2-STAB + 0.0514 NROG + 0.7247 XC
O2N3	8.54E-13	3.17E-13	-0.59	1.00	OLE2 + NO3 = 0.4352 RO2-R. + 0.7252 R2O2. + 0.0511 ISOPROD + 0.4204 NO2 + 0.2411 XN + 0.1201 RO2-N. + 0.0242 C-O2. + 0.0715 HCHO + 0.5018 CCHO + 0.1672 RCHO + 0.1104 ACET + 0.0014 MEK + 0.3347 RNO3 + 0.9588 XC

Table A-2 (continued)

Rxn. Label	Kinetic Parameters [a] k(300)	A	Ea	B	Reactions [b]
O2OP	1.99E-11	7.40E-12	-0.59	1.00	OLE2 + O3P = 0.0128 HO2. + 0.0118 RO2-R. + 0.0010 RO2-N. + 0.0118 ACROLEIN + 0.0118 CO + 0.0679 RCHO + 0.6489 MEK + 0.2705 PROD2 + 0.9532 XC
L1OH	2.61E-11	3.51E-12	-1.20	1.00	ALD1 + HO. = 0.0960 RO2-R. + 0.0931 R2O2. + 0.0233 RO2-N. + 0.8805 RCO-O2. + 0.0095 HCHO + 0.0136 CCHO + 0.0934 RCHO + 0.0403 CO + 0.0007 GLY + 0.0045 MGLY + 2.0713 XC
L1N3	2.72E-15	1.01E-15	-0.59	1.00	ALD1 + NO3 = RCO-O2. + XN + 2.1997 XC
L1HV	(Phot. Set = C2CHO)				HV + ALD1 = 0.2900 HO2. + 1.6674 RO2-R. + 0.0426 RO2-N. + 0.9574 RCHO + 1.0000 CO + 1.1141 XC
Reactions of Styrene: "Best Estimate" Mechanism (Model A) [d]					
syOH	5.80E-11	(No T Dependence)			HO. + STYRENE = 0.9 "RO2-R. + HCHO + BALD" + 0.1 RO2-N.
syO3	1.71E-17	(No T Dependence)			O3 + STYRENE = 0.4 "HCHO + RCHO2-STAB" + 0.6 "BALD + HCHO2-STAB"
syN3	1.51E-13	(No T Dependence)			NO3 + STYRENE = 0.1 "RO2-N. + XN "+ 0.675 "RO2-R. + RNO3" + 0.225 "BALD + HCHO + R2O2. + NO2" + 2.325 XC
syOP	1.76E-11	(No T Dependence)			O3P + STYRENE = PROD2 + 2 XC
Reactions of Styrene: "Radicals in O_3 Reaction" Mechanism [e]					
syOH	5.80E-11	(No T Dependence)			HO. + STYRENE = 0.9 "RO2-R. + HCHO + BALD" + 0.1 RO2-N.
syO3	1.71E-17	(No T Dependence)			O3 + STYRENE = 0.4 "HCHO + RCHO2-STAB" + 0.6 BALD + 0.072 RO2-R. + 0.072 HO. + 0.3 CO + 0.078 CO2 + 0.370 HCHO2-STAB + 1.6 XC
syN3	1.51E-13	(No T Dependence)			NO3 + STYRENE = 0.1 "RO2-N. + XN "+ 0.675 "RO2-R. + RNO3" + 0.225 "BALD + HCHO + R2O2. + NO2" + 2.325 XC
syOP	1.76E-11	(No T Dependence)			O3P + STYRENE = PROD2 + 2 XC
Reactions of Styrene: "100% Decomposition in NO_3 Reaction" Mechanism (Model B) [e]					
syOH	5.80E-11	(No T Dependence)			HO. + STYRENE = 0.9 "RO2-R. + HCHO + BALD" + 0.1 RO2-N.
syO3	1.71E-17	(No T Dependence)			O3 + STYRENE = 0.4 "HCHO + RCHO2-STAB" + 0.6 "BALD + HCHO2-STAB"
syN3	1.51E-13	(No T Dependence)			NO3 + STYRENE = 0.1 "RO2-N. + XN "+ 0.9 "BALD + HCHO + R2O2. + NO2" + 2.325 XC
syOP	1.76E-11	(No T Dependence)			O3P + STYRENE = PROD2 + 2 XC
Reactions used to Represent Chamber-Dependent Processes [f]					
O3W	(varied)	(No T Dependence)			O3 =
N25I	(varied)	(No T Dependence)			N2O5 = 2 NOX-WALL
N25S	(varied)	(No T Dependence)			N2O5 + H2O = 2 NOX-WALL
NO2W	(varied)	(No T Dependence)			NO2 = (yHONO) HONO + (1-yHONO) NOX-WALL
XSHC	(varied)	(No T Dependence)			HO. = HO2.
RNI	(Phot. Set = NO2)				HV + #RS/K1 = HONO + -1 NOX-WALL

[a] Except as noted, the expression for the rate constant is $k = A\ e^{Ea/RT}\ (T/300)^B$. Rate constants and A factor are in cm, molecule, sec. units. Units of Ea is kcal $mole^{-1}$. "Phot Set" means this is a photolysis reaction, with the absorption coefficients and quantum yields given in Table A-3. In addition, if "#(number)" or "#(parameter)" is given as a reactant, then the value of that number or parameter is multiplied by the result in the "rate constant expression" columns to obtain the rate constant used. Furthermore, "#RCONnn" as a reactant means that the rate constant for the reaction is obtained by multiplying the rate constant given by that for reaction "nn". Thus, the rate constant given is actually an equilibrium constant. "(Fast)" means that this is the only fate of a steady state species, and the solver treats it as occurring as soon as the reactant species is formed.

[b] The format of the reaction listing is the same as that used in the documentation of the detailed mechanism (Carter 1990).

[c] The rate constants and product yield parameters are based on the mixture of species in the base ROG mixture which are being represented.

[d] This is the version of the styrene mechanism is recommended for use in ambient modeling. See text.

[e] This version of the styrene mechanism was used for mechanism evaluation and sensitivity calculations only. See text.

[f] See Table A-4 for the values of the parameters used for the specific chamber simulations in this study.

Table A-3. Absorption cross sections and quantum yields for photolysis reactions.

WL (nm)	Abs (cm^2)	QY	WL (nm)	Abs (cm^2)	QY	WL (nm)	Abs (cm^2)	QY	WL (nm)	Abs (cm^2)	QY	WL (nm)	Abs (cm^2)	QY
Photolysis File = NO2														
205.0	4.31E-19	1.000	210.0	4.72E-19	1.000	215.0	4.95E-19	1.000	220.0	4.56E-19	1.000	225.0	3.79E-19	1.000
230.0	2.74E-19	1.000	235.0	1.67E-19	1.000	240.0	9.31E-20	1.000	245.0	4.74E-20	1.000	250.0	2.48E-20	1.000
255.0	1.95E-20	1.000	260.0	2.24E-20	1.000	265.0	2.73E-20	1.000	270.0	4.11E-20	1.000	275.0	4.90E-20	1.000
280.0	5.92E-20	1.000	285.0	7.39E-20	1.000	290.0	9.00E-20	1.000	295.0	1.09E-19	1.000	300.0	1.31E-19	1.000
305.0	1.57E-19	1.000	310.0	1.86E-19	1.000	315.0	2.15E-19	0.990	320.0	2.48E-19	0.990	325.0	2.81E-19	0.990
330.0	3.13E-19	0.990	335.0	3.43E-19	0.990	340.0	3.80E-19	0.990	345.0	4.07E-19	0.990	350.0	4.31E-19	0.990
355.0	4.72E-19	0.990	360.0	4.83E-19	0.980	365.0	5.17E-19	0.980	370.0	5.32E-19	0.980	375.0	5.51E-19	0.980
380.0	5.64E-19	0.970	385.0	5.76E-19	0.970	390.0	5.93E-19	0.960	395.0	5.85E-19	0.935	400.0	6.02E-19	0.820
405.0	5.78E-19	0.355	410.0	6.00E-19	0.130	411.0	5.93E-19	0.110	412.0	5.86E-19	0.094	413.0	5.79E-19	0.083
414.0	5.72E-19	0.070	415.0	5.65E-19	0.059	416.0	5.68E-19	0.048	417.0	5.71E-19	0.039	418.0	5.75E-19	0.030
419.0	5.78E-19	0.023	420.0	5.81E-19	0.018	421.0	5.72E-19	0.012	422.0	5.64E-19	0.008	423.0	5.55E-19	0.004
424.0	5.47E-19	0.000												
Photolysis File = NO3NO														
585.0	2.89E-18	0.000	586.0	3.32E-18	0.050	587.0	4.16E-18	0.100	588.0	5.04E-18	0.150	589.0	6.13E-18	0.200
590.0	5.96E-18	0.250	591.0	5.44E-18	0.280	592.0	5.11E-18	0.310	593.0	4.58E-18	0.340	594.0	4.19E-18	0.370
595.0	4.29E-18	0.400	596.0	4.62E-18	0.370	597.0	4.36E-18	0.340	598.0	3.67E-18	0.310	599.0	3.10E-18	0.280
600.0	2.76E-18	0.250	601.0	2.86E-18	0.240	602.0	3.32E-18	0.230	603.0	3.80E-18	0.220	604.0	4.37E-18	0.210
605.0	4.36E-18	0.200	606.0	3.32E-18	0.200	607.0	2.40E-18	0.200	608.0	1.85E-18	0.200	609.0	1.71E-18	0.200
610.0	1.77E-18	0.200	611.0	1.91E-18	0.180	612.0	2.23E-18	0.160	613.0	2.63E-18	0.140	614.0	2.55E-18	0.120
615.0	2.26E-18	0.100	616.0	2.09E-18	0.100	617.0	2.11E-18	0.100	618.0	2.39E-18	0.100	619.0	2.56E-18	0.100
620.0	3.27E-18	0.100	621.0	5.24E-18	0.090	622.0	1.02E-17	0.080	623.0	1.47E-17	0.070	624.0	1.21E-17	0.060
625.0	8.38E-18	0.050	626.0	7.30E-18	0.050	627.0	7.53E-18	0.050	628.0	7.37E-18	0.050	629.0	6.98E-18	0.050
630.0	6.76E-18	0.050	631.0	4.84E-18	0.046	632.0	3.27E-18	0.042	633.0	2.17E-18	0.038	634.0	1.64E-18	0.034
635.0	1.44E-18	0.030	636.0	1.69E-18	0.024	637.0	2.07E-18	0.018	638.0	2.03E-18	0.012	639.0	1.58E-18	0.006
640.0	1.23E-18	0.000												
Photolysis File = NO3NO2														
400.0	0.00E+00	1.000	401.0	0.00E+00	1.000	402.0	0.00E+00	1.000	403.0	2.00E-20	1.000	404.0	0.00E+00	1.000
405.0	3.00E-20	1.000	406.0	2.00E-20	1.000	407.0	1.00E-20	1.000	408.0	3.00E-20	1.000	409.0	0.00E+00	1.000
410.0	1.00E-20	1.000	411.0	2.00E-20	1.000	412.0	5.00E-20	1.000	413.0	5.00E-20	1.000	414.0	2.00E-20	1.000
415.0	6.00E-20	1.000	416.0	6.00E-20	1.000	417.0	7.00E-20	1.000	418.0	5.00E-20	1.000	419.0	8.00E-20	1.000
420.0	8.00E-20	1.000	421.0	8.00E-20	1.000	422.0	9.00E-20	1.000	423.0	1.10E-19	1.000	424.0	9.00E-20	1.000
425.0	7.00E-20	1.000	426.0	1.40E-19	1.000	427.0	1.40E-19	1.000	428.0	1.20E-19	1.000	429.0	1.10E-19	1.000
430.0	1.70E-19	1.000	431.0	1.30E-19	1.000	432.0	1.50E-19	1.000	433.0	1.80E-19	1.000	434.0	1.80E-19	1.000
435.0	1.60E-19	1.000	436.0	1.50E-19	1.000	437.0	1.80E-19	1.000	438.0	2.10E-19	1.000	439.0	2.00E-19	1.000
440.0	1.90E-19	1.000	441.0	1.80E-19	1.000	442.0	2.10E-19	1.000	443.0	1.80E-19	1.000	444.0	1.90E-19	1.000
445.0	2.00E-19	1.000	446.0	2.40E-19	1.000	447.0	2.90E-19	1.000	448.0	2.40E-19	1.000	449.0	2.80E-19	1.000
450.0	2.90E-19	1.000	451.0	3.00E-19	1.000	452.0	3.30E-19	1.000	453.0	3.10E-19	1.000	454.0	3.60E-19	1.000
455.0	3.60E-19	1.000	456.0	3.60E-19	1.000	457.0	4.00E-19	1.000	458.0	3.70E-19	1.000	459.0	4.20E-19	1.000
460.0	4.00E-19	1.000	461.0	3.90E-19	1.000	462.0	4.00E-19	1.000	463.0	4.10E-19	1.000	464.0	4.80E-19	1.000
465.0	5.10E-19	1.000	466.0	5.40E-19	1.000	467.0	5.70E-19	1.000	468.0	5.60E-19	1.000	469.0	5.80E-19	1.000
470.0	5.90E-19	1.000	471.0	6.20E-19	1.000	472.0	6.40E-19	1.000	473.0	6.20E-19	1.000	474.0	6.20E-19	1.000
475.0	6.80E-19	1.000	476.0	7.80E-19	1.000	477.0	7.70E-19	1.000	478.0	7.30E-19	1.000	479.0	7.30E-19	1.000
480.0	7.00E-19	1.000	481.0	7.10E-19	1.000	482.0	7.10E-19	1.000	483.0	7.20E-19	1.000	484.0	7.70E-19	1.000
485.0	8.20E-19	1.000	486.0	9.10E-19	1.000	487.0	9.20E-19	1.000	488.0	9.50E-19	1.000	489.0	9.60E-19	1.000
490.0	1.03E-18	1.000	491.0	9.90E-19	1.000	492.0	9.90E-19	1.000	493.0	1.01E-18	1.000	494.0	1.01E-18	1.000
495.0	1.06E-18	1.000	496.0	1.21E-18	1.000	497.0	1.22E-18	1.000	498.0	1.20E-18	1.000	499.0	1.17E-18	1.000
500.0	1.13E-18	1.000	501.0	1.11E-18	1.000	502.0	1.11E-18	1.000	503.0	1.11E-18	1.000	504.0	1.26E-18	1.000
505.0	1.28E-18	1.000	506.0	1.34E-18	1.000	507.0	1.28E-18	1.000	508.0	1.27E-18	1.000	509.0	1.35E-18	1.000
510.0	1.51E-18	1.000	511.0	1.73E-18	1.000	512.0	1.77E-18	1.000	513.0	1.60E-18	1.000	514.0	1.58E-18	1.000
515.0	1.58E-18	1.000	516.0	1.56E-18	1.000	517.0	1.49E-18	1.000	518.0	1.44E-18	1.000	519.0	1.54E-18	1.000
520.0	1.68E-18	1.000	521.0	1.83E-18	1.000	522.0	1.93E-18	1.000	523.0	1.77E-18	1.000	524.0	1.64E-18	1.000
525.0	1.58E-18	1.000	526.0	1.63E-18	1.000	527.0	1.81E-18	1.000	528.0	2.10E-18	1.000	529.0	2.39E-18	1.000
530.0	2.23E-18	1.000	531.0	2.09E-18	1.000	532.0	2.02E-18	1.000	533.0	1.95E-18	1.000	534.0	2.04E-18	1.000
535.0	2.30E-18	1.000	536.0	2.57E-18	1.000	537.0	2.58E-18	1.000	538.0	2.34E-18	1.000	539.0	2.04E-18	1.000
540.0	2.10E-18	1.000	541.0	2.04E-18	1.000	542.0	1.88E-18	1.000	543.0	1.68E-18	1.000	544.0	1.70E-18	1.000
545.0	1.96E-18	1.000	546.0	2.42E-18	1.000	547.0	2.91E-18	1.000	548.0	2.98E-18	1.000	549.0	2.71E-18	1.000
550.0	2.48E-18	1.000	551.0	2.43E-18	1.000	552.0	2.47E-18	1.000	553.0	2.53E-18	1.000	554.0	2.78E-18	1.000
555.0	3.11E-18	1.000	556.0	3.26E-18	1.000	557.0	3.29E-18	1.000	558.0	3.51E-18	1.000	559.0	3.72E-18	1.000
560.0	3.32E-18	1.000	561.0	2.98E-18	1.000	562.0	2.90E-18	1.000	563.0	2.80E-18	1.000	564.0	2.72E-18	1.000
565.0	2.73E-18	1.000	566.0	2.85E-18	1.000	567.0	2.81E-18	1.000	568.0	2.85E-18	1.000	569.0	2.89E-18	1.000
570.0	2.79E-18	1.000	571.0	2.76E-18	1.000	572.0	2.74E-18	1.000	573.0	2.78E-18	1.000	574.0	2.86E-18	1.000
575.0	3.08E-18	1.000	576.0	3.27E-18	1.000	577.0	3.38E-18	1.000	578.0	3.31E-18	1.000	579.0	3.24E-18	1.000
580.0	3.34E-18	1.000	581.0	3.55E-18	1.000	582.0	3.28E-18	1.000	583.0	2.93E-18	1.000	584.0	2.82E-18	1.000
585.0	2.89E-18	1.000	586.0	3.32E-18	0.950	587.0	4.16E-18	0.900	588.0	5.04E-18	0.850	589.0	6.13E-18	0.800
590.0	5.96E-18	0.750	591.0	5.44E-18	0.720	592.0	5.11E-18	0.690	593.0	4.58E-18	0.660	594.0	4.19E-18	0.630
595.0	4.29E-18	0.600	596.0	4.62E-18	0.590	597.0	4.36E-18	0.580	598.0	3.67E-18	0.570	599.0	3.10E-18	0.560
600.0	2.76E-18	0.550	601.0	2.86E-18	0.540	602.0	3.32E-18	0.530	603.0	3.80E-18	0.520	604.0	4.37E-18	0.510
605.0	4.36E-18	0.400	606.0	3.32E-18	0.380	607.0	2.40E-18	0.360	608.0	1.85E-18	0.340	609.0	1.71E-18	0.320
610.0	1.77E-18	0.300	611.0	1.91E-18	0.290	612.0	2.23E-18	0.280	613.0	2.63E-18	0.270	614.0	2.55E-18	0.260
615.0	2.26E-18	0.250	616.0	2.09E-18	0.240	617.0	2.11E-18	0.230	618.0	2.39E-18	0.220	619.0	2.56E-18	0.210
620.0	3.27E-18	0.200	621.0	5.24E-18	0.190	622.0	1.02E-17	0.180	623.0	1.47E-17	0.170	624.0	1.21E-17	0.160
625.0	8.38E-18	0.150	626.0	7.30E-18	0.130	627.0	7.53E-18	0.110	628.0	7.37E-18	0.090	629.0	6.98E-18	0.070
630.0	6.76E-18	0.050	631.0	4.84E-18	0.040	632.0	3.27E-18	0.030	633.0	2.17E-18	0.020	634.0	1.64E-18	0.010
635.0	1.44E-18	0.000												
Photolysis File = O3O3P														
175.4	8.11E-19	0.050	177.0	8.11E-19	0.050	178.6	7.99E-19	0.050	180.2	7.86E-19	0.050	181.8	7.63E-19	0.050
183.5	7.29E-19	0.050	185.2	6.88E-19	0.050	186.9	6.22E-19	0.050	188.7	5.76E-19	0.050	190.5	5.26E-19	0.050
192.3	4.76E-19	0.050	194.2	4.28E-19	0.050	196.1	3.83E-19	0.050	198.0	3.47E-19	0.050	200.0	3.23E-19	0.050
202.0	3.14E-19	0.050	204.1	3.26E-19	0.050	206.2	3.64E-19	0.050	208.3	4.34E-19	0.050	210.5	5.42E-19	0.050
212.8	6.99E-19	0.050	215.0	9.20E-19	0.050	217.4	1.19E-18	0.050	219.8	1.55E-18	0.050	222.2	1.99E-18	0.050
224.7	2.56E-18	0.050	227.3	3.23E-18	0.050	229.9	4.00E-18	0.050	232.6	4.83E-18	0.050	235.3	5.79E-18	0.050
238.1	6.86E-18	0.050	241.0	7.97E-18	0.050	243.9	9.00E-18	0.050	246.9	1.00E-17	0.050	250.1	1.08E-17	0.050

Table A-3. (continued)

WL (nm)	Abs (cm^2)	QY	WL (nm)	Abs (cm^2)	QY	WL (nm)	Abs (cm^2)	QY	WL (nm)	Abs (cm^2)	QY	WL (nm)	Abs (cm^2)	QY
253.2	1.13E-17	0.050	256.4	1.15E-17	0.050	259.7	1.12E-17	0.050	263.2	1.06E-17	0.050	266.7	9.65E-18	0.050
270.3	8.34E-18	0.050	274.0	6.92E-18	0.050	277.8	5.42E-18	0.050	281.7	4.02E-18	0.050	285.7	2.77E-18	0.050
289.9	1.79E-18	0.050	290.0	1.77E-18	0.050	294.1	1.09E-18	0.050	295.0	9.95E-19	0.050	298.5	6.24E-19	0.050
300.0	5.30E-19	0.050	303.0	3.43E-19	0.015	305.0	2.76E-19	0.020	306.0	2.42E-19	0.050	307.0	2.09E-19	0.123
307.7	1.85E-19	0.196	308.0	1.80E-19	0.227	309.0	1.61E-19	0.333	310.0	1.43E-19	0.400	311.0	1.25E-19	0.612
312.0	1.07E-19	0.697	312.5	9.80E-20	0.718	313.0	9.32E-20	0.738	314.0	8.36E-20	0.762	315.0	7.40E-20	0.765
316.0	6.44E-20	0.779	317.0	5.48E-20	0.791	317.5	5.00E-20	0.799	318.0	4.75E-20	0.806	319.0	4.25E-20	0.822
322.5	2.49E-20	0.906	327.5	1.20E-20	0.940	332.5	6.17E-21	0.950	337.5	2.74E-21	0.975	342.5	1.17E-21	1.000
347.5	5.90E-22	1.000	352.5	2.70E-22	1.000	357.5	1.10E-22	1.000	362.5	5.00E-23	1.000	367.5	0.00E+00	1.000
400.0	0.00E+00	1.000	410.0	1.20E-23	1.000	420.0	2.20E-23	1.000	440.0	1.12E-22	1.000	460.0	3.28E-22	1.000
480.0	6.84E-22	1.000	500.0	1.22E-21	1.000	520.0	1.82E-21	1.000	540.0	2.91E-21	1.000	560.0	3.94E-21	1.000
580.0	4.59E-21	1.000	600.0	5.11E-21	1.000	620.0	4.00E-21	1.000	640.0	2.96E-21	1.000	660.0	2.09E-21	1.000
680.0	1.36E-21	1.000	700.0	9.10E-22	1.000	750.0	3.20E-22	1.000	800.0	1.60E-22	1.000	900.0	0.00E+00	1.000
Photolysis File = O3O1D														
175.4	8.11E-19	0.870	177.0	8.11E-19	0.870	178.6	7.99E-19	0.870	180.2	7.86E-19	0.870	181.8	7.63E-19	0.870
183.5	7.29E-19	0.870	185.2	6.88E-19	0.870	186.9	6.22E-19	0.870	188.7	5.76E-19	0.870	190.5	5.26E-19	0.870
192.3	4.76E-19	0.870	194.2	4.28E-19	0.870	196.1	3.83E-19	0.870	198.0	3.47E-19	0.870	200.0	3.23E-19	0.870
202.0	3.14E-19	0.870	204.1	3.26E-19	0.870	206.2	3.64E-19	0.870	208.3	4.34E-19	0.870	210.5	5.42E-19	0.870
212.8	6.99E-19	0.870	215.0	9.20E-19	0.870	217.4	1.19E-18	0.870	219.8	1.55E-18	0.870	222.2	1.99E-18	0.870
224.7	2.56E-18	0.870	227.3	3.23E-18	0.870	229.9	4.00E-18	0.870	232.6	4.83E-18	0.870	235.3	5.79E-18	0.870
238.1	6.86E-18	0.870	241.0	7.97E-18	0.870	243.9	9.00E-18	0.870	246.9	1.00E-17	0.870	250.1	1.08E-17	0.870
253.2	1.13E-17	0.870	256.4	1.15E-17	0.870	259.7	1.12E-17	0.870	263.2	1.06E-17	0.870	266.7	9.65E-18	0.870
270.3	8.34E-18	0.870	274.0	6.92E-18	0.881	277.8	5.42E-18	0.896	281.7	4.02E-18	0.911	285.7	2.77E-18	0.926
289.9	1.79E-18	0.942	290.0	1.77E-18	0.942	294.1	1.09E-18	0.950	295.0	9.95E-19	0.950	298.5	6.24E-19	0.950
300.0	5.30E-19	0.950	303.0	3.43E-19	0.985	305.0	2.76E-19	0.980	306.0	2.42E-19	0.950	307.0	2.09E-19	0.877
307.7	1.85E-19	0.804	308.0	1.80E-19	0.773	309.0	1.61E-19	0.667	310.0	1.43E-19	0.600	311.0	1.25E-19	0.388
312.0	1.07E-19	0.303	312.5	9.80E-20	0.283	313.0	9.32E-20	0.262	314.0	8.36E-20	0.238	315.0	7.40E-20	0.235
316.0	6.44E-20	0.221	317.0	5.48E-20	0.209	317.5	5.00E-20	0.202	318.0	4.75E-20	0.194	319.0	4.25E-20	0.178
322.5	2.49E-20	0.095	327.5	1.20E-20	0.060	332.5	6.17E-21	0.050	337.5	2.74E-21	0.025	342.5	1.17E-21	0.000
347.5	5.90E-22	0.000												
Photolysis File = HONO-NO														
311.0	0.00E+00	0.411	312.0	2.00E-21	0.421	313.0	4.20E-21	0.432	314.0	4.60E-21	0.443	315.0	4.20E-21	0.454
316.0	3.00E-21	0.464	317.0	4.60E-21	0.475	318.0	3.60E-20	0.486	319.0	6.10E-20	0.496	320.0	2.10E-20	0.507
321.0	4.27E-20	0.518	322.0	4.01E-20	0.529	323.0	3.93E-20	0.539	324.0	4.01E-20	0.550	325.0	4.04E-20	0.561
326.0	3.13E-20	0.571	327.0	4.12E-20	0.582	328.0	7.55E-20	0.593	329.0	6.64E-20	0.604	330.0	7.29E-20	0.614
331.0	8.70E-20	0.625	332.0	1.38E-19	0.636	333.0	5.91E-20	0.646	334.0	5.91E-20	0.657	335.0	6.45E-20	0.668
336.0	5.91E-20	0.679	337.0	4.58E-20	0.689	338.0	1.91E-19	0.700	339.0	1.63E-19	0.711	340.0	1.05E-19	0.721
341.0	8.70E-20	0.732	342.0	3.35E-19	0.743	343.0	2.01E-19	0.754	344.0	1.02E-19	0.764	345.0	8.54E-20	0.775
346.0	8.32E-20	0.786	347.0	8.20E-20	0.796	348.0	7.49E-20	0.807	349.0	7.13E-20	0.818	350.0	6.83E-20	0.829
351.0	1.74E-19	0.839	352.0	1.14E-19	0.850	353.0	3.71E-19	0.861	354.0	4.96E-19	0.871	355.0	2.46E-19	0.882
356.0	1.19E-19	0.893	357.0	9.35E-20	0.904	358.0	7.78E-20	0.914	359.0	7.29E-20	0.925	360.0	6.83E-20	0.936
361.0	6.90E-20	0.946	362.0	7.32E-20	0.957	363.0	9.00E-20	0.968	364.0	1.21E-19	0.979	365.0	1.33E-19	0.989
366.0	2.13E-19	1.000	367.0	3.52E-19	1.000	368.0	4.50E-19	1.000	369.0	2.93E-19	1.000	370.0	1.19E-19	1.000
371.0	9.46E-20	1.000	372.0	8.85E-20	1.000	373.0	7.44E-20	1.000	374.0	4.77E-20	1.000	375.0	2.70E-20	1.000
376.0	1.90E-20	1.000	377.0	1.50E-20	1.000	378.0	1.90E-20	1.000	379.0	5.80E-20	1.000	380.0	7.78E-20	1.000
381.0	1.14E-19	1.000	382.0	1.40E-19	1.000	383.0	1.72E-19	1.000	384.0	1.99E-19	1.000	385.0	1.90E-19	1.000
386.0	1.19E-19	1.000	387.0	5.65E-20	1.000	388.0	3.20E-20	1.000	389.0	1.90E-20	1.000	390.0	1.20E-20	1.000
391.0	5.00E-21	1.000	392.0	0.00E+00	1.000									
Photolysis File = HONO-NO2														
311.0	0.00E+00	0.589	312.0	2.00E-21	0.579	313.0	4.20E-21	0.568	314.0	4.60E-21	0.557	315.0	4.20E-21	0.546
316.0	3.00E-21	0.536	317.0	4.60E-21	0.525	318.0	3.60E-20	0.514	319.0	6.10E-20	0.504	320.0	2.10E-20	0.493
321.0	4.27E-20	0.482	322.0	4.01E-20	0.471	323.0	3.93E-20	0.461	324.0	4.01E-20	0.450	325.0	4.04E-20	0.439
326.0	3.13E-20	0.429	327.0	4.12E-20	0.418	328.0	7.55E-20	0.407	329.0	6.64E-20	0.396	330.0	7.29E-20	0.386
331.0	8.70E-20	0.375	332.0	1.38E-19	0.364	333.0	5.91E-20	0.354	334.0	5.91E-20	0.343	335.0	6.45E-20	0.332
336.0	5.91E-20	0.321	337.0	4.58E-20	0.311	338.0	1.91E-19	0.300	339.0	1.63E-19	0.289	340.0	1.05E-19	0.279
341.0	8.70E-20	0.268	342.0	3.35E-19	0.257	343.0	2.01E-19	0.246	344.0	1.02E-19	0.236	345.0	8.54E-20	0.225
346.0	8.32E-20	0.214	347.0	8.20E-20	0.204	348.0	7.49E-20	0.193	349.0	7.13E-20	0.182	350.0	6.83E-20	0.171
351.0	1.74E-19	0.161	352.0	1.14E-19	0.150	353.0	3.71E-19	0.139	354.0	4.96E-19	0.129	355.0	2.46E-19	0.118
356.0	1.19E-19	0.107	357.0	9.35E-20	0.096	358.0	7.78E-20	0.086	359.0	7.29E-20	0.075	360.0	6.83E-20	0.064
361.0	6.90E-20	0.054	362.0	7.32E-20	0.043	363.0	9.00E-20	0.032	364.0	1.21E-19	0.021	365.0	1.33E-19	0.011
366.0	2.13E-19	0.000												
Photolysis File = HNO3														
190.0	1.36E-17	1.000	195.0	1.02E-17	1.000	200.0	5.88E-18	1.000	205.0	2.80E-18	1.000	210.0	1.04E-18	1.000
215.0	3.65E-19	1.000	220.0	1.49E-19	1.000	225.0	8.81E-20	1.000	230.0	5.75E-20	1.000	235.0	3.75E-20	1.000
240.0	2.58E-20	1.000	245.0	2.11E-20	1.000	250.0	1.97E-20	1.000	255.0	1.95E-20	1.000	260.0	1.91E-20	1.000
265.0	1.80E-20	1.000	270.0	1.62E-20	1.000	275.0	1.38E-20	1.000	280.0	1.12E-20	1.000	285.0	8.58E-21	1.000
290.0	6.15E-21	1.000	295.0	4.12E-21	1.000	300.0	2.63E-21	1.000	305.0	1.50E-21	1.000	310.0	8.10E-22	1.000
315.0	4.10E-22	1.000	320.0	2.00E-22	1.000	325.0	9.50E-23	1.000	330.0	4.30E-23	1.000	335.0	2.20E-23	1.000
340.0	1.00E-23	1.000	345.0	6.00E-24	1.000	350.0	4.00E-24	1.000	355.0	0.00E+00	1.000			
Photolysis File = HO2NO2														
190.0	1.01E-17	1.000	195.0	8.16E-18	1.000	200.0	5.63E-18	1.000	205.0	3.67E-18	1.000	210.0	2.39E-18	1.000
215.0	1.61E-18	1.000	220.0	1.18E-18	1.000	225.0	9.32E-19	1.000	230.0	7.88E-19	1.000	235.0	6.80E-19	1.000
240.0	5.79E-19	1.000	245.0	4.97E-19	1.000	250.0	4.11E-19	1.000	255.0	3.49E-19	1.000	260.0	2.84E-19	1.000
265.0	2.29E-19	1.000	270.0	1.80E-19	1.000	275.0	1.33E-19	1.000	280.0	9.30E-20	1.000	285.0	6.20E-20	1.000
290.0	3.90E-20	1.000	295.0	2.40E-20	1.000	300.0	1.40E-20	1.000	305.0	8.50E-21	1.000	310.0	5.30E-21	1.000
315.0	3.90E-21	1.000	320.0	2.40E-21	1.000	325.0	1.50E-21	1.000	330.0	9.00E-22	1.000	335.0	0.00E+00	1.000

Table A-3. (continued)

WL (nm)	Abs (cm^2)	QY	WL (nm)	Abs (cm^2)	QY	WL (nm)	Abs (cm^2)	QY	WL (nm)	Abs (cm^2)	QY	WL (nm)	Abs (cm^2)	QY
Photolysis File = H2O2														
190.0	6.72E-19	1.000	195.0	5.63E-19	1.000	200.0	4.75E-19	1.000	205.0	4.08E-19	1.000	210.0	3.57E-19	1.000
215.0	3.07E-19	1.000	220.0	2.58E-19	1.000	225.0	2.17E-19	1.000	230.0	1.82E-19	1.000	235.0	1.50E-19	1.000
240.0	1.24E-19	1.000	245.0	1.02E-19	1.000	250.0	8.30E-20	1.000	255.0	6.70E-20	1.000	260.0	5.30E-20	1.000
265.0	4.20E-20	1.000	270.0	3.30E-20	1.000	275.0	2.60E-20	1.000	280.0	2.00E-20	1.000	285.0	1.50E-20	1.000
290.0	1.20E-20	1.000	295.0	9.00E-21	1.000	300.0	6.80E-21	1.000	305.0	5.10E-21	1.000	310.0	3.90E-21	1.000
315.0	2.90E-21	1.000	320.0	2.20E-21	1.000	325.0	1.60E-21	1.000	330.0	1.30E-21	1.000	335.0	1.00E-21	1.000
340.0	7.00E-22	1.000	345.0	5.00E-22	1.000	350.0	4.00E-22	1.000	355.0	0.00E+00	1.000			
Photolysis File = COOH														
210.0	3.12E-19	1.000	215.0	2.09E-19	1.000	220.0	1.54E-19	1.000	225.0	1.22E-19	1.000	230.0	9.62E-20	1.000
235.0	7.61E-20	1.000	240.0	6.05E-20	1.000	245.0	4.88E-20	1.000	250.0	3.98E-20	1.000	255.0	3.23E-20	1.000
260.0	2.56E-20	1.000	265.0	2.11E-20	1.000	270.0	1.70E-20	1.000	275.0	1.39E-20	1.000	280.0	1.09E-20	1.000
285.0	8.63E-21	1.000	290.0	6.91E-21	1.000	295.0	5.51E-21	1.000	300.0	4.13E-21	1.000	305.0	3.13E-21	1.000
310.0	2.39E-21	1.000	315.0	1.82E-21	1.000	320.0	1.37E-21	1.000	325.0	1.05E-21	1.000	330.0	7.90E-22	1.000
335.0	6.10E-22	1.000	340.0	4.70E-22	1.000	345.0	3.50E-22	1.000	350.0	2.70E-22	1.000	355.0	2.10E-22	1.000
360.0	1.60E-22	1.000	365.0	1.20E-22	1.000	370.0	0.00E+00	1.000						
Photolysis File = HCHO_R														
240.0	6.40E-22	0.270	241.0	5.60E-22	0.272	242.0	1.05E-21	0.274	243.0	1.15E-21	0.276	244.0	8.20E-22	0.278
245.0	1.03E-21	0.280	246.0	9.80E-22	0.282	247.0	1.35E-21	0.284	248.0	1.91E-21	0.286	249.0	2.82E-21	0.288
250.0	2.05E-21	0.290	251.0	1.70E-21	0.291	252.0	2.88E-21	0.292	253.0	2.55E-21	0.293	254.0	2.55E-21	0.294
255.0	3.60E-21	0.295	256.0	5.09E-21	0.296	257.0	3.39E-21	0.297	258.0	2.26E-21	0.298	259.0	5.04E-21	0.299
260.0	5.05E-21	0.300	261.0	5.49E-21	0.308	262.0	5.20E-21	0.316	263.0	9.33E-21	0.324	264.0	8.23E-21	0.332
265.0	4.30E-21	0.340	266.0	4.95E-21	0.348	267.0	1.24E-20	0.356	268.0	1.11E-20	0.364	269.0	8.78E-21	0.372
270.0	9.36E-21	0.380	271.0	1.79E-20	0.399	272.0	1.23E-20	0.418	273.0	6.45E-21	0.437	274.0	6.56E-21	0.456
275.0	2.23E-20	0.475	276.0	2.42E-20	0.494	277.0	1.40E-20	0.513	278.0	1.05E-20	0.532	279.0	2.55E-20	0.551
280.0	2.08E-20	0.570	281.0	1.48E-20	0.586	282.0	8.81E-21	0.602	283.0	1.07E-20	0.618	284.0	4.49E-20	0.634
285.0	3.59E-20	0.650	286.0	1.96E-20	0.666	287.0	1.30E-20	0.682	288.0	3.36E-20	0.698	289.0	2.84E-20	0.714
290.0	1.30E-20	0.730	291.0	1.75E-20	0.735	292.0	8.32E-21	0.740	293.0	3.73E-20	0.745	294.0	6.54E-20	0.750
295.0	3.95E-20	0.755	296.0	2.33E-20	0.760	297.0	1.51E-20	0.765	298.0	4.04E-20	0.770	299.0	2.87E-20	0.775
300.0	8.71E-21	0.780	301.0	1.72E-20	0.780	302.0	1.06E-20	0.780	303.0	3.20E-20	0.780	304.0	6.90E-20	0.780
305.0	4.91E-20	0.780	306.0	4.63E-20	0.780	307.0	2.10E-20	0.780	308.0	1.49E-20	0.780	309.0	3.41E-20	0.780
310.0	1.95E-20	0.780	311.0	5.21E-21	0.764	312.0	1.12E-20	0.748	313.0	1.12E-20	0.732	314.0	4.75E-20	0.716
315.0	5.25E-20	0.700	316.0	2.90E-20	0.684	317.0	5.37E-20	0.668	318.0	2.98E-20	0.652	319.0	9.18E-21	0.636
320.0	1.26E-20	0.620	321.0	1.53E-20	0.585	322.0	6.69E-21	0.550	323.0	3.45E-21	0.515	324.0	8.16E-21	0.480
325.0	1.85E-20	0.445	326.0	5.95E-20	0.410	327.0	3.49E-20	0.375	328.0	1.09E-20	0.340	329.0	3.35E-20	0.305
330.0	3.32E-20	0.270	331.0	1.07E-20	0.243	332.0	2.89E-21	0.216	333.0	2.15E-21	0.189	334.0	1.71E-21	0.162
335.0	1.43E-21	0.135	336.0	1.94E-21	0.108	337.0	4.17E-21	0.081	338.0	2.36E-20	0.054	339.0	4.71E-20	0.027
340.0	2.48E-20	0.000												
Photolysis File = HCHO_M														
240.0	6.40E-22	0.490	241.0	5.60E-22	0.490	242.0	1.05E-21	0.490	243.0	1.15E-21	0.490	244.0	8.20E-22	0.490
245.0	1.03E-21	0.490	246.0	9.80E-22	0.490	247.0	1.35E-21	0.490	248.0	1.91E-21	0.490	249.0	2.82E-21	0.490
250.0	2.05E-21	0.490	251.0	1.70E-21	0.490	252.0	2.88E-21	0.490	253.0	2.55E-21	0.490	254.0	2.55E-21	0.490
255.0	3.60E-21	0.490	256.0	5.09E-21	0.490	257.0	3.39E-21	0.490	258.0	2.26E-21	0.490	259.0	5.04E-21	0.490
260.0	5.05E-21	0.490	261.0	5.49E-21	0.484	262.0	5.20E-21	0.478	263.0	9.33E-21	0.472	264.0	8.23E-21	0.466
265.0	4.30E-21	0.460	266.0	4.95E-21	0.454	267.0	1.24E-20	0.448	268.0	1.11E-20	0.442	269.0	8.78E-21	0.436
270.0	9.36E-21	0.430	271.0	1.79E-20	0.419	272.0	1.23E-20	0.408	273.0	6.45E-21	0.397	274.0	6.56E-21	0.386
275.0	2.23E-20	0.375	276.0	2.42E-20	0.364	277.0	1.40E-20	0.353	278.0	1.05E-20	0.342	279.0	2.55E-20	0.331
280.0	2.08E-20	0.320	281.0	1.48E-20	0.312	282.0	8.81E-21	0.304	283.0	1.07E-20	0.296	284.0	4.49E-20	0.288
285.0	3.59E-20	0.280	286.0	1.96E-20	0.272	287.0	1.30E-20	0.264	288.0	3.36E-20	0.256	289.0	2.84E-20	0.248
290.0	1.30E-20	0.240	291.0	1.75E-20	0.237	292.0	8.32E-21	0.234	293.0	3.73E-20	0.231	294.0	6.54E-20	0.228
295.0	3.95E-20	0.225	296.0	2.33E-20	0.222	297.0	1.51E-20	0.219	298.0	4.04E-20	0.216	299.0	2.87E-20	0.213
300.0	8.71E-21	0.210	301.0	1.72E-20	0.211	302.0	1.06E-20	0.212	303.0	3.20E-20	0.213	304.0	6.90E-20	0.214
305.0	4.91E-20	0.215	306.0	4.63E-20	0.216	307.0	2.10E-20	0.217	308.0	1.49E-20	0.218	309.0	3.41E-20	0.219
310.0	1.95E-20	0.220	311.0	5.21E-21	0.236	312.0	1.12E-20	0.252	313.0	1.12E-20	0.268	314.0	4.75E-20	0.284
315.0	5.25E-20	0.300	316.0	2.90E-20	0.316	317.0	5.37E-20	0.332	318.0	2.98E-20	0.348	319.0	9.18E-21	0.364
320.0	1.26E-20	0.380	321.0	1.53E-20	0.408	322.0	6.69E-21	0.436	323.0	3.45E-21	0.464	324.0	8.16E-21	0.492
325.0	1.85E-20	0.520	326.0	5.95E-20	0.548	327.0	3.49E-20	0.576	328.0	1.09E-20	0.604	329.0	3.35E-20	0.632
330.0	3.32E-20	0.660	331.0	1.07E-20	0.650	332.0	2.89E-21	0.640	333.0	2.15E-21	0.630	334.0	1.71E-21	0.620
335.0	1.43E-21	0.610	336.0	1.94E-21	0.600	337.0	4.17E-21	0.590	338.0	2.36E-20	0.580	339.0	4.71E-20	0.570
340.0	2.48E-20	0.560	341.0	7.59E-21	0.525	342.0	6.81E-21	0.490	343.0	1.95E-20	0.455	344.0	1.14E-20	0.420
345.0	3.23E-21	0.385	346.0	1.13E-21	0.350	347.0	6.60E-22	0.315	348.0	1.22E-21	0.280	349.0	3.20E-22	0.245
350.0	3.80E-22	0.210	351.0	1.04E-21	0.192	352.0	7.13E-21	0.174	353.0	2.21E-20	0.156	354.0	1.54E-20	0.138
355.0	6.76E-21	0.120	356.0	1.35E-21	0.102	357.0	3.60E-22	0.084	358.0	5.70E-23	0.066	359.0	5.80E-22	0.048
360.0	8.20E-22	0.000												
Photolysis File = CCHO_R														
262.0	2.44E-20	0.326	266.0	3.05E-20	0.358	270.0	3.42E-20	0.390	274.0	4.03E-20	0.466	278.0	4.19E-20	0.542
280.0	4.50E-20	0.580	281.0	4.69E-20	0.575	282.0	4.72E-20	0.570	283.0	4.75E-20	0.565	284.0	4.61E-20	0.560
285.0	4.49E-20	0.555	286.0	4.44E-20	0.550	287.0	4.59E-20	0.545	288.0	4.72E-20	0.540	289.0	4.77E-20	0.535
290.0	4.89E-20	0.530	291.0	4.78E-20	0.520	292.0	4.68E-20	0.510	293.0	4.53E-20	0.500	294.0	4.33E-20	0.490
295.0	4.27E-20	0.480	296.0	4.24E-20	0.470	297.0	4.38E-20	0.460	298.0	4.41E-20	0.450	299.0	4.26E-20	0.440
300.0	4.16E-20	0.430	301.0	3.99E-20	0.418	302.0	3.86E-20	0.406	303.0	3.72E-20	0.394	304.0	3.48E-20	0.382
305.0	3.42E-20	0.370	306.0	3.42E-20	0.354	307.0	3.36E-20	0.338	308.0	3.33E-20	0.322	309.0	3.14E-20	0.306
310.0	2.93E-20	0.290	311.0	2.76E-20	0.266	312.0	2.53E-20	0.242	313.0	2.47E-20	0.218	314.0	2.44E-20	0.194
315.0	2.20E-20	0.170	316.0	2.04E-20	0.156	317.0	2.07E-20	0.142	318.0	1.98E-20	0.128	319.0	1.87E-20	0.114
320.0	1.72E-20	0.100	321.0	1.48E-20	0.088	322.0	1.40E-20	0.076	323.0	1.24E-20	0.064	324.0	1.09E-20	0.052
325.0	1.14E-20	0.040	326.0	1.07E-20	0.032	327.0	8.58E-21	0.024	328.0	7.47E-21	0.016	329.0	7.07E-21	0.008
Photolysis File = C2CHO														
294.0	5.80E-20	0.890	295.0	5.57E-20	0.885	296.0	5.37E-20	0.880	297.0	5.16E-20	0.875	298.0	5.02E-20	0.870
299.0	5.02E-20	0.865	300.0	5.04E-20	0.860	301.0	5.09E-20	0.855	302.0	5.07E-20	0.850	303.0	4.94E-20	0.818
304.0	4.69E-20	0.786	305.0	4.32E-20	0.755	306.0	4.04E-20	0.723	307.0	3.81E-20	0.691	308.0	3.65E-20	0.659
309.0	3.62E-20	0.627	310.0	3.60E-20	0.596	311.0	3.53E-20	0.564	312.0	3.50E-20	0.532	313.0	3.32E-20	0.500

Table A-3. (continued)

WL (nm)	Abs (cm^2)	QY	WL (nm)	Abs (cm^2)	QY	WL (nm)	Abs (cm^2)	QY	WL (nm)	Abs (cm^2)	QY	WL (nm)	Abs (cm^2)	QY
314.0	3.06E-20	0.480	315.0	2.77E-20	0.460	316.0	2.43E-20	0.440	317.0	2.18E-20	0.420	318.0	2.00E-20	0.400
319.0	1.86E-20	0.380	320.0	1.83E-20	0.360	321.0	1.78E-20	0.340	322.0	1.66E-20	0.320	323.0	1.58E-20	0.300
324.0	1.49E-20	0.280	325.0	1.30E-20	0.260	326.0	1.13E-20	0.248	327.0	9.96E-21	0.236	328.0	8.28E-21	0.223
329.0	6.85E-21	0.211	330.0	5.75E-21	0.199	331.0	4.94E-21	0.187	332.0	4.66E-21	0.174	333.0	4.30E-21	0.162
334.0	3.73E-21	0.150	335.0	3.25E-21	0.133	336.0	2.80E-21	0.117	337.0	2.30E-21	0.100	338.0	1.85E-21	0.083
339.0	1.66E-21	0.067	340.0	1.55E-21	0.050	341.0	1.19E-21	0.033	342.0	7.60E-22	0.017	343.0	4.50E-22	0.000
Photolysis File = ACETONE														
250.0	2.47E-20	0.760	254.0	3.04E-20	0.776	258.0	3.61E-20	0.792	262.0	4.15E-20	0.768	266.0	4.58E-20	0.704
270.0	4.91E-20	0.640	274.0	5.06E-20	0.604	278.0	5.07E-20	0.568	280.0	5.05E-20	0.550	281.0	5.01E-20	0.525
282.0	4.94E-20	0.500	283.0	4.86E-20	0.475	284.0	4.76E-20	0.450	285.0	4.68E-20	0.425	286.0	4.58E-20	0.400
287.0	4.50E-20	0.375	288.0	4.41E-20	0.350	289.0	4.29E-20	0.325	290.0	4.19E-20	0.302	291.0	4.08E-20	0.284
292.0	3.94E-20	0.266	293.0	3.81E-20	0.249	294.0	3.67E-20	0.232	295.0	3.52E-20	0.217	296.0	3.35E-20	0.201
297.0	3.20E-20	0.187	298.0	3.07E-20	0.173	299.0	2.91E-20	0.160	300.0	2.77E-20	0.147	301.0	2.66E-20	0.135
302.0	2.53E-20	0.124	303.0	2.37E-20	0.114	304.0	2.24E-20	0.104	305.0	2.11E-20	0.095	306.0	1.95E-20	0.086
307.0	1.80E-20	0.078	308.0	1.66E-20	0.071	309.0	1.54E-20	0.064	310.0	1.41E-20	0.057	311.0	1.28E-20	0.052
312.0	1.17E-20	0.046	313.0	1.08E-20	0.042	314.0	9.67E-21	0.037	315.0	8.58E-21	0.033	316.0	7.77E-21	0.029
317.0	6.99E-21	0.026	318.0	6.08E-21	0.023	319.0	5.30E-21	0.020	320.0	4.67E-21	0.018	321.0	4.07E-21	0.016
322.0	3.44E-21	0.014	323.0	2.87E-21	0.012	324.0	2.43E-21	0.011	325.0	2.05E-21	0.009	326.0	1.68E-21	0.008
327.0	1.35E-21	0.007	328.0	1.08E-21	0.006	329.0	8.60E-22	0.005	330.0	6.70E-22	0.005	331.0	5.10E-22	0.004
332.0	4.00E-22	0.003	333.0	3.10E-22	0.003	334.0	2.60E-22	0.002	335.0	1.70E-22	0.002	336.0	1.40E-22	0.002
337.0	1.10E-22	0.002	338.0	9.00E-23	0.001	339.0	6.00E-23	0.001	340.0	5.00E-23	0.001	341.0	5.00E-23	0.001
342.0	3.00E-23	0.001	343.0	4.00E-23	0.001	344.0	2.00E-23	0.000						
Photolysis File = KETONE														
198.5	3.95E-19	1.000	199.0	1.61E-19	1.000	199.5	7.75E-20	1.000	200.0	3.76E-20	1.000	200.5	2.51E-20	1.000
201.0	1.83E-20	1.000	201.5	1.36E-20	1.000	202.0	1.16E-20	1.000	202.5	8.97E-21	1.000	203.0	4.62E-21	1.000
203.5	3.18E-21	1.000	204.0	2.42E-21	1.000	204.5	2.01E-21	1.000	205.0	1.77E-21	1.000	205.5	1.64E-21	1.000
206.0	1.54E-21	1.000	206.5	1.52E-21	1.000	207.0	1.54E-21	1.000	207.5	1.62E-21	1.000	208.0	1.64E-21	1.000
208.5	1.60E-21	1.000	209.0	1.57E-21	1.000	209.5	1.49E-21	1.000	210.0	1.47E-21	1.000	210.5	1.52E-21	1.000
211.0	1.50E-21	1.000	211.5	1.62E-21	1.000	212.0	1.81E-21	1.000	212.5	2.10E-21	1.000	213.0	2.23E-21	1.000
213.5	2.06E-21	1.000	214.0	1.69E-21	1.000	214.5	1.49E-21	1.000	215.0	1.42E-21	1.000	215.5	1.42E-21	1.000
216.0	1.42E-21	1.000	216.5	1.48E-21	1.000	217.0	1.48E-21	1.000	217.5	1.53E-21	1.000	218.0	1.56E-21	1.000
218.5	1.67E-21	1.000	219.0	1.68E-21	1.000	219.5	1.78E-21	1.000	220.0	1.85E-21	1.000	220.5	1.92E-21	1.000
221.0	2.01E-21	1.000	221.5	2.11E-21	1.000	222.0	2.23E-21	1.000	222.5	2.33E-21	1.000	223.0	2.48E-21	1.000
223.5	2.60E-21	1.000	224.0	2.74E-21	1.000	224.5	2.85E-21	1.000	225.0	3.04E-21	1.000	225.5	3.15E-21	1.000
226.0	3.33E-21	1.000	226.5	3.55E-21	1.000	227.0	3.73E-21	1.000	227.5	3.93E-21	1.000	228.0	4.11E-21	1.000
228.5	4.34E-21	1.000	229.0	4.56E-21	1.000	229.5	4.75E-21	1.000	230.0	5.01E-21	1.000	230.5	5.27E-21	1.000
231.0	5.53E-21	1.000	231.5	5.83E-21	1.000	232.0	6.15E-21	1.000	232.5	6.45E-21	1.000	233.0	6.73E-21	1.000
233.5	7.02E-21	1.000	234.0	7.42E-21	1.000	234.5	7.83E-21	1.000	235.0	8.11E-21	1.000	235.5	8.45E-21	1.000
236.0	8.82E-21	1.000	236.5	9.21E-21	1.000	237.0	9.65E-21	1.000	237.5	1.00E-20	1.000	238.0	1.05E-20	1.000
238.5	1.10E-20	1.000	239.0	1.15E-20	1.000	239.5	1.20E-20	1.000	240.0	1.23E-20	1.000	240.5	1.28E-20	1.000
241.0	1.32E-20	1.000	241.5	1.38E-20	1.000	242.0	1.44E-20	1.000	242.5	1.50E-20	1.000	243.0	1.57E-20	1.000
243.5	1.63E-20	1.000	244.0	1.68E-20	1.000	244.5	1.75E-20	1.000	245.0	1.81E-20	1.000	245.5	1.88E-20	1.000
246.0	1.96E-20	1.000	246.5	2.03E-20	1.000	247.0	2.11E-20	1.000	247.5	2.19E-20	1.000	248.0	2.25E-20	1.000
248.5	2.33E-20	1.000	249.0	2.40E-20	1.000	249.5	2.48E-20	1.000	250.0	2.56E-20	1.000	250.5	2.64E-20	1.000
251.0	2.73E-20	1.000	251.5	2.81E-20	1.000	252.0	2.88E-20	1.000	252.5	2.98E-20	1.000	253.0	3.07E-20	1.000
253.5	3.16E-20	1.000	254.0	3.25E-20	1.000	254.5	3.34E-20	1.000	255.0	3.43E-20	1.000	255.5	3.51E-20	1.000
256.0	3.59E-20	1.000	256.5	3.67E-20	1.000	257.0	3.75E-20	1.000	257.5	3.84E-20	1.000	258.0	3.94E-20	1.000
258.5	4.03E-20	1.000	259.0	4.13E-20	1.000	259.5	4.22E-20	1.000	260.0	4.28E-20	1.000	260.5	4.33E-20	1.000
261.0	4.41E-20	1.000	261.5	4.49E-20	1.000	262.0	4.57E-20	1.000	262.5	4.65E-20	1.000	263.0	4.72E-20	1.000
263.5	4.78E-20	1.000	264.0	4.85E-20	1.000	264.5	4.92E-20	1.000	265.0	4.99E-20	1.000	265.5	5.04E-20	1.000
266.0	5.12E-20	1.000	266.5	5.22E-20	1.000	267.0	5.28E-20	1.000	267.5	5.34E-20	1.000	268.0	5.41E-20	1.000
268.5	5.46E-20	1.000	269.0	5.51E-20	1.000	269.5	5.55E-20	1.000	270.0	5.59E-20	1.000	270.5	5.63E-20	1.000
271.0	5.66E-20	1.000	271.5	5.70E-20	1.000	272.0	5.74E-20	1.000	272.5	5.78E-20	1.000	273.0	5.81E-20	1.000
273.5	5.86E-20	1.000	274.0	5.90E-20	1.000	274.5	5.93E-20	1.000	275.0	5.96E-20	1.000	275.5	5.97E-20	1.000
276.0	5.98E-20	1.000	276.5	5.98E-20	1.000	277.0	5.99E-20	1.000	277.5	5.99E-20	1.000	278.0	5.98E-20	1.000
278.5	5.96E-20	1.000	279.0	5.96E-20	1.000	279.5	5.95E-20	1.000	280.0	5.94E-20	1.000	280.5	5.92E-20	1.000
281.0	5.90E-20	1.000	281.5	5.88E-20	1.000	282.0	5.86E-20	1.000	282.5	5.83E-20	1.000	283.0	5.79E-20	1.000
283.5	5.75E-20	1.000	284.0	5.71E-20	1.000	284.5	5.67E-20	1.000	285.0	5.61E-20	1.000	285.5	5.56E-20	1.000
286.0	5.51E-20	1.000	286.5	5.45E-20	1.000	287.0	5.41E-20	1.000	287.5	5.37E-20	1.000	288.0	5.33E-20	1.000
288.5	5.27E-20	1.000	289.0	5.21E-20	1.000	289.5	5.15E-20	1.000	290.0	5.08E-20	1.000	290.5	4.99E-20	1.000
291.0	4.89E-20	1.000	291.5	4.82E-20	1.000	292.0	4.73E-20	1.000	292.5	4.62E-20	1.000	293.0	4.53E-20	1.000
293.5	4.41E-20	1.000	294.0	4.32E-20	1.000	294.5	4.23E-20	1.000	295.0	4.15E-20	1.000	295.5	4.11E-20	1.000
296.0	4.01E-20	1.000	296.5	3.94E-20	1.000	297.0	3.88E-20	1.000	297.5	3.77E-20	1.000	298.0	3.69E-20	1.000
298.5	3.63E-20	1.000	299.0	3.54E-20	1.000	299.5	3.46E-20	1.000	300.0	3.36E-20	1.000	300.5	3.24E-20	1.000
301.0	3.16E-20	1.000	301.5	3.06E-20	1.000	302.0	2.95E-20	1.000	302.5	2.82E-20	1.000	303.0	2.70E-20	1.000
303.5	2.59E-20	1.000	304.0	2.49E-20	1.000	304.5	2.42E-20	1.000	305.0	2.34E-20	1.000	305.5	2.28E-20	1.000
306.0	2.19E-20	1.000	306.5	2.11E-20	1.000	307.0	2.04E-20	1.000	307.5	1.93E-20	1.000	308.0	1.88E-20	1.000
308.5	1.80E-20	1.000	309.0	1.73E-20	1.000	309.5	1.66E-20	1.000	310.0	1.58E-20	1.000	310.5	1.48E-20	1.000
311.0	1.42E-20	1.000	311.5	1.34E-20	1.000	312.0	1.26E-20	1.000	312.5	1.17E-20	1.000	313.0	1.13E-20	1.000
313.5	1.08E-20	1.000	314.0	1.04E-20	1.000	314.5	9.69E-21	1.000	315.0	8.91E-21	1.000	315.5	8.61E-21	1.000
316.0	7.88E-21	1.000	316.5	7.25E-21	1.000	317.0	6.92E-21	1.000	317.5	6.43E-21	1.000	318.0	6.07E-21	1.000
318.5	5.64E-21	1.000	319.0	5.19E-21	1.000	319.5	4.66E-21	1.000	320.0	4.36E-21	1.000	320.5	3.95E-21	1.000
321.0	3.64E-21	1.000	321.5	3.38E-21	1.000	322.0	3.17E-21	1.000	322.5	2.80E-21	1.000	323.0	2.62E-21	1.000
323.5	2.29E-21	1.000	324.0	2.13E-21	1.000	324.5	1.93E-21	1.000	325.0	1.70E-21	1.000	325.5	1.58E-21	1.000
326.0	1.48E-21	1.000	326.5	1.24E-21	1.000	327.0	1.20E-21	1.000	327.5	1.04E-21	1.000	328.0	9.51E-22	1.000
328.5	8.44E-22	1.000	329.0	7.26E-22	1.000	329.5	6.70E-22	1.000	330.0	6.08E-22	1.000	330.5	5.15E-22	1.000
331.0	4.56E-22	1.000	331.5	4.13E-22	1.000	332.0	3.56E-22	1.000	332.5	3.30E-22	1.000	333.0	2.97E-22	1.000
333.5	2.67E-22	1.000	334.0	2.46E-22	1.000	334.5	2.21E-22	1.000	335.0	1.93E-22	1.000	335.5	1.56E-22	1.000
336.0	1.47E-22	1.000	336.5	1.37E-22	1.000	337.0	1.27E-22	1.000	337.5	1.19E-22	1.000	338.0	1.09E-22	1.000
338.5	1.01E-22	1.000	339.0	9.09E-23	1.000	339.5	8.22E-23	1.000	340.0	7.66E-23	1.000	340.5	7.43E-23	1.000
341.0	6.83E-23	1.000	341.5	6.72E-23	1.000	342.0	6.04E-23	1.000	342.5	4.78E-23	1.000	343.0	0.00E+00	1.000
Photolysis File = IC3ONO2														
185.0	1.79E-17	1.000	188.0	1.81E-17	1.000	190.0	1.79E-17	1.000	195.0	1.61E-17	1.000	200.0	1.26E-17	1.000

Table A-3. (continued)

WL (nm)	Abs (cm^2)	QY	WL (nm)	Abs (cm^2)	QY	WL (nm)	Abs (cm^2)	QY	WL (nm)	Abs (cm^2)	QY	WL (nm)	Abs (cm^2)	QY
205.0	8.67E-18	1.000	210.0	4.98E-18	1.000	215.0	2.47E-18	1.000	220.0	1.17E-18	1.000	225.0	5.80E-19	1.000
230.0	3.10E-19	1.000	235.0	1.80E-19	1.000	240.0	1.10E-19	1.000	245.0	7.00E-20	1.000	250.0	5.70E-20	1.000
255.0	5.20E-20	1.000	260.0	4.90E-20	1.000	265.0	4.60E-20	1.000	270.0	4.10E-20	1.000	275.0	3.60E-20	1.000
280.0	2.90E-20	1.000	285.0	2.30E-20	1.000	290.0	1.70E-20	1.000	295.0	1.20E-20	1.000	300.0	8.10E-21	1.000
305.0	5.20E-21	1.000	310.0	3.20E-21	1.000	315.0	1.90E-21	1.000	320.0	1.10E-21	1.000	325.0	6.10E-22	1.000
330.0	3.70E-22	1.000	335.0	0.00E+00	1.000									
Photolysis File = GLY_R														
230.0	2.87E-21	1.000	235.0	2.87E-21	1.000	240.0	4.30E-21	1.000	245.0	5.73E-21	1.000	250.0	8.60E-21	1.000
255.0	1.15E-20	1.000	260.0	1.43E-20	1.000	265.0	1.86E-20	1.000	270.0	2.29E-20	1.000	275.0	2.58E-20	1.000
280.0	2.87E-20	1.000	285.0	3.30E-20	1.000	290.0	3.15E-20	1.000	295.0	3.30E-20	1.000	300.0	3.58E-20	1.000
305.0	2.72E-20	1.000	310.0	2.72E-20	1.000	312.5	2.87E-20	1.000	315.0	2.29E-20	1.000	320.0	1.43E-20	1.000
325.0	1.15E-20	1.000	327.5	1.43E-20	1.000	330.0	1.15E-20	1.000	335.0	2.87E-21	1.000	340.0	0.00E+00	1.000
345.0	0.00E+00	1.000	350.0	0.00E+00	1.000	355.0	0.00E+00	1.000	360.0	2.29E-21	1.000	365.0	2.87E-21	1.000
370.0	8.03E-21	1.000	375.0	1.00E-20	1.000	380.0	1.72E-20	0.972	382.0	1.58E-20	0.855	384.0	1.49E-20	0.737
386.0	1.49E-20	0.619	388.0	2.87E-20	0.502	390.0	3.15E-20	0.384	391.0	3.24E-20	0.326	392.0	3.04E-20	0.267
393.0	2.23E-20	0.208	394.0	2.63E-20	0.149	395.0	3.04E-20	0.090	396.0	2.63E-20	0.032	397.0	2.43E-20	0.000
398.0	3.24E-20	0.000	399.0	3.04E-20	0.000	400.0	2.84E-20	0.000	401.0	3.24E-20	0.000	402.0	4.46E-20	0.000
403.0	5.27E-20	0.000	404.0	4.26E-20	0.000	405.0	3.04E-20	0.000	406.0	3.04E-20	0.000	407.0	2.84E-20	0.000
408.0	2.43E-20	0.000	409.0	2.84E-20	0.000	410.0	6.08E-20	0.000	411.0	5.07E-20	0.000	411.5	6.08E-20	0.000
412.0	4.86E-20	0.000	413.0	8.31E-20	0.000	413.5	6.48E-20	0.000	414.0	7.50E-20	0.000	414.5	8.11E-20	0.000
415.0	8.11E-20	0.000	415.5	6.89E-20	0.000	416.0	4.26E-20	0.000	417.0	4.86E-20	0.000	418.0	5.88E-20	0.000
Photolysis File = GLY_ABS														
230.0	2.87E-21	1.000	235.0	2.87E-21	1.000	240.0	4.30E-21	1.000	245.0	5.73E-21	1.000	250.0	8.60E-21	1.000
255.0	1.15E-20	1.000	260.0	1.43E-20	1.000	265.0	1.86E-20	1.000	270.0	2.29E-20	1.000	275.0	2.58E-20	1.000
280.0	2.87E-20	1.000	285.0	3.30E-20	1.000	290.0	3.15E-20	1.000	295.0	3.30E-20	1.000	300.0	3.58E-20	1.000
305.0	2.72E-20	1.000	310.0	2.72E-20	1.000	312.5	2.87E-20	1.000	315.0	2.29E-20	1.000	320.0	1.43E-20	1.000
325.0	1.15E-20	1.000	327.5	1.43E-20	1.000	330.0	1.15E-20	1.000	335.0	2.87E-21	1.000	340.0	0.00E+00	1.000
355.0	0.00E+00	1.000	360.0	2.29E-21	1.000	365.0	2.87E-21	1.000	370.0	8.03E-21	1.000	375.0	1.00E-20	1.000
380.0	1.72E-20	1.000	382.0	1.58E-20	1.000	384.0	1.49E-20	1.000	386.0	1.49E-20	1.000	388.0	2.87E-20	1.000
390.0	3.15E-20	1.000	391.0	3.24E-20	1.000	392.0	3.04E-20	1.000	393.0	2.23E-20	1.000	394.0	2.63E-20	1.000
395.0	3.04E-20	1.000	396.0	2.63E-20	1.000	397.0	2.43E-20	1.000	398.0	3.24E-20	1.000	399.0	3.04E-20	1.000
400.0	2.84E-20	1.000	401.0	3.24E-20	1.000	402.0	4.46E-20	1.000	403.0	5.27E-20	1.000	404.0	4.26E-20	1.000
405.0	3.04E-20	1.000	406.0	3.04E-20	1.000	407.0	2.84E-20	1.000	408.0	2.43E-20	1.000	409.0	2.84E-20	1.000
410.0	6.08E-20	1.000	411.0	5.07E-20	1.000	411.5	6.08E-20	1.000	412.0	4.86E-20	1.000	413.0	8.31E-20	1.000
413.5	6.48E-20	1.000	414.0	7.50E-20	1.000	414.5	8.11E-20	1.000	415.0	8.11E-20	1.000	415.5	6.89E-20	1.000
416.0	4.26E-20	1.000	417.0	4.86E-20	1.000	418.0	5.88E-20	1.000	419.0	6.69E-20	1.000	420.0	3.85E-20	1.000
421.0	5.67E-20	1.000	421.5	4.46E-20	1.000	422.0	5.27E-20	1.000	422.5	1.05E-19	1.000	423.0	8.51E-20	1.000
424.0	6.08E-20	1.000	425.0	7.29E-20	1.000	426.0	1.18E-19	1.000	426.5	1.30E-19	1.000	427.0	1.07E-19	1.000
428.0	1.66E-19	1.000	429.0	4.05E-20	1.000	430.0	5.07E-20	1.000	431.0	4.86E-20	1.000	432.0	4.05E-20	1.000
433.0	3.65E-20	1.000	434.0	4.05E-20	1.000	434.5	6.08E-20	1.000	435.0	5.07E-20	1.000	436.0	8.11E-20	1.000
436.5	1.13E-19	1.000	437.0	5.27E-20	1.000	438.0	1.01E-19	1.000	438.5	1.38E-19	1.000	439.0	7.70E-20	1.000
440.0	2.47E-19	1.000	441.0	8.11E-20	1.000	442.0	6.08E-20	1.000	443.0	7.50E-20	1.000	444.0	9.32E-20	1.000
445.0	1.13E-19	1.000	446.0	5.27E-20	1.000	447.0	2.43E-20	1.000	448.0	2.84E-20	1.000	449.0	3.85E-20	1.000
450.0	6.08E-20	1.000	451.0	1.09E-19	1.000	451.5	9.32E-20	1.000	452.0	1.22E-19	1.000	453.0	2.39E-19	1.000
454.0	1.70E-19	1.000	455.0	3.40E-19	1.000	455.5	4.05E-19	1.000	456.0	1.01E-19	1.000	457.0	1.62E-20	1.000
458.0	1.22E-20	1.000	458.5	1.42E-20	1.000	459.0	4.05E-21	1.000	460.0	4.05E-21	1.000	460.5	6.08E-21	1.000
461.0	2.03E-21	1.000	462.0	0.00E+00	1.000									
Photolysis File = MGLY_ADJ														
219.0	9.84E-21	1.000	219.5	1.04E-20	1.000	220.0	1.06E-20	1.000	220.5	1.11E-20	1.000	221.0	1.15E-20	1.000
221.5	1.18E-20	1.000	222.0	1.22E-20	1.000	222.5	1.24E-20	1.000	223.0	1.26E-20	1.000	223.5	1.26E-20	1.000
224.0	1.25E-20	1.000	224.5	1.24E-20	1.000	225.0	1.25E-20	1.000	225.5	1.27E-20	1.000	226.0	1.27E-20	1.000
226.5	1.29E-20	1.000	227.0	1.31E-20	1.000	227.5	1.32E-20	1.000	228.0	1.35E-20	1.000	228.5	1.37E-20	1.000
229.0	1.40E-20	1.000	229.5	1.42E-20	1.000	230.0	1.48E-20	1.000	230.5	1.53E-20	1.000	231.0	1.57E-20	1.000
231.5	1.59E-20	1.000	232.0	1.61E-20	1.000	232.5	1.62E-20	1.000	233.0	1.61E-20	1.000	233.5	1.68E-20	1.000
234.0	1.74E-20	1.000	234.5	1.80E-20	1.000	235.0	1.84E-20	1.000	235.5	1.87E-20	1.000	236.0	1.89E-20	1.000
236.5	1.91E-20	1.000	237.0	1.93E-20	1.000	237.5	1.94E-20	1.000	238.0	1.96E-20	1.000	238.5	1.96E-20	1.000
239.0	2.01E-20	1.000	239.5	2.04E-20	1.000	240.0	2.08E-20	1.000	240.5	2.10E-20	1.000	241.0	2.14E-20	1.000
241.5	2.16E-20	1.000	242.0	2.19E-20	1.000	242.5	2.20E-20	1.000	243.0	2.23E-20	1.000	243.5	2.26E-20	1.000
244.0	2.28E-20	1.000	244.5	2.29E-20	1.000	245.0	2.30E-20	1.000	245.5	2.32E-20	1.000	246.0	2.33E-20	1.000
246.5	2.35E-20	1.000	247.0	2.38E-20	1.000	247.5	2.41E-20	1.000	248.0	2.46E-20	1.000	248.5	2.51E-20	1.000
249.0	2.57E-20	1.000	249.5	2.61E-20	1.000	250.0	2.65E-20	1.000	250.5	2.67E-20	1.000	251.0	2.69E-20	1.000
251.5	2.69E-20	1.000	252.0	2.71E-20	1.000	252.5	2.72E-20	1.000	253.0	2.73E-20	1.000	253.5	2.74E-20	1.000
254.0	2.76E-20	1.000	254.5	2.78E-20	1.000	255.0	2.82E-20	1.000	255.5	2.87E-20	1.000	256.0	2.93E-20	1.000
256.5	2.98E-20	1.000	257.0	3.07E-20	1.000	257.5	3.12E-20	1.000	258.0	3.17E-20	1.000	258.5	3.21E-20	1.000
259.0	3.26E-20	1.000	259.5	3.28E-20	1.000	260.0	3.29E-20	1.000	260.5	3.31E-20	1.000	261.0	3.33E-20	1.000
261.5	3.34E-20	1.000	262.0	3.36E-20	1.000	262.5	3.38E-20	1.000	263.0	3.42E-20	1.000	263.5	3.44E-20	1.000
264.0	3.48E-20	1.000	264.5	3.54E-20	1.000	265.0	3.59E-20	1.000	265.5	3.65E-20	1.000	266.0	3.73E-20	1.000
266.5	3.80E-20	1.000	267.0	3.87E-20	1.000	267.5	3.95E-20	1.000	268.0	4.02E-20	1.000	268.5	4.08E-20	1.000
269.0	4.13E-20	1.000	269.5	4.17E-20	1.000	270.0	4.20E-20	1.000	270.5	4.22E-20	1.000	271.0	4.22E-20	1.000
271.5	4.22E-20	1.000	272.0	4.23E-20	1.000	272.5	4.24E-20	1.000	273.0	4.27E-20	1.000	273.5	4.29E-20	1.000
274.0	4.31E-20	1.000	274.5	4.33E-20	1.000	275.0	4.37E-20	1.000	275.5	4.42E-20	1.000	276.0	4.48E-20	1.000
276.5	4.56E-20	1.000	277.0	4.64E-20	1.000	277.5	4.71E-20	1.000	278.0	4.78E-20	1.000	278.5	4.83E-20	1.000
279.0	4.87E-20	1.000	279.5	4.90E-20	1.000	280.0	4.92E-20	1.000	280.5	4.93E-20	1.000	281.0	4.94E-20	1.000
281.5	4.92E-20	1.000	282.0	4.90E-20	1.000	282.5	4.86E-20	1.000	283.0	4.83E-20	1.000	283.5	4.79E-20	1.000
284.0	4.76E-20	1.000	284.5	4.72E-20	1.000	285.0	4.70E-20	1.000	285.5	4.68E-20	1.000	286.0	4.66E-20	1.000
286.5	4.65E-20	1.000	287.0	4.65E-20	1.000	287.5	4.68E-20	1.000	288.0	4.73E-20	1.000	288.5	4.78E-20	1.000
289.0	4.84E-20	1.000	289.5	4.89E-20	1.000	290.0	4.92E-20	1.000	290.5	4.92E-20	1.000	291.0	4.90E-20	1.000
291.5	4.86E-20	1.000	292.0	4.81E-20	1.000	292.5	4.75E-20	1.000	293.0	4.70E-20	1.000	293.5	4.65E-20	1.000
294.0	4.58E-20	1.000	294.5	4.48E-20	1.000	295.0	4.38E-20	1.000	295.5	4.27E-20	1.000	296.0	4.17E-20	1.000
296.5	4.07E-20	1.000	297.0	3.99E-20	1.000	297.5	3.94E-20	1.000	298.0	3.88E-20	1.000	298.5	3.82E-20	1.000
299.0	3.76E-20	1.000	299.5	3.72E-20	1.000	300.0	3.69E-20	1.000	300.5	3.68E-20	1.000	301.0	3.70E-20	1.000
301.5	3.72E-20	1.000	302.0	3.74E-20	1.000	302.5	3.74E-20	1.000	303.0	3.75E-20	1.000	303.5	3.71E-20	1.000
304.0	3.62E-20	1.000	304.5	3.51E-20	1.000	305.0	3.38E-20	1.000	305.5	3.25E-20	1.000	306.0	3.15E-20	1.000

Table A-3. (continued)

WL (nm)	Abs (cm^2)	QY	WL (nm)	Abs (cm^2)	QY	WL (nm)	Abs (cm^2)	QY	WL (nm)	Abs (cm^2)	QY	WL (nm)	Abs (cm^2)	QY
306.5	3.04E-20	1.000	307.0	2.92E-20	1.000	307.5	2.80E-20	1.000	308.0	2.71E-20	1.000	308.5	2.63E-20	1.000
309.0	2.52E-20	1.000	309.5	2.43E-20	1.000	310.0	2.34E-20	1.000	310.5	2.25E-20	1.000	311.0	2.19E-20	1.000
311.5	2.12E-20	1.000	312.0	2.06E-20	1.000	312.5	2.02E-20	1.000	313.0	1.96E-20	1.000	313.5	1.92E-20	1.000
314.0	1.91E-20	1.000	314.5	1.88E-20	1.000	315.0	1.86E-20	1.000	315.5	1.85E-20	1.000	316.0	1.86E-20	1.000
316.5	1.87E-20	1.000	317.0	1.87E-20	1.000	317.5	1.87E-20	1.000	318.0	1.83E-20	1.000	318.5	1.75E-20	1.000
319.0	1.69E-20	1.000	319.5	1.60E-20	1.000	320.0	1.50E-20	1.000	320.5	1.41E-20	1.000	321.0	1.34E-20	1.000
321.5	1.27E-20	1.000	322.0	1.21E-20	1.000	322.5	1.18E-20	1.000	323.0	1.14E-20	1.000	323.5	1.08E-20	1.000
324.0	1.01E-20	1.000	324.5	9.62E-21	1.000	325.0	9.28E-21	1.000	325.5	8.75E-21	1.000	326.0	8.49E-21	1.000
326.5	8.21E-21	1.000	327.0	7.71E-21	1.000	327.5	7.38E-21	1.000	328.0	7.18E-21	1.000	328.5	6.86E-21	1.000
329.0	6.71E-21	1.000	329.5	6.63E-21	1.000	330.0	6.46E-21	1.000	330.5	6.29E-21	1.000	331.0	6.21E-21	1.000
331.5	6.18E-21	1.000	332.0	6.20E-21	1.000	332.5	5.49E-21	1.000	333.0	5.21E-21	1.000	333.5	5.38E-21	1.000
334.0	5.35E-21	1.000	334.5	5.04E-21	1.000	335.0	4.94E-21	1.000	335.5	4.90E-21	1.000	336.0	4.52E-21	1.000
336.5	4.26E-21	1.000	337.0	4.11E-21	1.000	337.5	3.76E-21	1.000	338.0	3.61E-21	1.000	338.5	3.58E-21	1.000
339.0	3.47E-21	1.000	339.5	3.32E-21	1.000	340.0	3.22E-21	1.000	340.5	3.10E-21	1.000	341.0	3.00E-21	1.000
341.5	2.94E-21	1.000	342.0	2.89E-21	1.000	342.5	2.86E-21	1.000	343.0	2.88E-21	1.000	343.5	2.88E-21	1.000
344.0	2.89E-21	0.992	344.5	2.91E-21	0.984	345.0	2.95E-21	0.976	345.5	3.00E-21	0.968	346.0	3.08E-21	0.960
346.5	3.18E-21	0.953	347.0	3.25E-21	0.945	347.5	3.30E-21	0.937	348.0	3.39E-21	0.929	348.5	3.51E-21	0.921
349.0	3.63E-21	0.913	349.5	3.73E-21	0.905	350.0	3.85E-21	0.897	350.5	3.99E-21	0.889	351.0	4.27E-21	0.881
351.5	4.47E-21	0.873	352.0	4.63E-21	0.865	352.5	4.78E-21	0.858	353.0	4.92E-21	0.850	353.5	5.07E-21	0.842
354.0	5.23E-21	0.834	354.5	5.39E-21	0.826	355.0	5.56E-21	0.818	355.5	5.77E-21	0.810	356.0	5.97E-21	0.802
356.5	6.15E-21	0.794	357.0	6.35E-21	0.786	357.5	6.56E-21	0.778	358.0	6.76E-21	0.770	358.5	6.95E-21	0.763
359.0	7.20E-21	0.755	359.5	7.44E-21	0.747	360.0	7.64E-21	0.739	360.5	7.89E-21	0.731	361.0	8.15E-21	0.723
361.5	8.43E-21	0.715	362.0	8.71E-21	0.707	362.5	9.02E-21	0.699	363.0	9.33E-21	0.691	363.5	9.65E-21	0.683
364.0	1.00E-20	0.675	364.5	1.04E-20	0.668	365.0	1.08E-20	0.660	365.5	1.11E-20	0.652	366.0	1.15E-20	0.644
366.5	1.19E-20	0.636	367.0	1.23E-20	0.628	367.5	1.27E-20	0.620	368.0	1.31E-20	0.612	368.5	1.35E-20	0.604
369.0	1.40E-20	0.596	369.5	1.44E-20	0.588	370.0	1.47E-20	0.580	370.5	1.51E-20	0.573	371.0	1.55E-20	0.565
371.5	1.59E-20	0.557	372.0	1.64E-20	0.549	372.5	1.70E-20	0.541	373.0	1.73E-20	0.533	373.5	1.77E-20	0.525
374.0	1.81E-20	0.517	374.5	1.86E-20	0.509	375.0	1.90E-20	0.501	375.5	1.96E-20	0.493	376.0	2.02E-20	0.486
376.5	2.06E-20	0.478	377.0	2.10E-20	0.470	377.5	2.14E-20	0.462	378.0	2.18E-20	0.454	378.5	2.24E-20	0.446
379.0	2.30E-20	0.438	379.5	2.37E-20	0.430	380.0	2.42E-20	0.422	380.5	2.47E-20	0.414	381.0	2.54E-20	0.406
381.5	2.62E-20	0.398	382.0	2.69E-20	0.391	382.5	2.79E-20	0.383	383.0	2.88E-20	0.375	383.5	2.96E-20	0.367
384.0	3.02E-20	0.359	384.5	3.10E-20	0.351	385.0	3.20E-20	0.343	385.5	3.29E-20	0.335	386.0	3.39E-20	0.327
386.5	3.51E-20	0.319	387.0	3.62E-20	0.311	387.5	3.69E-20	0.303	388.0	3.70E-20	0.296	388.5	3.77E-20	0.288
389.0	3.88E-20	0.280	389.5	3.97E-20	0.272	390.0	4.03E-20	0.264	390.5	4.12E-20	0.256	391.0	4.22E-20	0.248
391.5	4.29E-20	0.240	392.0	4.30E-20	0.232	392.5	4.38E-20	0.224	393.0	4.47E-20	0.216	393.5	4.55E-20	0.208
394.0	4.56E-20	0.201	394.5	4.59E-20	0.193	395.0	4.67E-20	0.185	395.5	4.80E-20	0.177	396.0	4.87E-20	0.169
396.5	4.96E-20	0.161	397.0	5.08E-20	0.153	397.5	5.19E-20	0.145	398.0	5.23E-20	0.137	398.5	5.39E-20	0.129
399.0	5.46E-20	0.121	399.5	5.54E-20	0.113	400.0	5.59E-20	0.106	400.5	5.77E-20	0.098	401.0	5.91E-20	0.090
401.5	5.99E-20	0.082	402.0	6.06E-20	0.074	402.5	6.20E-20	0.066	403.0	6.35E-20	0.058	403.5	6.52E-20	0.050
404.0	6.54E-20	0.042	404.5	6.64E-20	0.034	405.0	6.93E-20	0.026	405.5	7.15E-20	0.018	406.0	7.19E-20	0.011
406.5	7.32E-20	0.003	407.0	7.58E-20	0.000	407.5	7.88E-20	0.000	408.0	7.97E-20	0.000	408.5	7.91E-20	0.000
409.0	8.11E-20	0.000	409.5	8.41E-20	0.000	410.0	8.53E-20	0.000	410.5	8.59E-20	0.000	411.0	8.60E-20	0.000
411.5	8.80E-20	0.000	412.0	9.04E-20	0.000	412.5	9.45E-20	0.000	413.0	9.34E-20	0.000	413.5	9.37E-20	0.000
414.0	9.63E-20	0.000	414.5	9.71E-20	0.000	415.0	9.70E-20	0.000	415.5	9.65E-20	0.000	416.0	9.69E-20	0.000
416.5	9.89E-20	0.000	417.0	1.00E-19	0.000	417.5	1.02E-19	0.000	418.0	1.00E-19	0.000	418.5	1.02E-19	0.000
419.0	1.01E-19	0.000	419.5	1.01E-19	0.000	420.0	1.03E-19	0.000	420.5	1.01E-19	0.000	421.0	1.04E-19	0.000
Photolysis File = MGLY_ABS														
219.0	9.84E-21	1.000	219.5	1.04E-20	1.000	220.0	1.06E-20	1.000	220.5	1.11E-20	1.000	221.0	1.15E-20	1.000
221.5	1.18E-20	1.000	222.0	1.22E-20	1.000	222.5	1.24E-20	1.000	223.0	1.26E-20	1.000	223.5	1.26E-20	1.000
224.0	1.25E-20	1.000	224.5	1.24E-20	1.000	225.0	1.25E-20	1.000	225.5	1.27E-20	1.000	226.0	1.27E-20	1.000
226.5	1.29E-20	1.000	227.0	1.31E-20	1.000	227.5	1.32E-20	1.000	228.0	1.35E-20	1.000	228.5	1.37E-20	1.000
229.0	1.40E-20	1.000	229.5	1.42E-20	1.000	230.0	1.48E-20	1.000	230.5	1.53E-20	1.000	231.0	1.57E-20	1.000
231.5	1.59E-20	1.000	232.0	1.61E-20	1.000	232.5	1.62E-20	1.000	233.0	1.61E-20	1.000	233.5	1.68E-20	1.000
234.0	1.74E-20	1.000	234.5	1.80E-20	1.000	235.0	1.84E-20	1.000	235.5	1.87E-20	1.000	236.0	1.89E-20	1.000
236.5	1.91E-20	1.000	237.0	1.93E-20	1.000	237.5	1.94E-20	1.000	238.0	1.96E-20	1.000	238.5	1.96E-20	1.000
239.0	2.01E-20	1.000	239.5	2.04E-20	1.000	240.0	2.08E-20	1.000	240.5	2.10E-20	1.000	241.0	2.14E-20	1.000
241.5	2.16E-20	1.000	242.0	2.19E-20	1.000	242.5	2.20E-20	1.000	243.0	2.23E-20	1.000	243.5	2.26E-20	1.000
244.0	2.28E-20	1.000	244.5	2.29E-20	1.000	245.0	2.30E-20	1.000	245.5	2.32E-20	1.000	246.0	2.33E-20	1.000
246.5	2.35E-20	1.000	247.0	2.38E-20	1.000	247.5	2.41E-20	1.000	248.0	2.46E-20	1.000	248.5	2.51E-20	1.000
249.0	2.57E-20	1.000	249.5	2.61E-20	1.000	250.0	2.65E-20	1.000	250.5	2.67E-20	1.000	251.0	2.69E-20	1.000
251.5	2.69E-20	1.000	252.0	2.71E-20	1.000	252.5	2.72E-20	1.000	253.0	2.73E-20	1.000	253.5	2.74E-20	1.000
254.0	2.76E-20	1.000	254.5	2.78E-20	1.000	255.0	2.82E-20	1.000	255.5	2.87E-20	1.000	256.0	2.93E-20	1.000
256.5	2.98E-20	1.000	257.0	3.07E-20	1.000	257.5	3.12E-20	1.000	258.0	3.17E-20	1.000	258.5	3.21E-20	1.000
259.0	3.26E-20	1.000	259.5	3.28E-20	1.000	260.0	3.29E-20	1.000	260.5	3.31E-20	1.000	261.0	3.33E-20	1.000
261.5	3.34E-20	1.000	262.0	3.36E-20	1.000	262.5	3.38E-20	1.000	263.0	3.42E-20	1.000	263.5	3.44E-20	1.000
264.0	3.48E-20	1.000	264.5	3.54E-20	1.000	265.0	3.59E-20	1.000	265.5	3.65E-20	1.000	266.0	3.73E-20	1.000
266.5	3.80E-20	1.000	267.0	3.87E-20	1.000	267.5	3.95E-20	1.000	268.0	4.02E-20	1.000	268.5	4.08E-20	1.000
269.0	4.13E-20	1.000	269.5	4.17E-20	1.000	270.0	4.20E-20	1.000	270.5	4.22E-20	1.000	271.0	4.22E-20	1.000
271.5	4.22E-20	1.000	272.0	4.23E-20	1.000	272.5	4.24E-20	1.000	273.0	4.27E-20	1.000	273.5	4.29E-20	1.000
274.0	4.31E-20	1.000	274.5	4.33E-20	1.000	275.0	4.37E-20	1.000	275.5	4.42E-20	1.000	276.0	4.48E-20	1.000
276.5	4.56E-20	1.000	277.0	4.64E-20	1.000	277.5	4.71E-20	1.000	278.0	4.78E-20	1.000	278.5	4.83E-20	1.000
279.0	4.87E-20	1.000	279.5	4.90E-20	1.000	280.0	4.92E-20	1.000	280.5	4.93E-20	1.000	281.0	4.94E-20	1.000
281.5	4.92E-20	1.000	282.0	4.90E-20	1.000	282.5	4.86E-20	1.000	283.0	4.83E-20	1.000	283.5	4.79E-20	1.000
284.0	4.76E-20	1.000	284.5	4.72E-20	1.000	285.0	4.70E-20	1.000	285.5	4.68E-20	1.000	286.0	4.66E-20	1.000
286.5	4.65E-20	1.000	287.0	4.65E-20	1.000	287.5	4.68E-20	1.000	288.0	4.73E-20	1.000	288.5	4.78E-20	1.000
289.0	4.84E-20	1.000	289.5	4.89E-20	1.000	290.0	4.92E-20	1.000	290.5	4.92E-20	1.000	291.0	4.90E-20	1.000
291.5	4.86E-20	1.000	292.0	4.81E-20	1.000	292.5	4.75E-20	1.000	293.0	4.70E-20	1.000	293.5	4.65E-20	1.000
294.0	4.58E-20	1.000	294.5	4.48E-20	1.000	295.0	4.38E-20	1.000	295.5	4.27E-20	1.000	296.0	4.17E-20	1.000
296.5	4.07E-20	1.000	297.0	3.99E-20	1.000	297.5	3.94E-20	1.000	298.0	3.88E-20	1.000	298.5	3.82E-20	1.000
299.0	3.76E-20	1.000	299.5	3.72E-20	1.000	300.0	3.69E-20	1.000	300.5	3.68E-20	1.000	301.0	3.70E-20	1.000
301.5	3.72E-20	1.000	302.0	3.74E-20	1.000	302.5	3.74E-20	1.000	303.0	3.75E-20	1.000	303.5	3.71E-20	1.000
304.0	3.62E-20	1.000	304.5	3.51E-20	1.000	305.0	3.38E-20	1.000	305.5	3.25E-20	1.000	306.0	3.15E-20	1.000
306.5	3.04E-20	1.000	307.0	2.92E-20	1.000	307.5	2.80E-20	1.000	308.0	2.71E-20	1.000	308.5	2.63E-20	1.000
309.0	2.52E-20	1.000	309.5	2.43E-20	1.000	310.0	2.34E-20	1.000	310.5	2.25E-20	1.000	311.0	2.19E-20	1.000
311.5	2.12E-20	1.000	312.0	2.06E-20	1.000	312.5	2.02E-20	1.000	313.0	1.96E-20	1.000	313.5	1.92E-20	1.000

Table A-3. (continued)

WL (nm)	Abs (cm^2)	QY	WL (nm)	Abs (cm^2)	QY	WL (nm)	Abs (cm^2)	QY	WL (nm)	Abs (cm^2)	QY	WL (nm)	Abs (cm^2)	QY
314.0	1.91E-20	1.000	314.5	1.88E-20	1.000	315.0	1.86E-20	1.000	315.5	1.85E-20	1.000	316.0	1.86E-20	1.000
316.5	1.87E-20	1.000	317.0	1.87E-20	1.000	317.5	1.87E-20	1.000	318.0	1.83E-20	1.000	318.5	1.75E-20	1.000
319.0	1.69E-20	1.000	319.5	1.60E-20	1.000	320.0	1.50E-20	1.000	320.5	1.41E-20	1.000	321.0	1.34E-20	1.000
321.5	1.27E-20	1.000	322.0	1.21E-20	1.000	322.5	1.18E-20	1.000	323.0	1.14E-20	1.000	323.5	1.08E-20	1.000
324.0	1.01E-20	1.000	324.5	9.62E-21	1.000	325.0	9.28E-21	1.000	325.5	8.75E-21	1.000	326.0	8.49E-21	1.000
326.5	8.21E-21	1.000	327.0	7.71E-21	1.000	327.5	7.38E-21	1.000	328.0	7.18E-21	1.000	328.5	6.86E-21	1.000
329.0	6.71E-21	1.000	329.5	6.63E-21	1.000	330.0	6.46E-21	1.000	330.5	6.29E-21	1.000	331.0	6.21E-21	1.000
331.5	6.18E-21	1.000	332.0	6.20E-21	1.000	332.5	5.49E-21	1.000	333.0	5.21E-21	1.000	333.5	5.38E-21	1.000
334.0	5.35E-21	1.000	334.5	5.04E-21	1.000	335.0	4.94E-21	1.000	335.5	4.90E-21	1.000	336.0	4.52E-21	1.000
336.5	4.26E-21	1.000	337.0	4.11E-21	1.000	337.5	3.76E-21	1.000	338.0	3.61E-21	1.000	338.5	3.58E-21	1.000
339.0	3.47E-21	1.000	339.5	3.32E-21	1.000	340.0	3.22E-21	1.000	340.5	3.10E-21	1.000	341.0	3.00E-21	1.000
341.5	2.94E-21	1.000	342.0	2.89E-21	1.000	342.5	2.86E-21	1.000	343.0	2.88E-21	1.000	343.5	2.88E-21	1.000
344.0	2.89E-21	1.000	344.5	2.91E-21	1.000	345.0	2.95E-21	1.000	345.5	3.00E-21	1.000	346.0	3.08E-21	1.000
346.5	3.18E-21	1.000	347.0	3.25E-21	1.000	347.5	3.30E-21	1.000	348.0	3.39E-21	1.000	348.5	3.51E-21	1.000
349.0	3.63E-21	1.000	349.5	3.73E-21	1.000	350.0	3.85E-21	1.000	350.5	3.99E-21	1.000	351.0	4.27E-21	1.000
351.5	4.47E-21	1.000	352.0	4.63E-21	1.000	352.5	4.78E-21	1.000	353.0	4.92E-21	1.000	353.5	5.07E-21	1.000
354.0	5.23E-21	1.000	354.5	5.39E-21	1.000	355.0	5.56E-21	1.000	355.5	5.77E-21	1.000	356.0	5.97E-21	1.000
356.5	6.15E-21	1.000	357.0	6.35E-21	1.000	357.5	6.56E-21	1.000	358.0	6.76E-21	1.000	358.5	6.95E-21	1.000
359.0	7.20E-21	1.000	359.5	7.44E-21	1.000	360.0	7.64E-21	1.000	360.5	7.89E-21	1.000	361.0	8.15E-21	1.000
361.5	8.43E-21	1.000	362.0	8.71E-21	1.000	362.5	9.02E-21	1.000	363.0	9.33E-21	1.000	363.5	9.65E-21	1.000
364.0	1.00E-20	1.000	364.5	1.04E-20	1.000	365.0	1.08E-20	1.000	365.5	1.11E-20	1.000	366.0	1.15E-20	1.000
366.5	1.19E-20	1.000	367.0	1.23E-20	1.000	367.5	1.27E-20	1.000	368.0	1.31E-20	1.000	368.5	1.35E-20	1.000
369.0	1.40E-20	1.000	369.5	1.44E-20	1.000	370.0	1.47E-20	1.000	370.5	1.51E-20	1.000	371.0	1.55E-20	1.000
371.5	1.59E-20	1.000	372.0	1.64E-20	1.000	372.5	1.70E-20	1.000	373.0	1.73E-20	1.000	373.5	1.77E-20	1.000
374.0	1.81E-20	1.000	374.5	1.86E-20	1.000	375.0	1.90E-20	1.000	375.5	1.96E-20	1.000	376.0	2.02E-20	1.000
376.5	2.06E-20	1.000	377.0	2.10E-20	1.000	377.5	2.14E-20	1.000	378.0	2.18E-20	1.000	378.5	2.24E-20	1.000
379.0	2.30E-20	1.000	379.5	2.37E-20	1.000	380.0	2.42E-20	1.000	380.5	2.47E-20	1.000	381.0	2.54E-20	1.000
381.5	2.62E-20	1.000	382.0	2.69E-20	1.000	382.5	2.79E-20	1.000	383.0	2.88E-20	1.000	383.5	2.96E-20	1.000
384.0	3.02E-20	1.000	384.5	3.10E-20	1.000	385.0	3.20E-20	1.000	385.5	3.29E-20	1.000	386.0	3.39E-20	1.000
386.5	3.51E-20	1.000	387.0	3.62E-20	1.000	387.5	3.69E-20	1.000	388.0	3.70E-20	1.000	388.5	3.77E-20	1.000
389.0	3.88E-20	1.000	389.5	3.97E-20	1.000	390.0	4.03E-20	1.000	390.5	4.12E-20	1.000	391.0	4.22E-20	1.000
391.5	4.29E-20	1.000	392.0	4.30E-20	1.000	392.5	4.38E-20	1.000	393.0	4.47E-20	1.000	393.5	4.55E-20	1.000
394.0	4.56E-20	1.000	394.5	4.59E-20	1.000	395.0	4.67E-20	1.000	395.5	4.80E-20	1.000	396.0	4.87E-20	1.000
396.5	4.96E-20	1.000	397.0	5.08E-20	1.000	397.5	5.19E-20	1.000	398.0	5.23E-20	1.000	398.5	5.39E-20	1.000
399.0	5.46E-20	1.000	399.5	5.54E-20	1.000	400.0	5.59E-20	1.000	400.5	5.77E-20	1.000	401.0	5.91E-20	1.000
401.5	5.99E-20	1.000	402.0	6.06E-20	1.000	402.5	6.20E-20	1.000	403.0	6.35E-20	1.000	403.5	6.52E-20	1.000
404.0	6.54E-20	1.000	404.5	6.64E-20	1.000	405.0	6.93E-20	1.000	405.5	7.15E-20	1.000	406.0	7.19E-20	1.000
406.5	7.32E-20	1.000	407.0	7.58E-20	1.000	407.5	7.88E-20	1.000	408.0	7.97E-20	1.000	408.5	7.91E-20	1.000
409.0	8.11E-20	1.000	409.5	8.41E-20	1.000	410.0	8.53E-20	1.000	410.5	8.59E-20	1.000	411.0	8.60E-20	1.000
411.5	8.80E-20	1.000	412.0	9.04E-20	1.000	412.5	9.45E-20	1.000	413.0	9.34E-20	1.000	413.5	9.37E-20	1.000
414.0	9.63E-20	1.000	414.5	9.71E-20	1.000	415.0	9.70E-20	1.000	415.5	9.65E-20	1.000	416.0	9.69E-20	1.000
416.5	9.89E-20	1.000	417.0	1.00E-19	1.000	417.5	1.02E-19	1.000	418.0	1.00E-19	1.000	418.5	1.02E-19	1.000
419.0	1.01E-19	1.000	419.5	1.01E-19	1.000	420.0	1.03E-19	1.000	420.5	1.01E-19	1.000	421.0	1.04E-19	1.000
421.5	1.05E-19	1.000	422.0	1.06E-19	1.000	422.5	1.04E-19	1.000	423.0	1.05E-19	1.000	423.5	1.05E-19	1.000
424.0	1.01E-19	1.000	424.5	1.01E-19	1.000	425.0	1.05E-19	1.000	425.5	1.03E-19	1.000	426.0	1.02E-19	1.000
426.5	1.01E-19	1.000	427.0	9.77E-20	1.000	427.5	9.81E-20	1.000	428.0	1.00E-19	1.000	428.5	1.02E-19	1.000
429.0	9.89E-20	1.000	429.5	9.85E-20	1.000	430.0	1.04E-19	1.000	430.5	1.08E-19	1.000	431.0	1.05E-19	1.000
431.5	1.02E-19	1.000	432.0	9.64E-20	1.000	432.5	1.01E-19	1.000	433.0	1.06E-19	1.000	433.5	1.09E-19	1.000
434.0	1.04E-19	1.000	434.5	1.03E-19	1.000	435.0	1.07E-19	1.000	435.5	1.16E-19	1.000	436.0	1.09E-19	1.000
436.5	1.11E-19	1.000	437.0	9.81E-20	1.000	437.5	9.71E-20	1.000	438.0	1.06E-19	1.000	438.5	1.16E-19	1.000
439.0	1.08E-19	1.000	439.5	1.05E-19	1.000	440.0	9.70E-20	1.000	440.5	1.01E-19	1.000	441.0	1.04E-19	1.000
441.5	1.07E-19	1.000	442.0	1.02E-19	1.000	442.5	9.68E-20	1.000	443.0	1.00E-19	1.000	443.5	1.14E-19	1.000
444.0	1.13E-19	1.000	444.5	1.03E-19	1.000	445.0	9.74E-20	1.000	445.5	8.46E-20	1.000	446.0	8.70E-20	1.000
446.5	9.97E-20	1.000	447.0	1.01E-19	1.000	447.5	9.15E-20	1.000	448.0	9.41E-20	1.000	448.5	8.99E-20	1.000
449.0	1.10E-19	1.000	449.5	9.12E-20	1.000	450.0	8.56E-20	1.000	450.5	8.28E-20	1.000	451.0	6.15E-20	1.000
451.5	5.56E-20	1.000	452.0	6.47E-20	1.000	452.5	7.27E-20	1.000	453.0	5.75E-20	1.000	453.5	5.08E-20	1.000
454.0	4.38E-20	1.000	454.5	3.81E-20	1.000	455.0	3.61E-20	1.000	455.5	3.61E-20	1.000	456.0	3.13E-20	1.000
456.5	2.72E-20	1.000	457.0	2.44E-20	1.000	457.5	2.22E-20	1.000	458.0	1.82E-20	1.000	458.5	1.43E-20	1.000
459.0	1.32E-20	1.000	459.5	1.05E-20	1.000	460.0	8.95E-21	1.000	460.5	8.90E-21	1.000	461.0	7.94E-21	1.000
461.5	7.04E-21	1.000	462.0	6.46E-21	1.000	462.5	5.63E-21	1.000	463.0	4.78E-21	1.000	463.5	3.94E-21	1.000
464.0	3.26E-21	1.000	464.5	2.97E-21	1.000	465.0	2.65E-21	1.000	465.5	2.46E-21	1.000	466.0	2.27E-21	1.000
466.5	2.08E-21	1.000	467.0	1.86E-21	1.000	467.5	1.76E-21	1.000	468.0	1.60E-21	1.000	468.5	1.44E-21	1.000
469.0	1.34E-21	1.000	469.5	1.20E-21	1.000	470.0	1.07E-21	1.000	470.5	1.02E-21	1.000	471.0	9.92E-22	1.000
471.5	9.97E-22	1.000	472.0	8.87E-22	1.000	472.5	8.27E-22	1.000	473.0	7.76E-22	1.000	473.5	7.15E-22	1.000
474.0	6.71E-22	1.000	474.5	6.67E-22	1.000	475.0	6.10E-22	1.000	475.5	6.17E-22	1.000	476.0	5.54E-22	1.000
476.5	5.22E-22	1.000	477.0	5.10E-22	1.000	477.5	5.17E-22	1.000	478.0	4.80E-22	1.000	478.5	4.71E-22	1.000
479.0	4.60E-22	1.000	479.5	4.35E-22	1.000	480.0	3.90E-22	1.000	480.5	3.71E-22	1.000	481.0	3.62E-22	1.000
481.5	3.52E-22	1.000	482.0	3.05E-22	1.000	482.5	3.05E-22	1.000	483.0	2.86E-22	1.000	483.5	2.53E-22	1.000
484.0	2.75E-22	1.000	484.5	2.59E-22	1.000	485.0	2.47E-22	1.000	485.5	2.36E-22	1.000	486.0	2.12E-22	1.000
486.5	1.89E-22	1.000	487.0	1.93E-22	1.000	487.5	1.86E-22	1.000	488.0	1.82E-22	1.000	488.5	1.75E-22	1.000
489.0	1.74E-22	1.000	489.5	1.72E-22	1.000	490.0	1.66E-22	1.000	490.5	1.75E-22	1.000	491.0	1.54E-22	1.000
491.5	1.74E-22	1.000	492.0	1.63E-22	1.000	492.5	1.53E-22	1.000	493.0	1.52E-22	1.000	493.5	5.85E-23	1.000
494.0	0.00E+00	1.000												
Photolysis File = BACL_ADJ														
230.0	1.30E-20	1.000	232.5	1.46E-20	1.000	235.0	1.68E-20	1.000	237.5	1.84E-20	1.000	240.0	2.16E-20	1.000
242.5	2.49E-20	1.000	245.0	2.65E-20	1.000	247.5	2.71E-20	1.000	250.0	3.03E-20	1.000	252.5	3.46E-20	1.000
255.0	3.46E-20	1.000	257.5	3.57E-20	1.000	260.0	3.95E-20	1.000	262.5	4.17E-20	1.000	265.0	4.17E-20	1.000
267.5	4.22E-20	1.000	270.0	4.60E-20	1.000	272.5	4.54E-20	1.000	275.0	4.33E-20	1.000	277.5	4.22E-20	1.000
280.0	4.44E-20	1.000	282.5	4.33E-20	1.000	285.0	3.90E-20	1.000	287.5	3.57E-20	1.000	290.0	3.25E-20	1.000
292.5	2.92E-20	1.000	295.0	2.60E-20	1.000	297.5	2.16E-20	1.000	300.0	1.79E-20	1.000	302.5	1.73E-20	1.000
305.0	1.46E-20	1.000	307.5	1.08E-20	1.000	310.0	9.20E-21	1.000	312.5	7.03E-21	1.000	315.0	6.49E-21	1.000
317.5	5.41E-21	1.000	320.0	5.41E-21	1.000	322.5	5.41E-21	1.000	325.0	4.33E-21	1.000	327.5	3.25E-21	1.000
330.0	3.79E-21	1.000	332.5	3.79E-21	1.000	335.0	4.33E-21	1.000	337.5	4.87E-21	1.000	340.0	5.41E-21	1.000
342.5	5.95E-21	1.000	345.0	6.49E-21	1.000	347.5	7.03E-21	1.000	350.0	8.12E-21	0.995	352.5	7.57E-21	0.960
355.0	9.20E-21	0.925	357.5	9.74E-21	0.890	360.0	1.08E-20	0.855	362.5	1.19E-20	0.820	365.0	1.41E-20	0.785

Table A-3. (continued)

WL (nm)	Abs (cm^2)	QY	WL (nm)	Abs (cm^2)	QY	WL (nm)	Abs (cm^2)	QY	WL (nm)	Abs (cm^2)	QY	WL (nm)	Abs (cm^2)	QY
367.5	1.51E-20	0.750	370.0	1.79E-20	0.715	372.5	2.00E-20	0.680	375.0	2.11E-20	0.645	377.5	2.33E-20	0.610
380.0	2.60E-20	0.575	382.5	2.81E-20	0.540	385.0	3.14E-20	0.505	387.5	3.46E-20	0.470	390.0	3.90E-20	0.435
392.5	4.11E-20	0.399	395.0	4.33E-20	0.364	397.5	4.38E-20	0.329	400.0	4.65E-20	0.294	402.5	4.81E-20	0.259
405.0	5.19E-20	0.224	407.5	5.84E-20	0.189	410.0	6.06E-20	0.154	412.5	6.49E-20	0.119	415.0	6.92E-20	0.084
417.5	6.87E-20	0.049	420.0	6.82E-20	0.014	422.5	6.71E-20	0.000	425.0	6.49E-20	0.000	427.5	5.95E-20	0.000
430.0	5.73E-20	0.000	432.5	6.28E-20	0.000	435.0	6.01E-20	0.000	437.5	5.84E-20	0.000	440.0	5.95E-20	0.000
442.5	6.49E-20	0.000	445.0	5.95E-20	0.000	447.5	4.98E-20	0.000	450.0	3.79E-20	0.000	452.5	2.81E-20	0.000
455.0	1.73E-20	0.000	457.5	1.08E-20	0.000	460.0	5.41E-21	0.000	462.5	3.79E-21	0.000	465.0	2.16E-21	0.000
467.5	1.08E-21	0.000	470.0	1.08E-21	0.000	472.5	0.00E+00	0.000						
Photolysis File = BZCHO														
299.0	1.78E-19	1.000	304.0	7.40E-20	1.000	306.0	6.91E-20	1.000	309.0	6.41E-20	1.000	313.0	6.91E-20	1.000
314.0	6.91E-20	1.000	318.0	6.41E-20	1.000	325.0	8.39E-20	1.000	332.0	7.65E-20	1.000	338.0	8.88E-20	1.000
342.0	8.88E-20	1.000	346.0	7.89E-20	1.000	349.0	7.89E-20	1.000	354.0	9.13E-20	1.000	355.0	8.14E-20	1.000
364.0	5.67E-20	1.000	368.0	6.66E-20	1.000	369.0	8.39E-20	1.000	370.0	8.39E-20	1.000	372.0	3.45E-20	1.000
374.0	3.21E-20	1.000	376.0	2.47E-20	1.000	377.0	2.47E-20	1.000	380.0	3.58E-20	1.000	382.0	9.90E-21	1.000
386.0	0.00E+00	1.000												
Photolysis File = ACROLEIN														
250.0	1.80E-21	1.000	252.0	2.05E-21	1.000	253.0	2.20E-21	1.000	254.0	2.32E-21	1.000	255.0	2.45E-21	1.000
256.0	2.56E-21	1.000	257.0	2.65E-21	1.000	258.0	2.74E-21	1.000	259.0	2.83E-21	1.000	260.0	2.98E-21	1.000
261.0	3.24E-21	1.000	262.0	3.47E-21	1.000	263.0	3.58E-21	1.000	264.0	3.93E-21	1.000	265.0	4.67E-21	1.000
266.0	5.10E-21	1.000	267.0	5.38E-21	1.000	268.0	5.73E-21	1.000	269.0	6.13E-21	1.000	270.0	6.64E-21	1.000
271.0	7.20E-21	1.000	272.0	7.77E-21	1.000	273.0	8.37E-21	1.000	274.0	8.94E-21	1.000	275.0	9.55E-21	1.000
276.0	1.04E-20	1.000	277.0	1.12E-20	1.000	278.0	1.19E-20	1.000	279.0	1.27E-20	1.000	280.0	1.27E-20	1.000
281.0	1.26E-20	1.000	282.0	1.26E-20	1.000	283.0	1.28E-20	1.000	284.0	1.33E-20	1.000	285.0	1.38E-20	1.000
286.0	1.44E-20	1.000	287.0	1.50E-20	1.000	288.0	1.57E-20	1.000	289.0	1.63E-20	1.000	290.0	1.71E-20	1.000
291.0	1.78E-20	1.000	292.0	1.86E-20	1.000	293.0	1.95E-20	1.000	294.0	2.05E-20	1.000	295.0	2.15E-20	1.000
296.0	2.26E-20	1.000	297.0	2.37E-20	1.000	298.0	2.48E-20	1.000	299.0	2.60E-20	1.000	300.0	2.73E-20	1.000
301.0	2.85E-20	1.000	302.0	2.99E-20	1.000	303.0	3.13E-20	1.000	304.0	3.27E-20	1.000	305.0	3.39E-20	1.000
306.0	3.51E-20	1.000	307.0	3.63E-20	1.000	308.0	3.77E-20	1.000	309.0	3.91E-20	1.000	310.0	4.07E-20	1.000
311.0	4.25E-20	1.000	312.0	4.39E-20	1.000	313.0	4.44E-20	1.000	314.0	4.50E-20	1.000	315.0	4.59E-20	1.000
316.0	4.75E-20	1.000	317.0	4.90E-20	1.000	318.0	5.05E-20	1.000	319.0	5.19E-20	1.000	320.0	5.31E-20	1.000
321.0	5.43E-20	1.000	322.0	5.52E-20	1.000	323.0	5.60E-20	1.000	324.0	5.67E-20	1.000	325.0	5.67E-20	1.000
326.0	5.62E-20	1.000	327.0	5.63E-20	1.000	328.0	5.71E-20	1.000	329.0	5.76E-20	1.000	330.0	5.80E-20	1.000
331.0	5.95E-20	1.000	332.0	6.23E-20	1.000	333.0	6.39E-20	1.000	334.0	6.38E-20	1.000	335.0	6.24E-20	1.000
336.0	6.01E-20	1.000	337.0	5.79E-20	1.000	338.0	5.63E-20	1.000	339.0	5.56E-20	1.000	340.0	5.52E-20	1.000
341.0	5.54E-20	1.000	342.0	5.53E-20	1.000	343.0	5.47E-20	1.000	344.0	5.41E-20	1.000	345.0	5.40E-20	1.000
346.0	5.48E-20	1.000	347.0	5.90E-20	1.000	348.0	6.08E-20	1.000	349.0	6.00E-20	1.000	350.0	5.53E-20	1.000
351.0	5.03E-20	1.000	352.0	4.50E-20	1.000	353.0	4.03E-20	1.000	354.0	3.75E-20	1.000	355.0	3.55E-20	1.000
356.0	3.45E-20	1.000	357.0	3.46E-20	1.000	358.0	3.49E-20	1.000	359.0	3.41E-20	1.000	360.0	3.23E-20	1.000
361.0	2.95E-20	1.000	362.0	2.81E-20	1.000	363.0	2.91E-20	1.000	364.0	3.25E-20	1.000	365.0	3.54E-20	1.000
366.0	3.30E-20	1.000	367.0	2.78E-20	1.000	368.0	2.15E-20	1.000	369.0	1.59E-20	1.000	370.0	1.19E-20	1.000
371.0	8.99E-21	1.000	372.0	7.22E-21	1.000	373.0	5.86E-21	1.000	374.0	4.69E-21	1.000	375.0	3.72E-21	1.000
376.0	3.57E-21	1.000	377.0	3.55E-21	1.000	378.0	2.83E-21	1.000	379.0	1.69E-21	1.000	380.0	8.29E-24	1.000
381.0	0.00E+00	1.000												

Table A-4. Values of chamber-dependent parameters used in the model simulations of the environmental chamber experiments for this study.

Parm.	Value(s)	Discussion
k(1)	0.131 → 0.121 min^{-1}	Derived from actinometry results and by modeling trends in d(O_3-NO) formation in the base case surrogate runs as discussed in the text.
k(O3W)	$8.5x10^{-4}$ min^{-1}	k(O3W) is rate constant for unimolecular wall loss of O_3. The default value used is based on results of early O_3 dark decay experiments in this chamber, which are consistent with results of more recent runs.
k(N25I) k(N25S)	$2.8\ x10^{-3}$ min^{-1}, $1.5x10^{-6}$ - k_g ppm^{-1} min^{-1}	k(N25I) is unimolecular decay of N_2O_5 to the walls. K(N25S) is the rate constant for bimolecular reaction with H_2O, forming 2 HNO3. The value used is based on the N_2O_5 decay rate measurements in a similar chamber reported by Tuazon et al. (1983). The same rate constants are used for all Teflon bag chambers (Carter et al., 1995c).
k(NO2W) yHONO	$1.6x10^{-4}$ min^{-1} 0.2	k(NO2W) is the rate constant for a unimolecular decay of NO_2 to the walls, forming HONO with a yield of yHOHO. The values used are based on dark NO_2 decay and HONO formation measured in a similar chamber by Pitts et al. (1984). This is assumed to be the same in all Teflon bag chambers (Carter et al. 1995c).
k(XSHC)	250 min^{-1}	k(XSHC) is the rate constant for conversion of HO to HO_2 due to background VOC reactants. This is estimated by modeling pure air irradiations. This is not an important parameter for experiments discussed here.
RN/K1	0.092 ppb (CTC244-255) 0.066 ppb (CTC256-277)	The continuous chamber radical source and NO_x offgasing from the chamber walls are represented as a light-dependent flux of HONO, whose rate is given by the NO_2 photolysis rate (k_1) multiplied by the parameter RN/K1. Previously these two processes were represented separately (Carter et al, 1995c,d), but based on their similar magnitudes they are currently assumed to be due the same process. RN/K1 is derived from model simulations of n-butane or CO - NO_x experiments as discussed by Carter et al. (1995c,d). The values for runs DTC256-277 are based on averages which fit the characterization runs carried out during this period and during previous periods, which are not significantly different. The characterization runs carried out around the time of CTC244-255 indicated slightly higher radical sources, so a separate average for this period was used when modeling those runs.
HONO-F	0.012 (CTC244-255) 0.010 (CTC256-267)	HONO-F is the fraction of initially present NO_2 which is assumed to be converted to HONO prior to the start of the run, present as an impurity in the NO_x. When the radical source is represented by a continuous flux of HONO, best fits to most n-butane or CO - NO_x experiments are obtained if HONO-F is treated as a second adjustable parameter when deriving RN/K1. The values used are the averages of the best fit values derived from these optimizations.